DISTRIBUTED MODELING OF SPENCER CREEK WATERSHED AND ASSESSMENT OF FUTURE CHANGES IN HYDROLOGICAL PROCESSES

DISTRIBUTED MODELING OF SPENCER CREEK WATERSHED AND ASSESSMENT OF FUTURE CHANGES IN HYDROLOGICAL PROCESSES

By

ZAKIA SULTANA

Bachelor of Science in Civil Engineering (Bangladesh Univ. of Engg. & Tech.)

A Thesis

Submitted to the School of Graduate Studies

In Partial Fulfillment of the Requirements

For the Degree

Master of Applied Science

McMaster University

Department of Civil Engineering

MASTER OF APPLIED SCIENCE (2009) **McMaster University**

Civil Engineering Hamilton, Ontario

TITLE: Distributed Modeling of Spencer Creek Watershed and Assessment of Future Changes in Hydrological Processes

AUTHOR: Zakia Sultana

B.Sc. Engg. (Civil), (Bangladesh Univ. of Engg. & Tech.)

SUPERVISOR: Dr. Paulin Coulibaly

NUMBER OF PAGES: xii, 119

ABSTRACT

The main purpose of this research is to implement and evaluate the effectiveness of a coupled model (MIKE SHE / MIKE 11) for Spencer Creek watershed (Ontario), and later to use this model for climate change impact study using Canadian Global Climate Model (CGCM 3.1) data and Canadian Regional Climate Model (CRCM 4.2) data. Both the CRCM and the CGCM data are downscaled using a Statistical Downscaling Method (SDSM) and a Time Lagged Feedforward Neural Network (TLFN).

The hydrologic modeling results show that the coupled model captured the snow storage quite well with a correlation coefficient of 0.5-0.8. It also provided a good representation of evapotranspiration (ET) in the catchment with higher values in late spring and early summer months. The simulated streamflows are consistent with the observed flows at different sites with a Nash-Sutcliffe coefficient of around 0.4-0.5. The model couldn't capture the extreme or mixed events such as freezing rain in winter and rain on snow processes in early spring. Using a conservative climate change scenario, downscaled RCM with TLFN and SDSM yields smaller changes than raw RCM projections, but the downscaling with SDSM produces smaller changes than TLFN. With downscaled GCM scenarios, the coupled MIKE SHE/MIKE 11 model predicted 1-5% annual decrease in snow storage for 2050s and 5-22% increase with RCM scenarios. Similarly, with downscaled GCM scenarios, the coupled model predicted 1-10% increase in annual ET for 2050s and 2-22% increase with TLFN downscaled RCM scenario. But with SDSM downscaled RCM scenario, the model showed around 10% decrease in annual ET. Those results are consistent with the downscaled results for maximum and minimum temperatures. The coupled model predicted 10-25% increase in annual streamflows for all the stations with downscaled GCM scenarios– which is consistent with the predicted changes in the snow storage and ET. With raw RCM scenarios, the model predicted 5-12% increase in annual streamflow, and 3-30% decrease with downscaled RCM results showing consistency with predicted increase in ET and the negative to small increase in precipitation. Overall, the wide range of projected future changes in hydrologic processes predicted by this study can be useful for understanding the integrated effect of climate change in this complex catchment.

ACKNOWLEDGEMENTS

I would like to gratefully acknowledge my supervisor Dr. Paulin Coulibaly, for his continuous guidance and heartiest support for this study. Without his suggestions on various aspects of the work, I would have not finished my research.

I would like to thank Mr. George Stojanovic, Water Resources Engineering Manager and Mr. Adalbert Z. Orbang, Water Resources Technician at Hamilton Conservation Authority for providing the database used in this study.

Thanks to Dr. R. L. Wilby, Professor, Department of Geography, Loughborough University, UK for his valuable advice on various aspects of the downscaling work with SDSM.

I also acknowledge Ms. Ying Qiao, Project Hydrogeologist, Danish Hydraulic Institute for providing suggestions and resolving issues regarding the MIKE-SHE/MIKE11 model.

Thanks to my colleagues in the Water Resources and Hydrology Research Group: Xiaoli Liu, Manu Sharma, Sadik Ahmed and Dr. Jos Samuel for helping me time to time whenever I had any problem.

Above all, I would like to gratefully acknowledge my family members, my always inspiring mom (Mrs. Tahera Begum) and dad (Md. Nurul Islam) and finally my loving husband (Md. Kamrul Islam) for supporting through my endeavours. Without their love, support and understanding, it would not have been possible for me to proceed with my studies.

TABLE OF CONTENTS

LIST OF TABLES

LIST OF FIGURES

Pg no.

Pg no.

Pg no.

LIST OF SYMBOLS

LAI	Leaf Area index
RD	Root depth
Kc	Crop coefficient
ETo	Reference crop evapotranspiration (mm/day)
w_t	Conditional probability of precipitation occurrence on day *t*
u_{tj}	Normalized predictors for SDSM
α_j	Estimated regression coefficients in SDSM
r_t	Computer generated uniformly distributed stochastic number
m	Size of the hidden layer in TLFN
n	Time step
w_j	Weight vector for the connection between the hidden and output layers
w_{jl}	Weight matrix for the connection between the input and hidden layers
φ 1, φ2	Transfer functions at the output and hidden layers respectively
b_j, bo	Additional network parameters or biases to be determined during training
Z_g (x,y)	Ground surface level
h(x,y)	Flow depth above the ground surface
u(x,y),v(x,y)	Flow velocities in x- and y-directions respectively
i(x,y)	Net rainfall less infiltration
S_0	Slope of the ground surface
S_f	Friction slope
K_x , K_y	Strickler coefficients
uh,vh	Discharge per unit area in the x- and y-directions respectively

CHAPTER 1

INTRODUCTION

1.1 BACKGROUND

Over the last decades of the 20th century, sustainable development and management of regional water resources has become a major concern at national and international levels. Many studies reported the loss and degradation of these resources due to natural disasters (floods, droughts, etc.) as well as human activities (agricultural, industrial, residential, etc.). Hydrological information and modeling tools are central to the management and restoration of existing water resources. Before incorporating any hydrological modifications or remedial measures, it is very important for the decision makers and planners to evaluate the consequences of these actions. Now-a-days, modeling has become an efficient tool to represent the hydrological processes as well as to assess the changes in these processes due to alternate management practices. Thompson et al. (2004) reported hydrologic modeling as a fast and less expensive technique for the evaluation of different management strategies, avoiding undesirable outcomes and targeting limited resources available for watershed management authorities and conservation practitioners. So, different hydrological models, both conceptual/statistical, and physically distributed, have been developed by scientists/engineers and several studies are performed with these models to obtain reliable hydrological information.

The conceptual or lumped hydrological models, such as HBV (Linden & Harlin, 2000), Stanford Watershed Model (Crawford & Linsey, 1966), have been widely used to simulate the hydrologic conditions for watershed management. These models are preferred by the hydrologists because of their lower data requirements and lower computational cost. But they represent the physical processes of the watershed with far less details (Liu, 2007) as they use lumped or spatially averaged model parameters, that can provide reasonable results only if there are no significant changes in the watershed conditions (Sahoo et al., 2006).

Physically distributed models, such as MIKE SHE (Jasper et al., 2002; Feyen et al., 2000; Johnson et al., 2003; Refsgaard, 1997), SHETRAN (Ewen et al., 2000), are developed in an attempt to overcome the limitations of conceptual models, thus they provide a detailed representation of the physical characteristics (topography, soil conditions, land cover, etc.) of the watershed. While the conceptual models can be used to study only one component of the hydrologic cycle at a time, physically distributed models can represent various components (unsaturated and saturated zone, overland flow) and so are preferred for integrated modeling of complex hydrological regimes. While Abbott et al. (1986) pointed to the conceptual models' inability to evaluate the impacts of different land use scenarios; Shalini (2006) applied a physically distributed model (MIKE SHE) to assess the hydrological changes in a complex watershed for different land use scenarios, such as urbanization, deforestation, etc. But these models require a large amount of spatially and temporally distributed input data and model parameters for reliable representation of the watershed hydrology. It is very difficult to set up a physically distributed model for large catchments with wide range of soil and aquifer properties; moreover the models require longer computational time. These facts limited the use of physically distributed hydrological models for watershed management.

In addition to developing an efficient hydrologic model to represent the present hydrological processes, the assessment of hydrological impacts due to climate change has become a very important issue in today's world. Climate change is supposed to affect the local hydrologic regimes, such as streamflows that support aquatic ecosystems, navigation, hydropower, etc., not only by changing the total flow volume in the rivers but also changing the frequency and severity of floods (Dibike & Coulibaly, 2007). So, different hydrological impact studies are being performed to predict the changes in the quantity and quality of regional water resources as well as to make flood forecasting so that water management plans can be made accordingly to protect and sustain these resources and also the necessary precautions can be taken to protect people from the damage and severity of floods.

Many climate change impact studies showed that if snowmelt is the major proportion of the stream flow for a basin, then regional temperature increase due to global warming will cause an earlier spring runoff for accelerated snowmelt and depending on the combined effects of precipitation changes and midwinter thaw events, there may be either an amplification or attenuation of flood magnitude (Mareuil et al., 2007). Dibike & Coulibaly (2005) showed an overall increasing trend in the mean annual river flow and reservoir inflow and also earlier spring peak flows for 2050s and 2080s. For more examples, readers are referred to Dibike & Coulibaly, 2006; Minville et al., 2008; Regonada et al., 2005; Simnovic & Li, 2004; Whitfield & Cannon, 2000.

The most widely used approach to study the hydrological impacts of climate change is to link climate change scenario outputs from general circulation models (GCMs), to a conceptual hydrological model so that future river runoff regimes can be generated to be compared with current runoff conditions (Mareuil et al., 2007; Dibike & Coulibaly, 2007). These climate models provide estimations of atmospheric variables, like precipitation, maximum and minimum temperature, wind speed, etc., for both current and future conditions under different climate change scenarios. But the spatial resolution of GCMs is quite coarse, usually in the order of 300 x 300 km and at this scale ,spatial heterogeneities of physiography is lost which makes accurate modeling of land phase very difficult (Dibike & Coulibaly, 2005). So, different downscaling techniques have been developed to convert these climate model outputs to the scale of the watershed concerned, though none of them is completely accurate. The use of several downscaling techniques with different models and emission scenarios better reflects the uncertainties in predicting future climate changes and model performance should be evaluated using simulations of present day conditions (Salathé Jr, 2005). Very few studies are done using an empirical downscaling technique for regional climate model data, and recent studies pointed out that regional climate model data should be further statistically downscaled (Murphy, 2000; Sharma, 2009) before using them in hydrologic impact study at the catchment scale.

The conceptual hydrologic models are preferred by the hydrologists for climate change impact study due to their lower data and computational time requirements. But these models can assess the change in only one hydrologic process at a time and these have been largely used in various previous studies mainly to assess the future changes in streamflow (Dibike & Coulibaly, 2005; Dibike & Coulibaly, 2007). As the physically distributed models are integrated ones, they can simulate future changes in different hydrologic components (streamflow, ET, snowmelt, groundwater level, etc.) for a complex watershed that will help to implement more effective watershed management plans. These models have high potential for climate change impact studies as they can provide changes in other water balance components. In this study an attempt is made to implement a distributed model for the Spencer Creek watershed and to further use the distributed model for climate change impact study.

1.2 RESEARCH OBJECTIVES

Spencer Creek watershed in Southern Ontario is a complex watershed with heterogeneous soil and aquifer properties. It has a drainage area of approximately 291 km^2 which is characterized by an extensive network of rivers and streams to collect surface runoff into Cootes Paradise at the Western end of Lake Ontario (HRCA, 1990). It contains different types of land uses, such as wetlands, forests, idle farmlands, rural croplands, urban developments, hydraulic structures, conservation areas and escarpments

(HRCA, 1990). A physically distributed and integrated modeling approach is required to reliably represent the complex hydrologic conditions in this watershed.

MIKE SHE is a physically-based, fully distributed model that incorporates both single-event and continuous simulation (Shalini, 2006). It is an efficient modeling technique for a wide range of applications due to its flexible structure, distributed nature and ability to employ physical laws to interpret hydrological processes (Abbott et al., 1986). MIKE SHE is also an integrated modeling approach for modeling surface and sub-surface flow processes. MIKE 11, which is a river modeling system, should be coupled with MIKE SHE for reliable representation of the interaction between surface runoff and groundwater. In this study, a coupled MIKE SHE/MIKE 11 model is implemented and tested for the Spencer Creek watershed.

Flooding occurred most frequently along Spencer Creek and snowmelt or rainfall-on-snowmelt are the key factors in generating high flows in this area. It reveals the importance of climate change impact study in this area mainly to assess the severity of floods in future so that proper adaptation or remediation measures can be taken in advance. Many climate change impact studies have been performed over the last decade using conceptual or lumped hydrologic models; but very few studies (Shalini, 2006) tried to use a physically distributed hydrologic model like MIKE SHE to study the effects of climate change in complex watersheds. So, an attempt has been made here to perform a climate change impact study with the coupled MIKE SHE/MIKE 11 model.

Therefore, this study has two major objectives:

a) firstly, to develop a physically distributed hydrologic model for Spencer Creek watershed using MIKE SHE and MIKE 11 modeling systems; and

b) later to use the coupled MIKE SHE/MIKE11 model to assess future changes in key hydrologic processes using climate change scenario results (precipitation and air temperature) from Canadian Global Climate model (CGCM) and Canadian Regional Climate model (CRCM).

Specifically, the coupled MIKE SHE/MIKE 11 model is used in this study to model three important hydrologic processes in the watershed: streamflow, total snow storage and evapotranspiration. Future changes in these hydrologic components are predicted using future climate scenarios obtained by downscaling CGCM and CRCM simulations.

1.3 STRUCTURE OF THE THESIS

This thesis consists of seven chapters including the introduction, which is Chapter 1. Chapter 2 provides a detailed description of the study area; the data collected for both downscaling and the hydrological model and the data preparation and correction processes. Chapter 3 provides a literature review of various downscaling techniques focusing particularly on SDSM and TLFN. In Chapter 4, MIKE SHE and MIKE 11 models are reviewed along with their applications in previous hydrology studies. Chapter 5 represents the model setups in two parts: first part for the downscaling model setups; and second part for the hydrological model setup and the calibration of the coupled model. In Chapter 6, the study results are discussed in two parts: first the downscaling results with SDSM and TLFN using both CGCM and CRCM along with the future projections for precipitation and maximum and minimum temperature are discussed; in the second part the current period results from the hydrological model are presented followed by the future projections using a conservative climate change scenario. The last Chapter (Chapter 7) provides the conclusions and significance of this study and the recommendations for future work.

CHAPTER 2

STUDY AREA AND DATA

2.1 STUDY AREA

The study area is Spencer Creek watershed located in the Southern Ontario. The three distinct water bodies in Hamilton Harbour are the main Harbour (central), Cootes Paradise (west) and the Winderemere basin (south-east). Spencer Creek flows through the western end of Lake Ontario by Cootes Paradise and has a drainage area of approximately 291 km^2. The watershed contains wetlands like the Beverly Swamp, forests and the main land use is pasture, idle farmland and rural cropland. In the upper part of the basin, there are some scattered communities and some urban developments in its lower part. About 10% of Spencer Creek watershed has urban land use that includes residential, commercial and industrial land uses (James, 1994; HRCA, 1990).

The flow in Spencer Creek, that has a total length of about 40 km along the main channel, is controlled by two dams and reservoirs: Valens Dam and Reservoir; and Christie Dam and Reservoir. The headwaters, located in the springs and seepage areas of the Galt Moraine within Puslinch Township, flows in a southeast direction into the Valens reservoir from an elevation of 340 meters (approximate). The Valens Dam and reservoir constructed in 1966 serves two important purposes: low flow augmentation and reducing downstream flooding during spring. The Beverly Swamp, downstream of Highway No. 97 at the joining of the main branch and Fletcher Creek, occupies an area of 20 km^2 and affects the hydrology of Spencer Creek significantly. It tends to reduce the flood peaks during high flow periods and augments the downstream flow in addition to recharging groundwater during low flow periods. The Christie Dam and Reservoir just upstream of Greensville were mainly constructed to reduce flooding within the Dundas town during the spring (Caron, 2007; HRCA, 1990; HRCA, 1983; Woo, 1978; Ontario Dept. of Lands and Forests, 1962). Fig 1 provides a detailed representation of the watershed including the streams and tributaries.

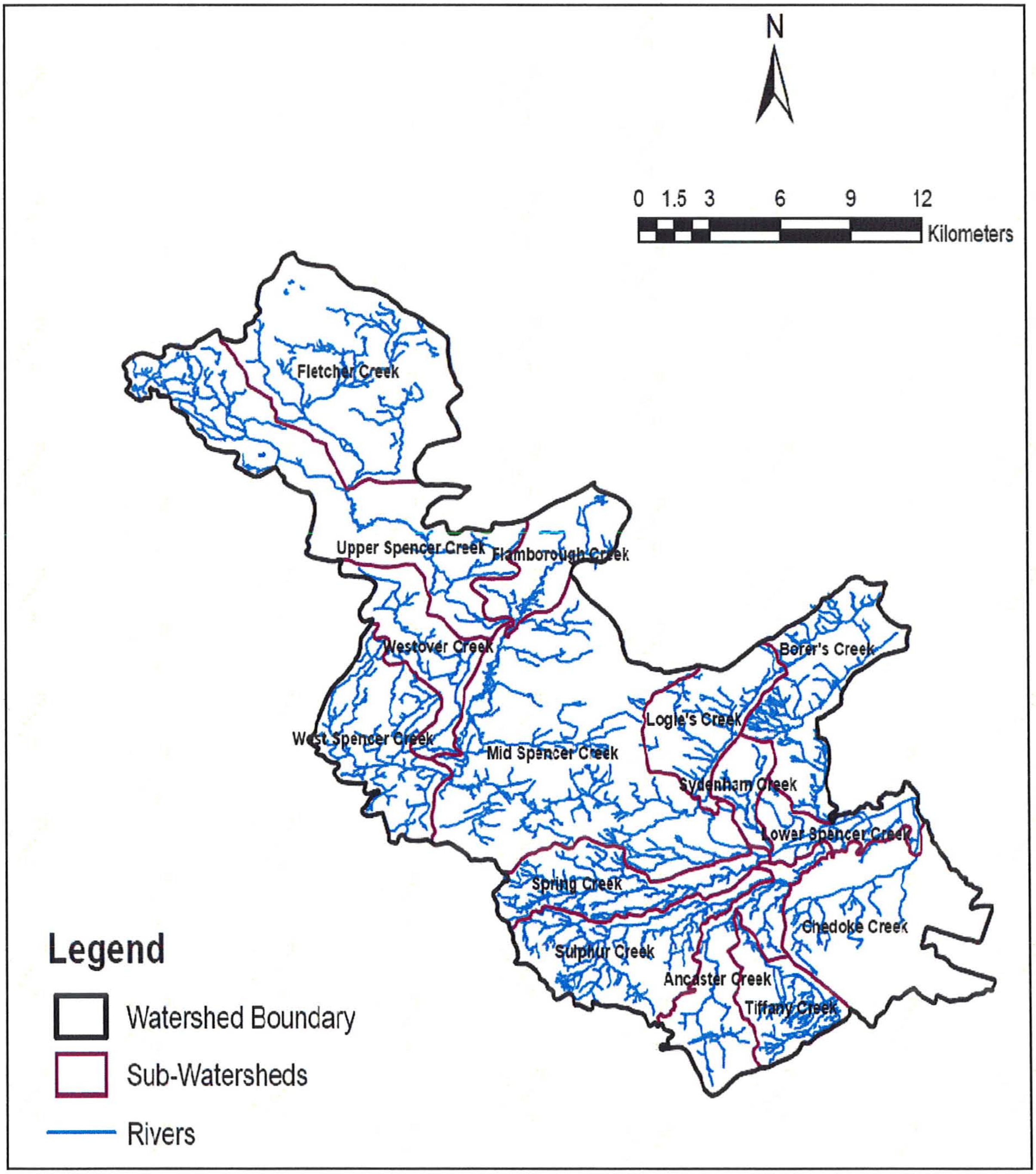

Fig 1: Spencer Creek watershed

2.2 DATA FOR DOWNSCALING

In this study, two meteorological stations, Hamilton Airport and Hamilton Royal Botanical Garden (RBG), are used as enough data for daily precipitation and daily maximum and minimum temperature is available for these two stations. The Hamilton RBG station was shut down in 1997 and so some data is collected from a closer new station Hamilton RBG CS. Table 1 provides the details of these stations.

Table 1: Meteorological stations in Spencer Creek Watershed

STATION NAME	CLIMATE ID	LATITUDE	LONGITUDE
Hamilton Airport	6153194	43° 10'12" N	79° 55'48" W
Hamilton RBG	6153300	43° 16'48" N	79° 52'48" W
Hamilton RBG CS	6153301	43° 17'24" N	79° 54'36" W

For the two stations: Hamilton Airport and Hamilton RBG, daily precipitation (mm) and daily maximum and minimum temperature data (^{o}C) for 1961-1990 are collected from Environment Canada. There were some missing values in the data set for both the stations. Those were filled in using the data from the closest station for precipitation and by regression for temperature.

Precipitation and temperature are downscaled using two Canadian climate model data: Canadian global climate model (CGCM) and Canadian regional climate model (CRCM). The T63 version of the third generation coupled Canadian global climate model, CGCM 3.1 is used for this study that has a surface grid resolution of 2.8^{o} lat/long and 31 levels in the vertical (CCCma, 2009); the data is collected from the Canadian Centre for Climate Modeling and Analysis website at the grid point 43^{o}15' N, 78^{o}45' W as it is the closest grid point to the two meteorological stations. Observed daily data of large scale predictor variables representing the current climatic conditions is derived from the National Center for Environmental Prediction (NCEP) reanalysis data set, which is used to build the downscaling models to be used for future prediction based on CGCM3.1 predictors.

The latest version of Canadian regional climate model, CRCM4.2 is chosen for this study and the data is provided by Environment Canada. RCMs are actually limited area models nested within GCMs that provide a higher spatial resolution as compared to the GCMs and can be set to run on a domain covering any part of the globe (CCCma, 2009). For a detailed description about CRCMs, readers are referred to CCCma, 2009; Caya & Laprise, 1999; Music & Caya, 2007.

Canadian climate models provide the current period data as well as the future period data for four climate scenarios: SRES A1B, SRES B1, SRES A2 and COMMIT. The scenarios predict future conditions based on different assumptions (CCCma, 2009). Fig 2 represents the variations in greenhouse gas concentrations and aerosol loadings for the scenarios. SRES A2 or the "business as usual" scenario is used in this study for climate change impact studies.

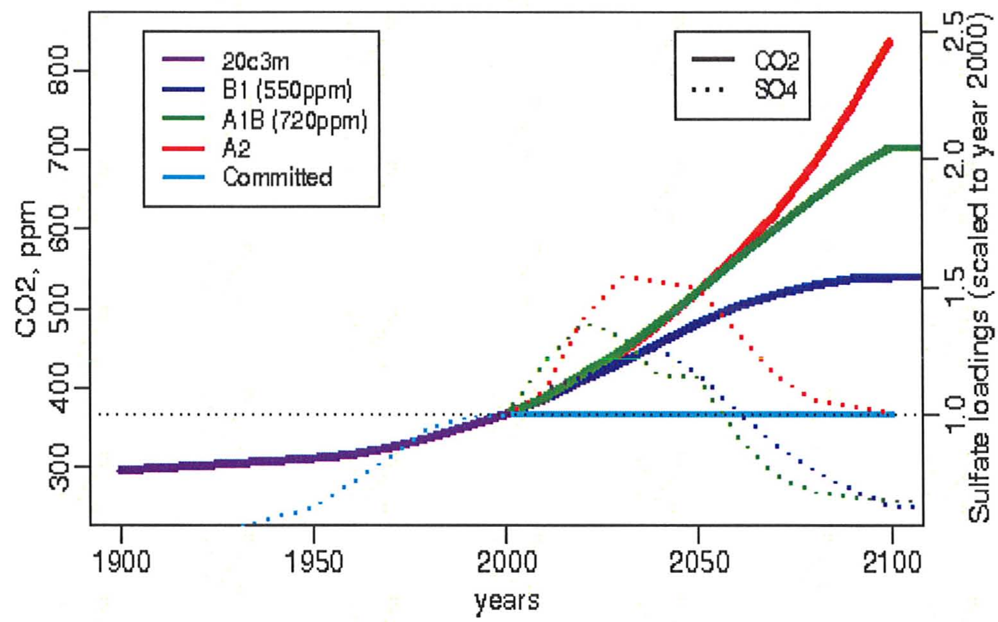

Fig 2: Climate change scenarios (CCCma, 2009)

The NCEP, CGCM3.1 and CRCM4.2 predictors used here are normalized with respect to 1961-1990 mean and standard deviation and are listed in Table 1A and 2A in the Appendix. The data for the current period are for 1961-1990 and the GCM and RCM data for SRES A2 are arranged for 2046-2065 (2050s) to facilitate trend analysis.

2.3 DATA FOR MIKE SHE MODEL

Topographic Data

A 50-meter DEM file for the watershed was provided by Hamilton Conservation Authority (HCA). It had some missing values near the outlet and those were filled in from the contours shape file using Arc Map. Later this 50-meter DEM file was used to prepare the topography grid file. HCA also provided a shape file named "subwatershed" to define the model domain.

Land use

The land use data used in this project is obtained from the shape file SOLRIS_2000_V1 from Mills library at McMaster University, clipped by the Spencer creek watershed. The original land use file included 30 different land types, and it was lumped into six types. A station-based shape file (Fig 3) for land use is created which contains six types of vegetation: built up, crops, forest, open water, marsh and bare fields. A vegetation property template file, provided by the Danish Hydraulic Institute (DHI), is used for temporal distribution of each vegetation type. In this vegetation property file, user defined vegetation development is chosen for each type of vegetation and the evapotranspiration parameters are set as default value except for forest. The variation of leaf area index (LAI), root depth (RD) and crop coefficient (K_C) is considered in this file throughout a year (365 days).

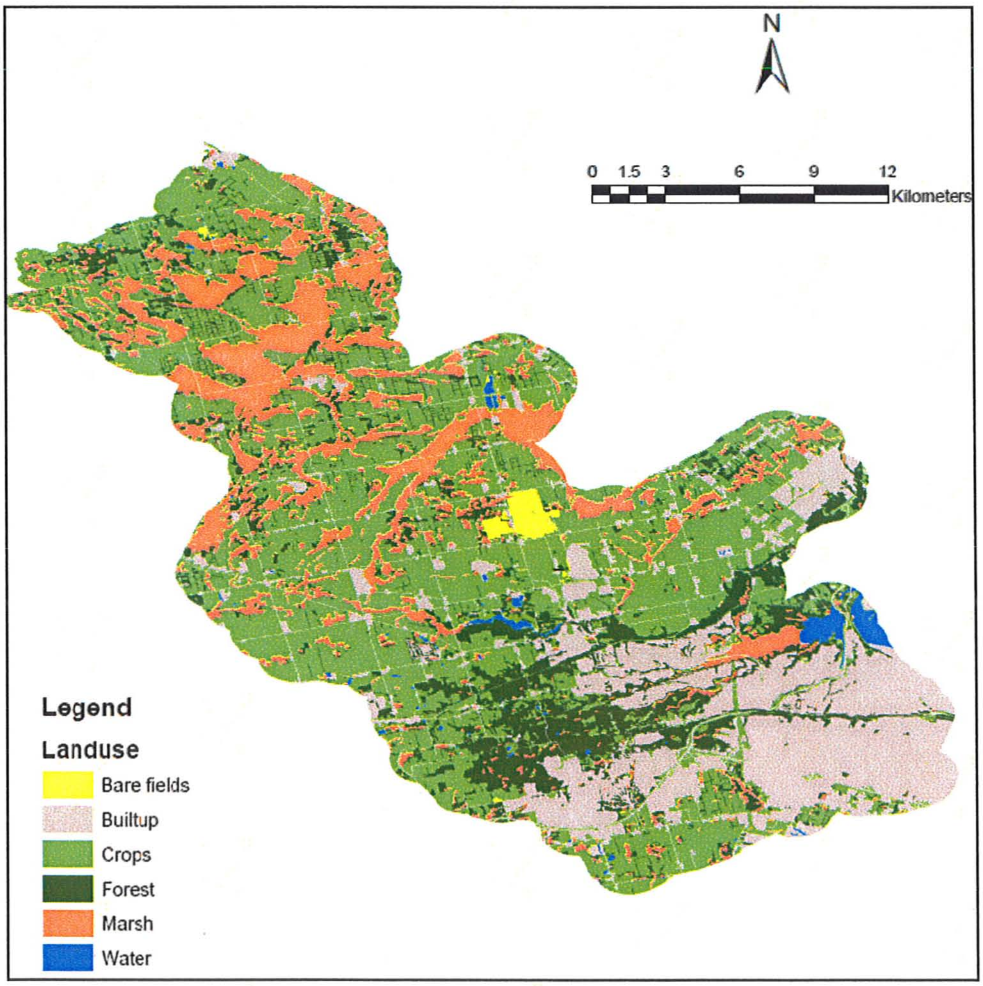

Fig 3: Land use types in Spencer creek watershed

Soil classification

The unsaturated zone soil profiles are obtained from the well data provided by HCA and 45 wells are selected to cover the whole watershed. Finally, 16 observation wells are used to divide the watershed into 16 zones with varying soil characteristics. The *geological layer* data for the saturated zone is also created from this well data. To simplify the model, the dominating soil type for each zone is identified which is the topmost soil layer for that zone and instead of using the vertical discretization of the soils, only that one dominant soil type is used for that particular zone. Fig 4 provides the final soil distribution used in the model.

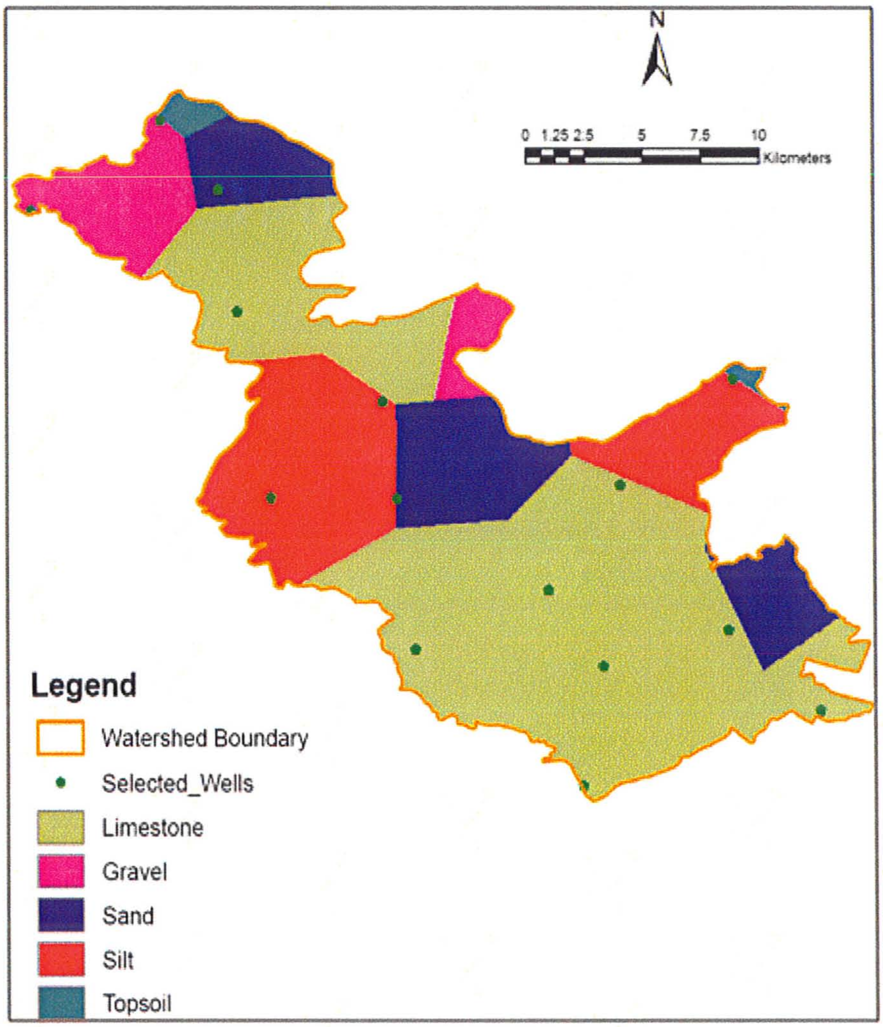

Fig 4: Soil distribution in the unsaturated zone

Groundwater data

Groundwater level data from eight wells is provided by HCA. A spatial distribution map of water level is created based on the wells' data (figure 5) and later distributed water level data recorded at a given time is used as time constant groundwater table for lower unsaturated zone boundary. Figure 5 is showing six wells, two wells are overlapped and so are not visible. The water depths vary from 1.1 to 8.7 meters.

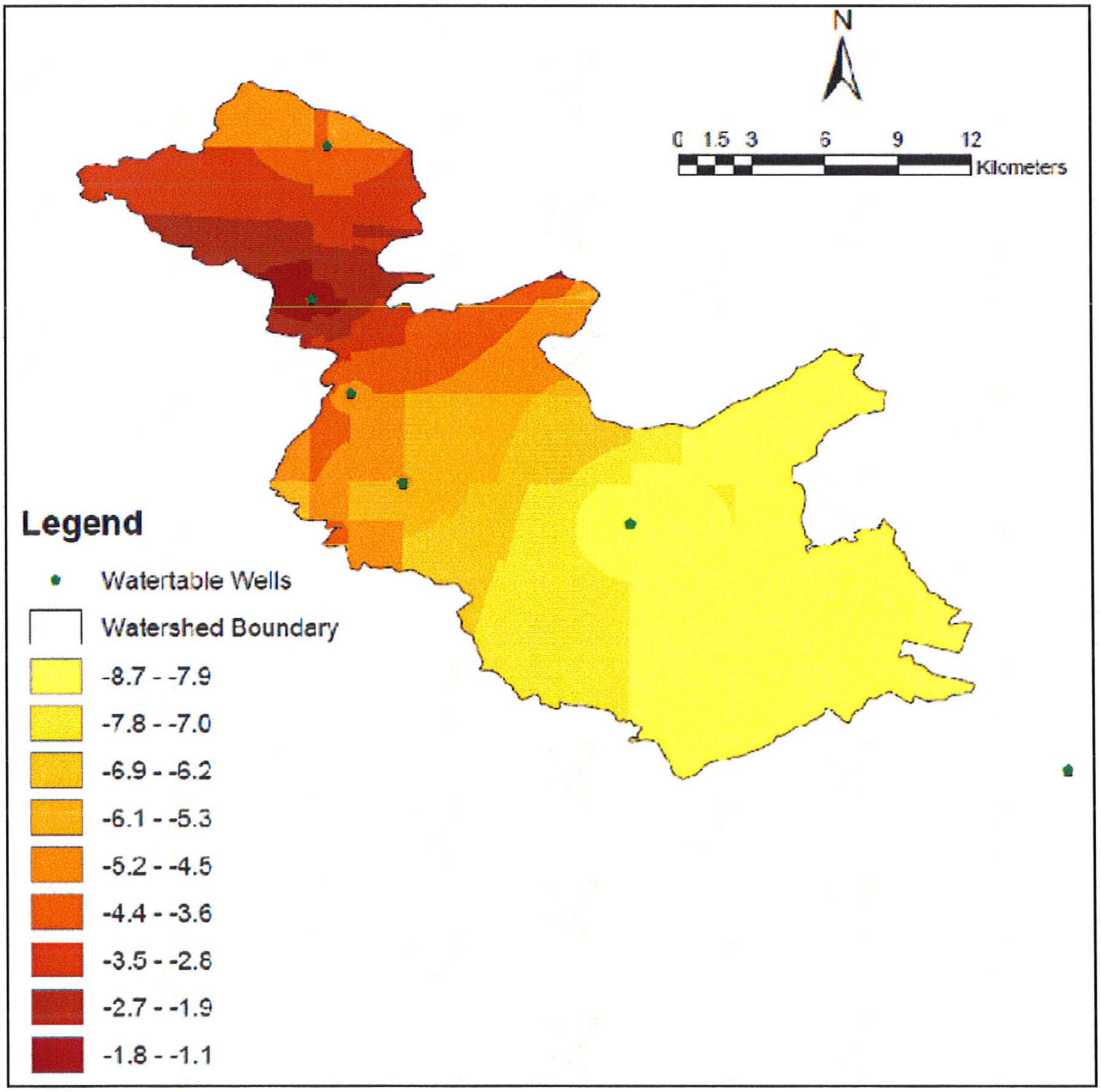

Fig 5: Map of Groundwater Depth Distribution

Meteorological datasets

The meteorological inputs for this model are collected from two stations: Hamilton Airport and Hamilton RBG. For each station, daily maximum and minimum temperature and daily precipitation data for 20 years (1989-2008) are collected from Environment Canada. A plot (figure 1A) for the cumulative precipitation in these stations is provided in Appendix A that shows that the precipitation data from the stations are consistent.

Using the daily maximum and minimum temperature data, monthly average daily evapotranspiration (ET) for each station are calculated using Blaney-Criddle method (Tollner, 2002; Brouwer & Heibloem, 1986).

The Blaney-Criddle formula is:

$$ETo = p\,(0.46\ T\ mean + 8);\ \text{where,}$$

ETo = Reference crop evapotranspiration (mm/day)

T mean = mean daily temperature (°C)

= (monthly average max. temp + monthly average min. temp)/2.

p = mean daily percentage of annual daytime hours (Table 3A in Appendix)

The Thiessen Polygon method is used to prepare a spatial distribution map of precipitation in the study area.

Snow Cover

Some snow data provided by HCA is used in the model to verify whether the model can efficiently simulate the snow storage or not. The snow courses are detailed in table 2; for each snow course, snowpack depth (cm) and water equivalent (mm) information is collected. These data are not continuous as snow sampling is usually done by HCA at the beginning and middle of each month during the winter/spring period.

Table 2: Snow course locations

Snow course	**Latitude**	**Longitude**	**Elevation (mASL)**
Dundas Valley	43°14'24" N	79°59'24" W	144.50
Valens	43°22' 48" N	80°8'24" W	277.10
Christie	43 °16' 48" N	80°1' 48" W	191.25

Hydrologic datasets

Twenty years' (1989-2008) daily flow data for four stations (Table 3) in the Spencer Creek watershed are prepared. The hourly flow data for this period is provided by HCA. Then daily data are prepared from the hourly data and compared with the available daily flow data from Water Survey Canada (WSC) to check the consistency of data. When compared, it is observed that the HCA data sometimes showed large deviations from the WSC flows except for the Ancaster station, for some years HCA data showed high flows in winter and comparatively low flows in spring. So, the streamflows from the flow stations are compared with corresponding precipitation data (figure 6 & 2A-4A) to select the reliable data source.

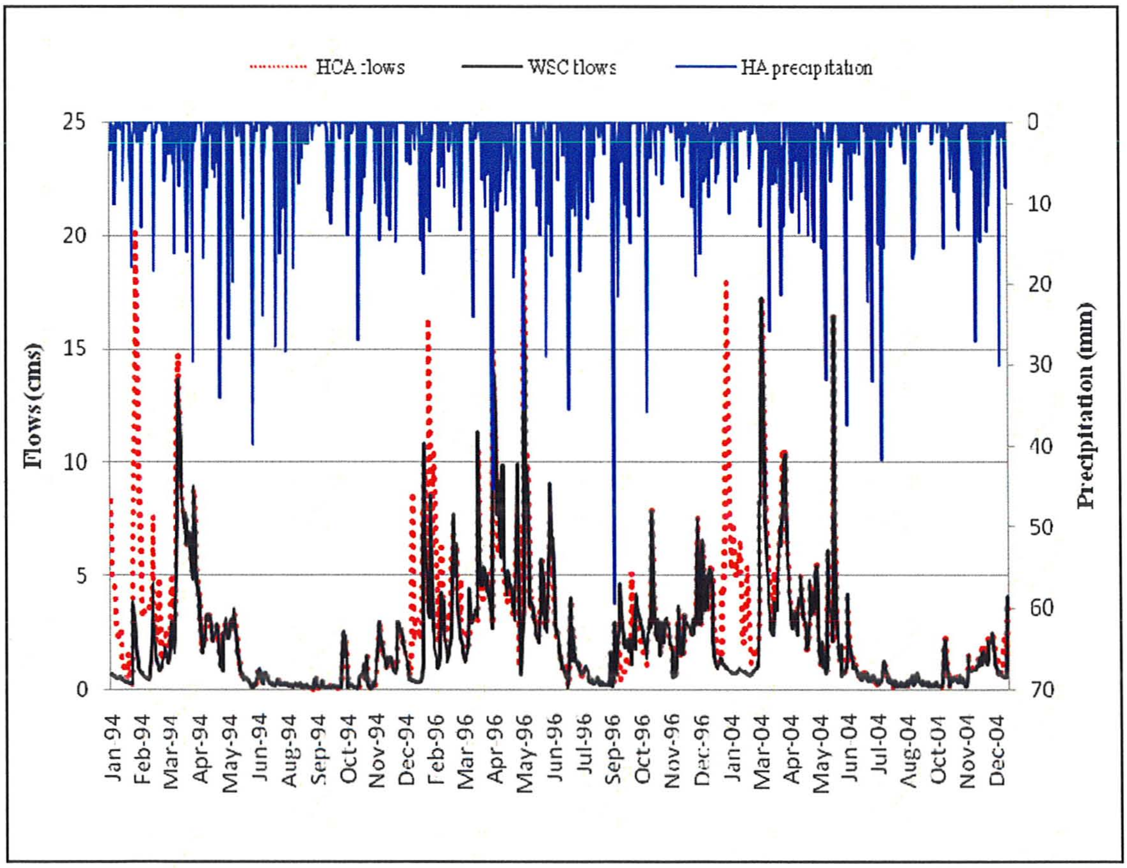

Fig 6: Comparison of WSC and HCA flows for Dundas with the precipitation at Hamilton Airport

For Dundas (figure 6), HCA data indicates high flows in winter; but precipitation (mainly snow) in winter is very low and moreover no snow melting occurs in this season. So, the high flows in winter are not reasonable and as WSC flows are more consistent, it is a more reliable data source for flow in Dundas. Same trend is observed for Westover and HWY5 (figures 2A, 3A).

WSC data is used when they are available (Westover: 1971-1998; HWY5: 1987-1997, 1999-2005, 2007, 2008; Dundas: 1989-2004, 2005, 2007, 2008); for the remaining part HCA data is used after comparing the flows for Dundas, Westover and HWY5 to make sure that they follow the same pattern, even then the flows in this part may be erroneous but data from any other source is not available for that period.

2.4 DATA FOR MIKE 11 MODEL

River Network

A river network image file is provided by HCA and based on that the network is delineated in MIKE 11 and it covers most of the rivers and ignores some of the tributaries.

Cross-section

For each rivers and tributaries, at least two cross-sections are required, one upstream and the other one at the junction of each river and tributary. A total of 174 Cross sections' data are provided by HCA. Fig 7 and 8 represent the model river network along with the cross-sections and the flow stations along with the meteorological stations used in this study.

Boundary data

For Valens dam, the hourly flows are collected from HCA that are used as the boundary data after converting them into daily flows. For this dam, the regulation rules and the historical water level data are also provided by HCA. The flow data was for 2003-2008. A dummy file is prepared to have continuous flow data from 1989-2008 for the boundary conditions.

Hydrodynamic parameters

Some of the water level and discharge data particularly at the flow stations are used as the initial conditions in MIKE 11.

Table 3: Flow Stations in Spencer Creek Watershed (WSC, 2009)

STATION NAME	STATION NO.	DRAINAGE AREA (km^2)	LATITUDE	LONGITUDE
Spencer Creek near Westover	02HB015	63.5	43°21' N	80°4'48" W
Spencer Creek at HWY5	02HB023	132	43°16'48" N	80°3' W
Spencer Creek at Dundas Crossing	02HB010	166	43°15'36" N	79°57'36" W
Ancaster Creek at Ancaster	02HB021	9.14	43°13'48" N	79°58'12" W

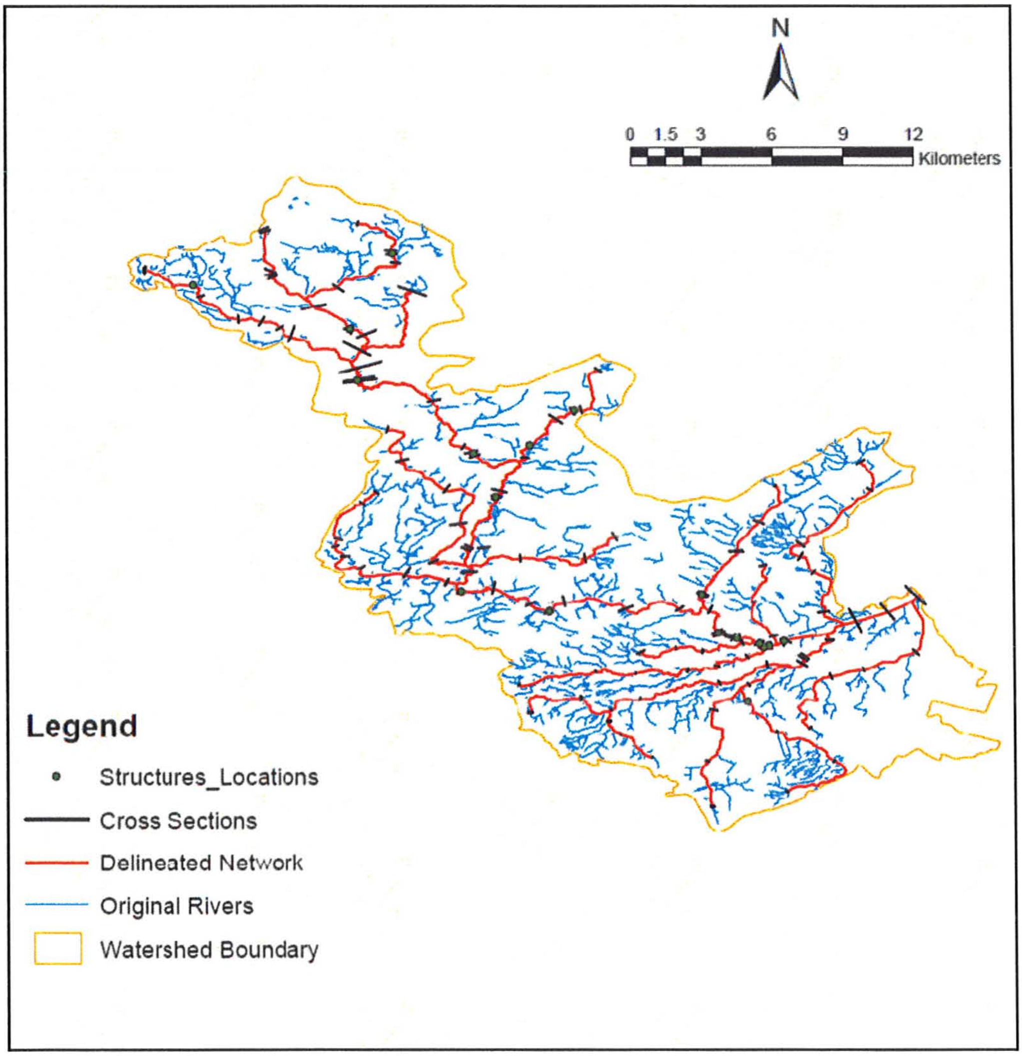

Fig 7: River network in Spencer Creek watershed with the hydraulic structures

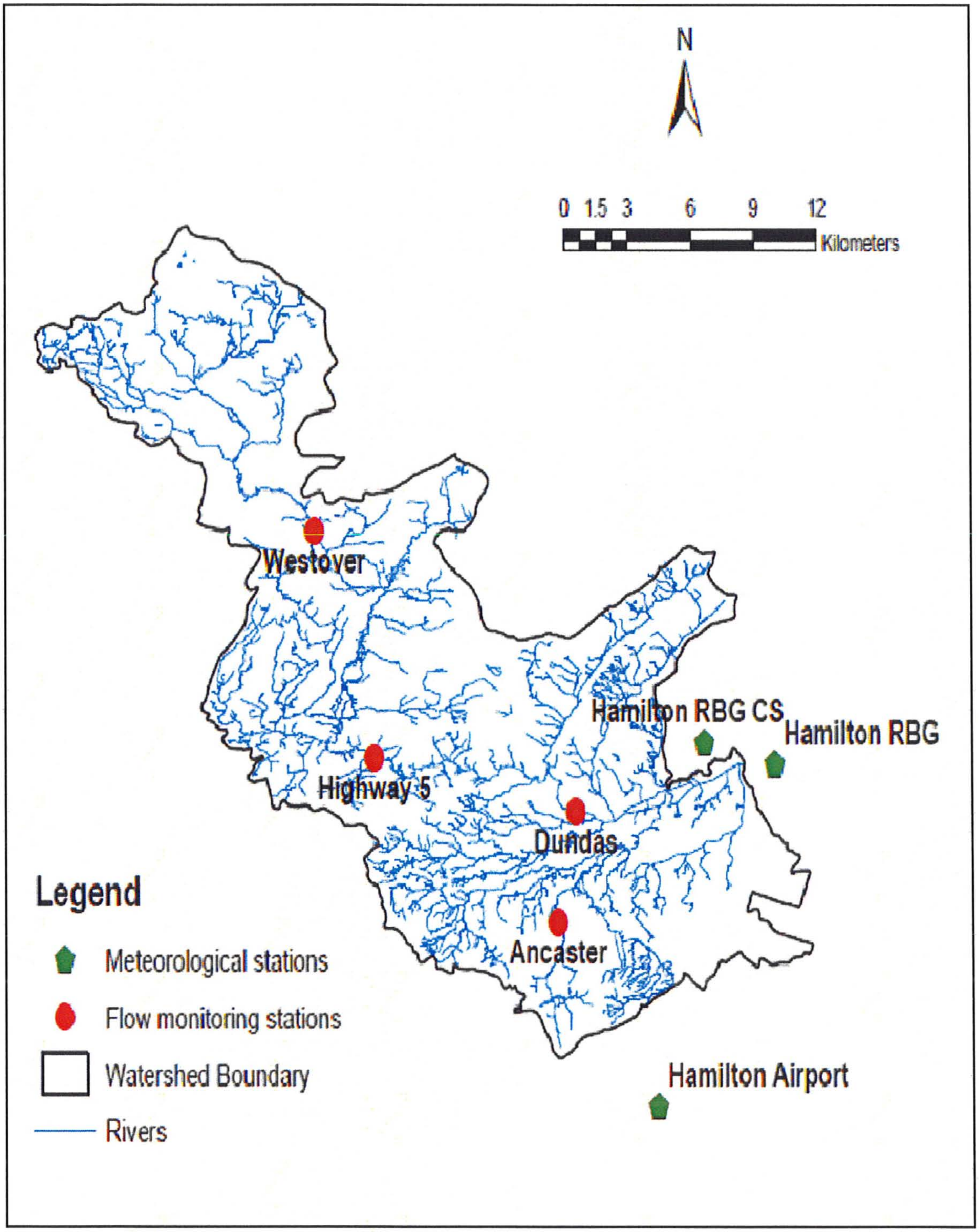

Fig 8: Meteorological and flow stations in Spencer Creek watershed

CHAPTER 3

DOWNSCALING METHODS

3.1 LITERATURE REVIEW

General Circulation Models (GCMs) can be used for reasonable representation of the global distribution of basic climate parameters. But outputs from GCMs have too coarse spatial resolution (typically of the order 50,000 km^2) to use them in local climate impact studies (Wilby et al., 2007) especially when the area has a complex topography (Schubert, 1998) or to use them for practical comprehensive planning situations, such as hydrological modeling for flood-risk analysis (Wetterhall et al., 2006). Though RCMs have higher spatial resolution, the study by Sharma (2009) showed that even for RCMs, downscaling provides better results. For any hydrological impact studies, GCM or RCM outputs should be converted to give a reliable daily precipitation and temperature time series at the scale of the watershed concerned.

As a result, various downscaling techniques have emerged that convert the large scale outputs from climate models into local meteorological variables (Coulibaly et al., 2005) and now scientists are focusing their studies to the development of new and more efficient downscaling techniques so that the outputs can be efficiently used for local climate impact studies. Basically, downscaling transfers large scale changes of atmospheric variables, reliably simulated from GCMs, to local weather series (Wetterhall et al., 2006).

Liu (2007) used three downscaling techniques in her study: statistical downscaling model (SDSM), evolutionary polynomial regression (EPR) and time-lagged-feedforward neural network (TLFN). While SDSM performed poorly in downscaling precipitation for all the seasons, TLFN and EPR gave good results for winter, spring and autumn, but poor results for summer. Again, for temperature, all the models performed better. While SDSM better captures the variability in precipitation, TLFN always underestimates the variance (Sharma, 2009). So, it is obvious that a particular downscaling technique may produce reasonably good results for a specific area under certain weather conditions and may produce very poor results for another case. Moreover, it is not clear which method to use to have reliable estimates of daily rainfall and temperature for the future (Xu, 1999). That's why different downscaling techniques should be compared to get reliable results for the study area.

3.2 DOWNSCALING TECHNIQUES

There are many downscaling methods but according to Nguyen (2005) and Wilby et al. (2007), all these fall into two broad categories:

- Dynamical Downscaling
- Statistical Downscaling

3.2.1 Dynamical Downscaling

Basically, this method uses a higher resolution Regional Climate Model (RCM) within a coarse resolution GCM (Wilby et al., 2007; Nguyen, 2005; McGregor, 1997). The RCM uses horizontal grid spacing of 20-50 km to model the physical dynamics of the atmosphere within a finite domain and the time-varying boundary conditions around this domain are defined by the GCM (Wilby et al., 2007). Because of finer horizontal resolution, RCMs represent important physical processes more accurately as compared to the GCMs. RCMs can be used efficiently to represent smaller scale atmospheric features such as orographic precipitation or low level jets and also to get an idea of the relative significance of different external forcings such as terrestrial-ecosystem or atmospheric chemistry changes (Wilby et al., 2007).

But the RCMs are expensive compared to statistical downscaling techniques because RCMs are computationally demanding as GCMs (Liu, 2007), and they also experience the similar bias problems (Hay et al., 1991; Hay & Clark, 2003; Liu, 2007). Moreover, RCMs generate scenarios that are highly dependent on the boundary conditions specified (Wilby et al., 2002) and they are inefficient particularly over complex terrain or for direct coupling to hydrologic models (Giogri & Means, 1999). Besides, they are not so flexible in the sense that if the study area is a little bit expanded or a slightly different area is chosen, then the entire experiment has to be redone, which makes RCMs really expensive (Crane and Hewitson, 1998).

3.2.2 Statistical Downscaling

According to Nguyen (2005), these methods are used to develop a relationship between local weather variables and the large scale GCM results. The statistical downscaling methods are less expensive than the dynamical ones and relatively fast.

They can be categorized into the following three groups based on the computational techniques they use:

- Synoptic weather typing;
- Stochastic weather generation;
- Regression-based or transfer function approaches.

Synoptic Weather Typing

It groups local, meteorological data related to the prevailing patterns of atmospheric circulation (Hay et al., 1991; Bardossy & Plate, 1992; Wilby et al., 2007) and is based on the sensible linkages between climate on the large scale and weather at small scale (Nguyen, 2005; Wilby et al., 2007). Re-sampling from the observed data is done to generate climate change scenarios. Though it can be used for a wide variety of environmental variables, it's a poor basis for downscaling rare events (Wilby et al., 2007). The major limitation of this method is that precipitation changes produced by changes in the weather frequency patterns may be inconsistent with those produced by the host GCM in most of the cases (Nguyen, 2005; Wilby et al., 2002; Wilby et al., 2007).

Stochastic Weather Generation

These methods, such as the weather generator model (WGEN) (Wilks, 1999), Long Ashton Research Station Weather Generator (LARS-WG) (Semenov & Burrow, 1997), modify the conventional weather generator parameters and use revised parameter sets scaled in line with the outputs from a host GCM to stochastically generate climate change scenarios (Wilby et al.,2002; Wilby et al., 2007). These techniques are widely used particularly for agricultural impact assessment because of their ability to reproduce many observed climate statistics exactly (Nguyen, 2005). But these techniques can seldom reproduce inter-annual to decadal climate variability and are not able to anticipate the effects of changes to precipitation occurrence on the secondary variables like temperature (Wilby et al., 2007).

Transfer Function Approaches

They rely on empirical relationships between local scale variables (predictands) and regional scale variables (predictors) (Nguyen, 2005; Wilby et al., 2007). There are various methods depending on the choice of mathematical transfer functions, predictor

variables or statistical fitting procedures such as linear and nonlinear regression, artificial neural networks, canonical correlation, etc. (Wilby et al., 2007). Basically, all of these follow more or less a common procedure: (i) selecting a local scale predictor, G that controls the local parameter, L; (ii) establishing a statistical relationship between L and G and using independent data to validate that relationship; (iii) after the relation is being confirmed, derivation of G from GCM experiments to estimate L (Liu, 2007).
Though these methods can be applied very easily because of their low computational demands (Nguyen, 2005), they represent only a fraction of the observed climate variability and are highly sensitive to the choice of predictor variables and statistical form. Moreover, downscaling future extreme events using these approaches are problematic as they assume that the estimated model parameters are valid under future conditions (Nguyen, 2005; Wilby et al., 2007).

3.3 STATISTICAL DOWNSCALING MODEL (SDSM)

SDSM can be described as a hybrid of stochastic weather generation and transfer function or regression based approaches (Wetterhall et al., 2007; Nguyen, 2005). This is because in SDSM, local scale weather generator parameters like precipitation occurrence and intensity are linearly conditioned using large scale circulation patterns and atmospheric moisture variables; and to better match with observations, stochastic techniques are used to inflate the variance of the downscaled daily time series artificially (Wilby et al., 2002; Liu, 2007). This model uses multiple linear regression techniques for spatial downscaling of daily predictor-predictand relationships and generates synthetic predictand (dependent variable) that represents the generated local weather (Nguyen, 2005). SDSM also allows different data transformations, such as logarithms, squares, cubes, etc.; to the predictor variables prior to model calibration to produce nonlinear regression models and data series can also be shifted forward or backward to produce lagged predictors (Coulibaly et al., 2005). Now-a-days, SDSM has been widely used for various meteorological, hydrological and environmental assessments.

In SDSM, the gridded predictors such as the mean sea level pressure have to be normalized first by their own mean and standard deviation and then should be used for model calibration; it eliminates the GCM's bias and also allows the reproduction of observed mean and standard deviation in the GCM-downscaled time series (Huth et al., 2002).

According to Wetterhall et al. (2006), SDSM models precipitation using the first order Markov chain which can be described by the following equation,

$$w_t=\alpha_0+\sum_{j=1}^{n}(\alpha j)\,(utj)$$

Here, w_t is the conditional probability of precipitation occurrence on day *t*, u_{tj} are the normalized predictors and α_j are the estimated regression coefficients. Precipitation occurs when $w_t \leq r_t$, where r_t is computer generated uniformly distributed stochastic number. As temperatures on successive days are linearly related, SDSM uses auto-regressive model for modeling temperature.

The whole procedure of modeling using SDSM is briefly described by Wilby et al., 2007 (Figure 9). In short, the model is first fit to the calibration period (usually 75% of the entire observation period) and then model performance is verified for the test period (usually 25% of the entire observation period) through a process called validation. Finally, the model is used to generate future scenarios, i.e. to estimate the predictand variables beyond the observation period.

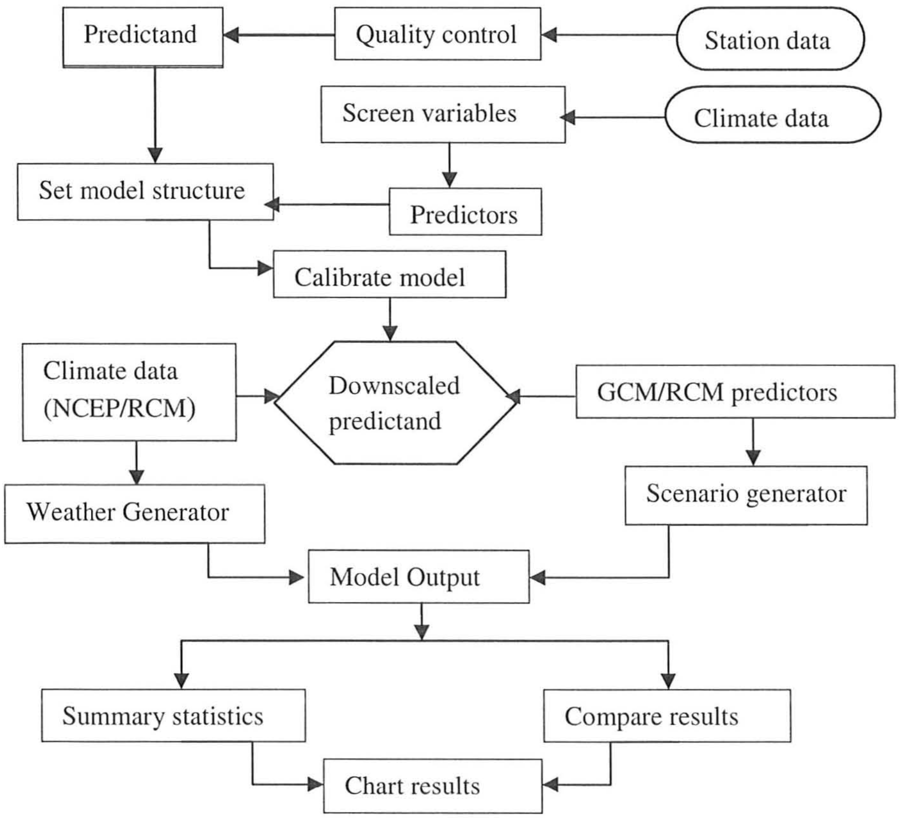

Fig 9: SDSM Version 4.2 climate scenario generation (modified after Wilby et al., 2007)

3.4 TIME-LAGGED-FEEDFORWARD NEURAL NETWORKS (TLFN)

Artificial neural networks have been efficiently used in many studies to model qualitative and quantitative water resource variables (Karunanithini et al., 1994; Smith and Eli, 1995) as they have a high potential for complex, nonlinear and time varying input-output mapping (Coulibaly et al., 2001).

ANNs are sophisticated information processing networks inspired by biological nervous systems like the brain and they employ a massive interconnection of simple computing cells, namely neurons or processing elements to perform useful computations through a learning process (Haykin, 1999). Neural networks are characterized by their architecture represented by the network topology and pattern of connection between the nodes, their method of determining the connection weights and the activation functions employed (Coulibaly et al., 2005). Neural networks can be classified based on the number of layers they possess (single-Hopfield nets, bi-layer-Carpenter/Grossberg adaptive resonance networks and multilayer perceptrons); and by the direction of flow (feed-forward or recurrent) (Sharma, 2009). Multilayer perceptrons (MLPs) contain a hierarchy of processing units organized in a series of two or more mutually exclusive sets of neurons or layers; in the network the information flow occurs in layer by layer, from the input to the output and so it is called a feed-forward network (Coulibaly et al., 2005). ANNs can approximate highly nonlinear relationships because of its unique structure and the non-linear transfer function associated with each hidden and output node; moreover ANNs allow the data to define the functional form and they are believed to be more powerful compared to the other regression-based downscaling techniques (Coulibaly et al., 2005). ANNs can account for some heavy rainfall events that are unidentifiable by the linear regression techniques (Weichert & Burger, 1998); moreover an ensemble ANN downscaling model can predict changes in streamflows by using only large scale atmospheric conditions (Cannon & Whitfield, 2002). In almost 90% hydrology studies, the conventional feedforward neural network, which is actually the standard multilayer perceptron (MLP) trained with the back-propagation algorithm, have been used successfully (Coulibaly et al., 2001).

TLFN is a type of neural network in which the neurons in the input layer of an MLP are replaced with a memory structure, namely a *tap delay* line and so it is particularly suitable when lagged predictor variables are to be included in the downscaling (Coulibaly et al., 2005). The size of the *tap delay* depends on the number of past samples needed to describe the input characteristics and it must be determined on a case-by-case basis; the major assumption in using TLFN is that the present large-scale atmospheric states as well as the past states condition the local weather (Coulibaly et al., 2005). Delay-line processing elements (PEs) are used in TLFN that implement memory by delay as shown in the figure 10. In a feed-forward network, there can be several hidden layers, each layer having one or more nodes and the information passes from the input to the output side (Coulibaly et al., 2005).The output, y of such a network with one hidden layer is given by the following equation,

$$y(n)=\Phi 1\left(\sum_{j=1}^{m} w_j y_j(n)+bo\right)$$

$$=\Phi 1\left\{\sum_{j=1}^{m} w_j \Phi 2\left[\sum_{l=0}^{k} w_{jl}\, x(n-l)+b_j\right]+bo\right\}$$

where 'm' is the size of the hidden layer, 'n' is the time step, w_j is the weight vector for the connection between the hidden and output layers, w_{jl} is the weight matrix for the connection between the input and hidden layers; Φ1 and Φ2 are transfer functions at the output and hidden layers respectively, and b_j, bo are additional network parameters or biases to be determined during training (Coulibaly et al., 2005).

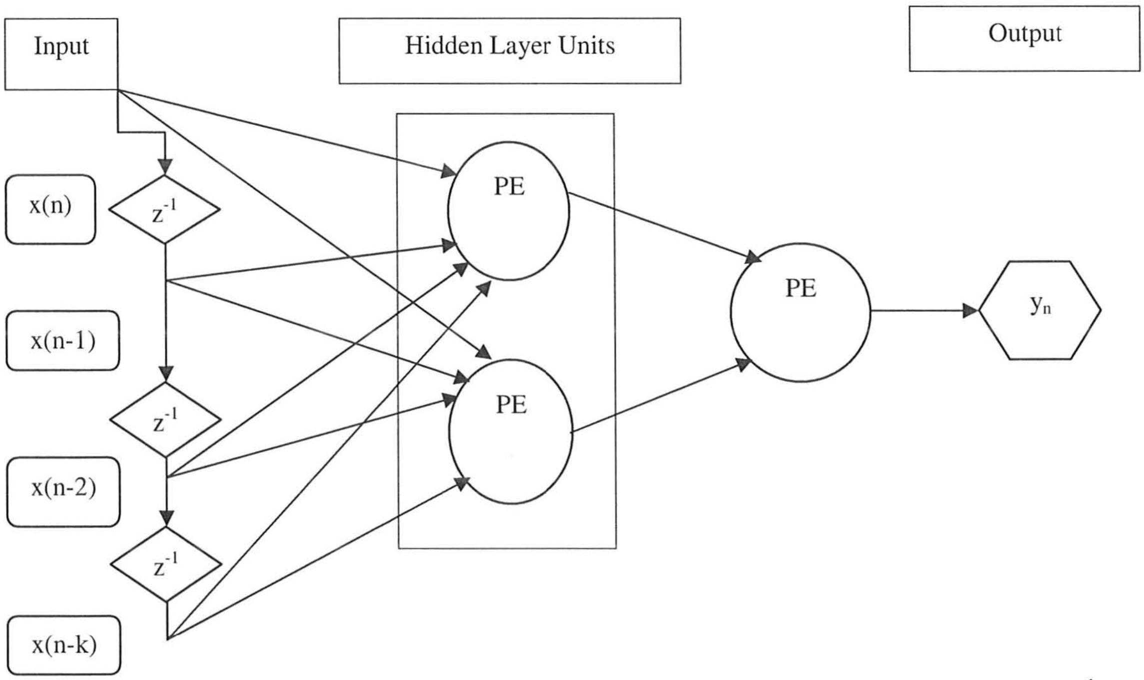

Fig 10: TLFN with one input, one hidden layer, and a tap delay line with k+1 taps [z^{-1} is an operator that delays the input by one sample] (modified after Coulibaly et al., 2005)

MLPs often provide suboptimal solutions and do not perform temporal pre-processing because the vector space input encoding provides the model no hint of the temporal relationship of the inputs (Giles at al., 1997). But time-lagged feed-forward neural networks (TLFN) have temporal processing capabilities without restoring to complex and costly training methods (Coulibaly et al., 2005). However, while using any type of ANNs, the users must have a good understanding of network architecture and transformations present within the network; otherwise there is an increased risk of errors associated with the structure of potentially complex networks (Coulibaly et al., 2005).

CHAPTER 4

MIKE SHE AND MIKE 11

4.1 MIKE SHE MODEL OVERVIEW

MIKE SHE is a deterministic, fully distributed and physically based hydrologic modeling system based on the SHE ("Systeme Hydrologique Europeen") model (Abbott et al., 1986; Refsgaard and Storm, 1995). It was developed to model water movement including overland flow, rivers and lakes, saturated and unsaturated flow and evapotranspiration and other main physical processes of the hydrological cycle (Refsgaard, 1997). The modular structure of its water movement module consists of the following six process-oriented components (Figure 11) that describe the major physical processes in the land phase of the hydrological cycle (Thompson et al., 2004):

a) Interception/Evapotranspiration;
b) Overland/Channel flow;
c) Unsaturated zone;
d) Saturated zone;
e) Snow melt; and
f) The exchange between aquifers and rivers.

To represent the spatial variability in parameters such as elevation, soil hydraulic properties, precipitation and potential evapotranspiration, the catchment is horizontally discretized into an orthogonal network of grid squares and within each grid square, a number of horizontal layers with variable depths are used to describe the vertical variations in soil and hydrogeological characteristics; between the grid squares, the lateral flow is either overland flow or subsurface saturated zone flow (Thompson et al., 2004). MIKE SHE model is most frequently used to simulate streamflow at different locations in the rivers and groundwater levels for different points and also the transport of solutes (Christiaens and Feyen, 2001). MIKE SHE has been successfully applied for irrigation planning and management (Jayatilaka et al., 1998; Singh et al., 1999), flood forecasting (Jasper et al., 2002), characterization of soil hydraulic properties (Romano and Palladino, 2002; Christiaens and Feyen, 2001), groundwater contamination assessment (Refsgaard et al., 1999), and analyzing surface and groundwater hydrology (Feyen et al., 2000; Andersen et al., 2001; Johnson et al., 2003; Refsgaard, 1997). A short description of the water movement module components is provided in the following sections. For detailed explanation, readers are referred to other sources such as DHI, 2007.

4.1.1 Overland Flow

Overland flow usually occurs after a precipitation event. When the net precipitation exceeds the infiltration capacity of the soil, then the rest of the water is available for surface runoff. The route and the amount of surface runoff is largely affected by the topography of the catchment concerned, the flow resistance as well as the evaporation and infiltration losses along the flow path.

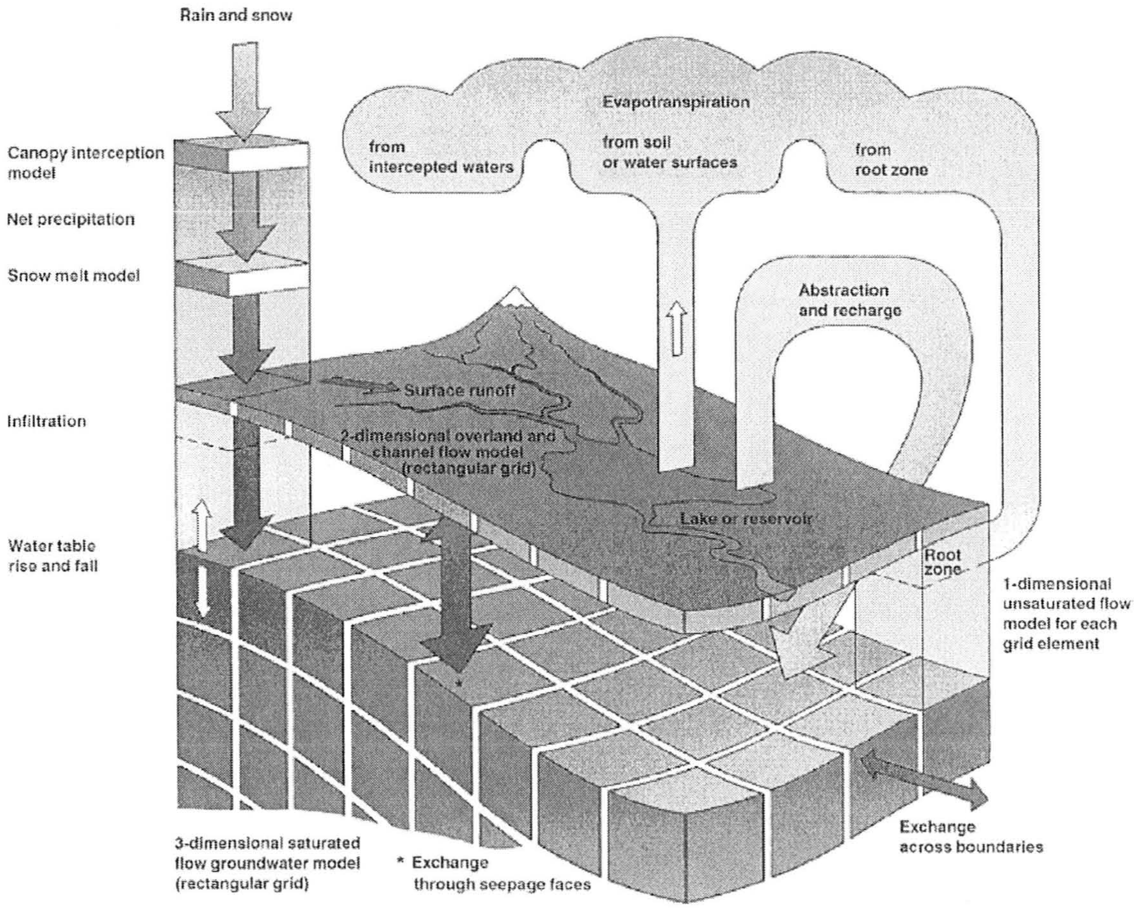

Fig 11: Schematic representation of MIKE SHE model (Refsgaard and Storm, 1995)

MIKE SHE uses diffusive wave approximation of the Saint Venant equations and finite difference formulation to calculate the surface runoff (DHI, 2007). The whole process is shortly described below (DHI, 2007).

Diffusive wave approximation

The two-dimensional Saint Venant equations are:

$$\frac{\partial h}{\partial t}+\frac{\partial}{\partial x}(uh)+\frac{\partial}{\partial y}(vh)=i$$

$$S_{fx}=S_{Ox}-\frac{\partial h}{\partial x}-\frac{u\partial u}{g\partial x}-\frac{1}{g}\frac{\partial u}{\partial t}-\frac{qu}{gh}$$

$$S_{fy}=S_{Oy}-\frac{\partial h}{\partial y}-\frac{v\partial v}{g\partial y}-\frac{1}{g}\frac{\partial v}{\partial t}-\frac{qv}{gh}$$

where Z_g (x,y) is the ground surface level, h(x,y) is the flow depth above the ground surface, u(x,y) and v(x,y) are the flow velocities in x- and y-directions respectively, i(x,y) is the net rainfall less infiltration, S_O is the slope of the ground surface and S_f is the friction slope. The solution of these equations gives a fully dynamic description of two-dimensional free surface flow (DHI, 2007).

The following assumptions are made to simplify the Saint Venant equations (DHI, 2007):

- Momentum losses due to local and convective acceleration and lateral inflows perpendicular to the flow direction are ignored which is known as diffusive wave approximation;

- Friction slope is assumed equal to the ground surface slope (S_f=S_o) which is known as kinematic wave approximation.

Then using the Strickler/Manning-type law for each friction slope, the Saint Venant equations get the following form:

$$S_{fx}=\frac{u^2}{h^{4/3}K_x^2} \qquad uh=Kx\left(-\frac{\partial z}{\partial x}\right)^{1/2}h^{5/3}$$

$$S_{fy}=\frac{v^2}{h^{4/3}K_y^2} \qquad vh=Ky\left(-\frac{\partial z}{\partial y}\right)^{1/2}h^{5/3}$$

where K_x and K_y are Strickler coefficients which are equivalent to Manning's M, uh and vh are the discharge per unit area in the x- and y-directions respectively (DHI, 2007).

Finite Difference Formulation

To further simplify the Saint Venant equations, let us consider the overland flow in a small region of a MIKE SHE model (Figure 12a) with side lengths Δx and Δy and a water depth h(t) at time t. Now using a finite difference approach, the final estimate for the flow, Q between two grid squares (Figure 12b) is,

$$Q=\frac{K\Delta x}{\Delta x^{1/2}}(Z_U-Z_D)^{1/2}h_u^{5/3}$$

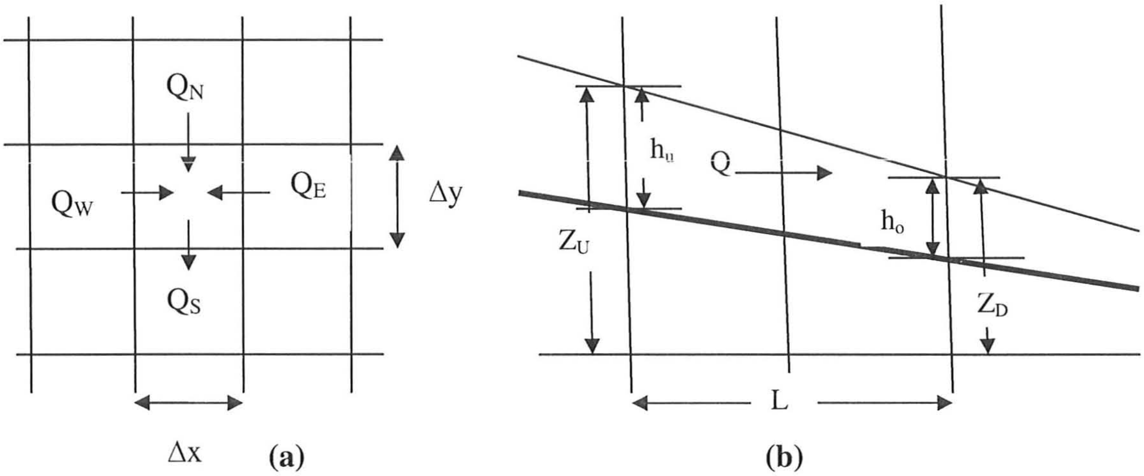

Fig 12: (**a**) Square Grid System in a small Region of a MIKE SHE model; (**b**) Overland flow across grid square boundary (modified after DHI, 2007)

where Z_U and Z_D are the higher and lower water levels for the two grid cells considered, h_U and h_D are corresponding water depths, K is the appropriate Strickler coefficient and h_u is the water depth that can freely flow into the next cell (DHI, 2007).

4.1.2 Channel Flow

The channel flow usually indicates the water flow in the rivers, canals, i.e. various surface water bodies. In present studies, MIKE SHE is coupled with MIKE 11 to provide a better idea of the interaction between groundwater flow and surface runoff (DHI, 2007) and this coupling also enables

- the one dimensional river flow and water level simulation by the fully dynamic Saint Venant equations;
- the simulation of hydraulic control structures like weirs, gates and culverts;
- area-inundation modeling that uses a simple flood-mapping procedure based on simulated river water levels and a digital terrain model; and
- the full, dynamic coupling of surface and sub-surface flow processes in MIKE SHE and MIKE 11.

A more detailed explanation of various terms and processes related to channel flow is provided by DHI (2007).

4.1.3 Evapotranspiration (ET)

Evapotranspiration usually refers to the total water vapour released from the earth's surface through both evaporation and transpiration. Various meteorological and vegetative data are required to predict the total ET and net rainfall due to

- interception of rainfall by the canopy;
- drainage from the canopy to the soil surface;
- evaporation from the canopy surface;
- evaporation from the soil surface; and
- uptake of water by plant roots and its transpiration, based on soil moisture in the unsaturated root zone.

MIKE SHE splits up the ET processes and models them in the following order (DHI, 2007):

1) part of water evaporates from the rainfall intercepted by the vegetation canopy;
2) the remaining water that reaches the soil surface either percolates to the unsaturated zone or produce surface runoff;
3) a portion of the infiltrating water evaporates from the upper part of the root zone or transpires by the plant roots; and
4) the remaining water infiltrates to the groundwater table in the saturated zone.

MIKE SHE usually applies the Kristensen and Jensen model to estimate evapotranspiration, but in the present study a simple two-layer UZ/ET model is also included that divides the unsaturated zone into a root zone from which ET can occur, and a zone below the root zone, where ET doesn't occur; it provides an estimate of the actual ET and the amount of water that recharges the saturated zone (DHI, 2007).

4.1.4 Unsaturated Zone

The unsaturated flow in this case is the flow of water between the surface and the aquifer that lies below. The most important factor in this regard is the vertical soil profile as both retention and conductivity versus water content vary with the soil type that affects this flow. Based on the assumption that subsurface flow is negligible compared to vertical flow, water flow in this zone is considered to be one-dimensional (Christiaens and Feyen, 2001). MIKE SHE can apply the following three options to calculate the vertical flow in the unsaturated zone (DHI, 2007):

1) the full Richards equation for which a tabular or functional relationship is required for both the moisture-retention curve and the effective conductivity;
2) a simplified gravity flow module that assumes a uniform vertical gradient and ignores capillary forces; and
3) a simple two layer water balance method for shallow water tables.

In present study, the simple two layer water balance method is used that gives the actual Evapotranspiration and the groundwater recharge. This method is good enough for wetland areas with a shallow groundwater table where the actual ET rate is close to the potential rate. But for areas with deeper and drier unsaturated zones, this module is not suitable. It also assumes some average conditions and doesn't consider the relation between the unsaturated hydraulic conductivity and soil moisture content; so for a detailed study of the unsaturated zone this method is not the first choice. It is used in the present study as it requires less computational time compared to other two processes and also in this case the main concern is the surface runoff, not the groundwater flow.

4.1.5 Saturated Zone

This feature of MIKE SHE is used to predict the subsurface flow in the catchment. MIKE SHE has the option for shifting conditions between unconfined and confined conditions for the fully three-dimensional flow in a heterogeneous aquifer. It uses the non-linear Boussinesq equation and solves it numerically by an iterative implicit finite difference technique to represent the spatial and temporal variability of the dependent variables like hydraulic head.

MIKE SHE uses two groundwater modules: (a) the SOR groundwater module based on a successive over-relaxation solution technique; and (b) the PCG groundwater module based on a pre-conditioned conjugate gradient solution technique. In MIKE SHE, the saturated zone component interacts with the other components of the module mainly through the boundary flows from other components implicitly or explicitly as sources and sinks.

A detailed description of all these processes is provided by DHI (2007).

4.2 MIKE 11 MODEL OVERVIEW

MIKE 11 is a river modeling system developed by the Danish Hydraulic Institute (DHI) to simulate channel flow, analyze water quality and sediment transport in surface water bodies such as rivers, estuaries, etc. (DHI, 2005). It's based on the complete dynamic wave formulation of the Saint Venant equations (Thompson et al., 2004; Liu et al., 2007) that can represent hydraulic structures like weirs, gates, bridges, etc. commonly found within wetlands (Thompson et al., 2004) and can be used efficiently for detailed analysis, design, management and operation of simple as well as complex river and channel systems (DHI, 2005).

MIKE 11 has an integrated modular structure with various add-on modules such as the hydrodynamic (HD) module, advection-dispersion module, sediment transport module and so on. Among these, the HD module is the basis for most modules and can be applied to flood forecasting, simulation of flood control measures, channel system design, tidal and storm surge studies in rivers and estuaries, etc. (DHI,2005).

The HD module in MIKE 11 has the following major components (Larson, 2005; DHI, 2005):

(a) ***River Network***: To have a clear idea of the water behaviour, it is important to set the river network very carefully as it affects the interaction between MIKE SHE and MIKE 11 model.
(b) ***River Cross-sections:*** The Mike 11 model cannot predict river flows or floods without cross-section data as it helps the model to predict water levels in different rivers.
(c) ***Boundary data:*** The boundary data specifies the initial flow into the river network if only a segment of a catchment is being modeled and also provides the outlet boundary conditions.
(d) ***Hydrodynamic parameters:*** The hydrodynamic parameter file contains various input possibilities, but the only section that is typically used is the initial conditions of the water levels at various points in the river network (Larson, 2005).

For detailed description of these components, readers are referred to DHI (2005).

4.3 COUPLING OF MIKE SHE AND MIKE 11

MIKE SHE and MIKE 11 models are coupled whenever a reliable representation of the dynamic interaction between surface water and groundwater is concerned (Figure 13) as MIKE SHE can't do that alone efficiently, particularly for a smaller stream width compared to the grid size in MIKE SHE. Moreover only MIKE 11 hydrodynamic (HD) module can express the hydrodynamics for a complex branch-system-bearing loop and flood unit (Liu et al., 2007).

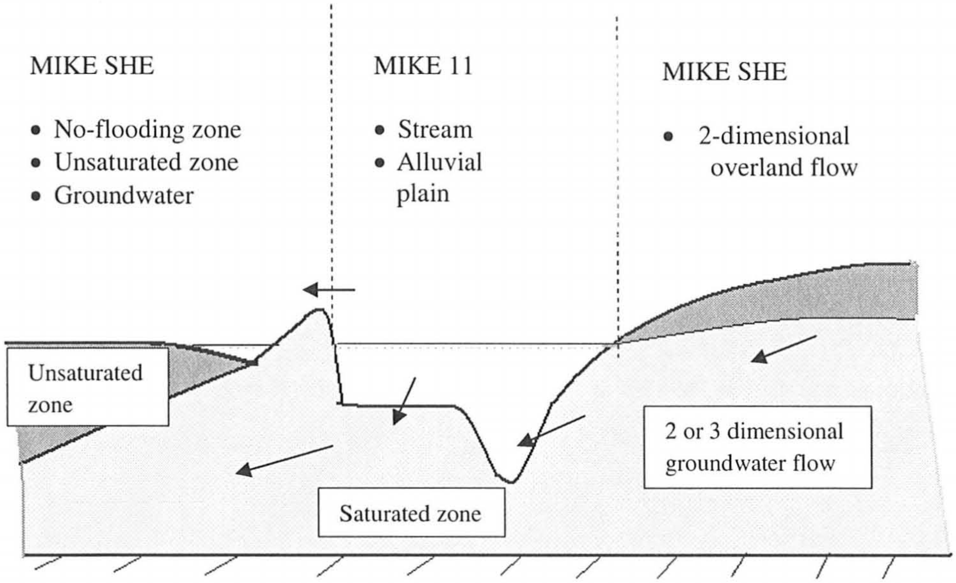

Fig 13: Coupling structure of MIKE SHE and MIKE 11 (modified after Liu et al., 2007)

MIKE SHE and MIKE 11 are dynamically coupled through river links that are line segments between adjacent MIKE SHE grid squares (Figure 14). The river link locations depend on the co-ordinates of the MIKE 11 river points that define the model branches. River links are established only for the coupled reaches specified in the hydraulic model and MIKE SHE only exchanges water with those reaches. During simulation, water levels at MIKE 11 H-points (points for which water levels are calculated; Figure 14) within the coupled reaches are transferred to adjacent MIKE SHE river links. Then MIKE SHE calculates the overland flow to each river link from adjacent grid squares and also the river-aquifer exchange that are later used as lateral inflows or outflows to the corresponding MIKE 11 H-points for the next computational time step (DHI, 2007).

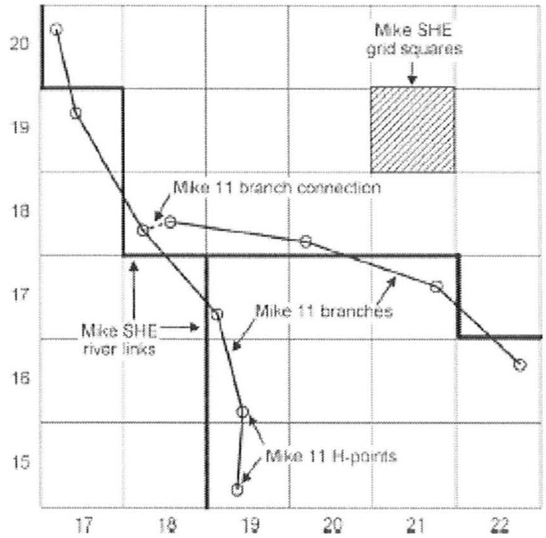

Fig 14: MIKE 11 branches and H-points for corresponding river links in a MIKE SHE model grid (DHI, 2007)

The coupled model also simulates the inundation from MIKE 11 river model into MIKE SHE grid squares using a simple flood mapping procedure that compares the topography of potentially flooded grid squares (identified automatically or specified manually) in MIKE SHE to the water level at MIKE 11 H-points. A grid square is flooded when its topographic level is lower than corresponding MIKE 11 H-point water level and in that case level of water in the flooded grid square is equal to the H-point water level. As soon as a grid square is flooded, MIKE SHE calculates the infiltration/seepage, overland flow and evapotranspiration in the same way as for a grid square ponded with surface water due to precipitation and surface runoff or the water table intercepting the ground surface (Thompson et al., 2004).

4.4 MIKE SHE AND MIKE 11 MODEL APPLICATIONS IN HYDROLOGY

MIKE SHE is used successfully in many hydrologic studies to predict stream flows, groundwater levels, soil moisture and so on. As it is a distributed model, it can be used to model various hydrologic processes at different locations of the study area, while the conceptual models can be used just for flow at the catchment outlet. Some of the earlier studies in groundwater and surface water hydrology using MIKE SHE and MIKE 11 are summarized in table 4.

Table 4: MIKE SHE and MIKE 11 studies in hydrology

AUTHOR	STUDY AREA	OBJECTIVE	MAJOR FINDINGS
Xevi et al., 1997	Neuenkirchen catchment, Braunschweig, Germany (research catchment: 1 km^2).	Prediction of stream flow at the catchment outlet with a MIKE SHE model.	MIKE SHE model is very sensitive to heterogeneities in soil and aquifer properties and so a detailed sensitivity analysis should be performed even for a small catchment to identify the proper calibration parameters. Nash-Sutcliffe coefficient for streamflows was around 0.2-0.7.
Jayatilaka et al., 1998	Tragowel plains, Australia (salt-affected irrigation bay: 9 ha/ around 1km^2).	Use of MIKE SHE model to quantify the processes affecting surface drainage and groundwater levels.	MIKE SHE can give an insight of effective flow processes in flood irrigated areas; it can't represent variations in rapid flow through macropores due to soil cracking and swelling. Correlation coefficient (R^2) for groundwater level was 0.8-0.9.
Feyen et al., 2000	GETE catchment (Grote Gete and Klein Gete sub-basins), Brussels, Belgium (600 km^2).	Modeling stream flow and groundwater levels with a MIKE SHE model.	MIKE SHE provides considerably worse results for stream flow or water table at internal stations of the catchment, not used in the calibration of the model as compared to the stations used in the calibration. Nash-Sutcliffe coefficient for streamflows was around 0.65-0.75.
Andersen et al., 2001	Senegal river basin, Sahel region, West Africa (375,000 km^2).	MIKE SHE model construction with conventional data; its parameterization, calibration and validation; and identifying the model limitations.	Reliable discharge data is required for calibration to obtain good model performance; multi-site calibration provides better results than one-site calibration. For multi-site calibrated model, Nash-Sutcliffe coefficient for streamflows was 0.85-0.95.
Thompson et al., 2004	Elmley Marshes, UK (lowland wet grasslands: 8.7 km^2).	Use of a coupled MIKE SHE/MIKE 11 model to predict flood flow and year-round high water table in the lowland wet grassland.	MIKE SHE can represent the seasonal dynamics of groundwater and ditchwater levels for a wetland. It has the potential for climate change impact study. Nash-Sutcliffe coefficient for groundwater level was around 0.4-0.9.
McMichael et al., 2006	Jameson catchment, California, USA (semi-arid shrublands: 34 km^2).	Stream flow prediction for a range of rainfall and fire conditions with MIKE SHE.	The model simulated moderate and low flow conditions well; but couldn't predict it accurately for large storms and extensive fires. Nash-Sutcliffe coefficient for streamflows was 0.7-0.9.
Sahoo et al., 2006	Manoa-Palolo watershed, Oahu, USA (Hawaii streams, flashy area: 3-25 km^2).	Application of MIKE SHE model to predict streamflow and determine the sensitivity of different model parameters on streamflow prediction.	Manning's roughness and hydraulic conductivity affected the shape of the hydrographs. By using spatially distributed hydraulic conductivity values, better results can be achieved. Correlation coefficients for streamflows were 0.5-0.7.
Shalini, 2006	Canagagigue Creek, South-western Ontario, Canada (143 km^2).	Modeling surface runoff and assessing hydrologic impact of different land use practices with MIKE SHE.	MIKE SHE can be used to assess impacts of alternative management practices (land use) and for climate change impact study. Nash-Sutcliffe coefficient for surface runoff was around 0.4-0.6.
Liu et al., 2007	Yingsu subwatershed, Tarim Basin, China (arid area: 92 km^2).	Simulation of overland flow and groundwater levels using a coupled MIKE SHE/MIKE 11 model.	Groundwater level increases along the direction of stream flow. Nash-Sutcliffe coefficient for simulated groundwater levels was 0.8-0.9.

Xevi et al. (1997) used the MIKE SHE model to simulate stream flows in Neuenkirchen catchment for two years and calibrated the model for parameters such as grid size and time step, Strickler coefficient for overland and channel flow, saturated zone horizontal hydraulic conductivity, unsaturated zone vertical saturated hydraulic conductivity, drainage coefficient and specific storage and vegetation characteristics. A denser grid size increased the peak overland and peak drain discharge. The vertical saturated hydraulic conductivity affected the overland flow by limiting the infiltration rate; while high values of horizontal saturated hydraulic conductivity increased the base flows. The model showed a higher sensitivity to Strickler coefficient particularly at lower values. Vegetation characteristics had a direct influence on the unsaturated zone variables like water uptake and moisture content. The Nash-Sutcliffe efficiency coefficient, R^2 for simulated streamflows was 0.65 for calibration, but only 0.17 for validation; it might have happened because of not accounting for the dynamic near-surface processes. This study highlights the benefit of performing sensitivity analysis followed by calibration of a physically distributed model like MIKE SHE.

Jayatilaka et al. (1998) applied the MIKE SHE model to represent the flow processes within the irrigation bay in the Tragowel plains and calibrated the model (by adjusting hydraulic conductivity values) against observed piezometric levels, drain flow and soil moisture data for 19 months to represent different flow conditions under seasonal changes. Model simulations were generally consistent with the observed data for piezometric levels and drain flow; but not for the soil moisture levels. The model provided a well representation of the conceptual processes in the irrigation site. Because of the constant bypass fraction used in the model, it was unable to simulate time-varying bypass flow through desiccation cracks. Apart from that, this study demonstrated the effects of flow processes in flood irrigated areas with shallow water table conditions and their role in transporting salt to waterways.

Feyen et al. (2000) developed a MIKE SHE model for daily discharge and water table simulations for two years; calibrated it for horizontal and vertical saturated hydraulic conductivity and specific yield and finally validated the model with a simple split-sample test. Higher vertical conductivity results in lower and flatter peaks due to an increased vertical flow to the deeper soil zones; while horizontal conductivity mainly affects the base flow. The model was validated with simple split sample test and later was applied to two internal flow stations and six wells, not used in model calibration. The simulated stream flows were in good agreement with the observed ones (Nash-Sutcliffe efficiency coefficient, R^2=0.65-0.75); but the results for water table differed a lot among different wells, with acceptable results for some wells and worse results for the others, may be due to scale effects and poor quality data in certain areas of the catchment. The validation results for the internal stations were not as well as those for the stations used in calibration which indicates the model's incapability of simulating internal state variables. The authors pointed to the fact that reliable representation of spatial variability of hydrological characteristics with a physically distributed model like MIKE SHE requires a vast amount of continuous and reliable distributed data.

Andersen et al. (2001) developed three MIKE SHE models to simulate daily discharge for 11 years in the Senegal River basin to examine the effects of calibration and to enable internal model validation tests. The first model was an uncalibrated model based on estimates from field data, literature and previous studies; the second one was a one-site calibrated model obtained by calibrating the first model against one flow station and the third one was a multi-site calibrated model obtained by calibrating the second model against all the 9 flow stations. The uncalibrated model results were poor for all the stations except for the most-downstream one as the deviations in discharge from different subcatchments balanced each other due to aggregation in larger catchment areas. The one-site calibrated model gave better results for all the stations compared to the uncalibrated one, while the multi-site calibrated model gave the best results.

Thompson et al.(2004) developed a coupled MIKE SHE/MIKE 11 model for the lowland wet grasslands of the Elmley Marshes in UK to represent the observed hydrological conditions for a 36 month period and calibrated the model for the MIKE SHE calibration parameters like Manning's roughness coefficient for overland flow, bypass flow ratio, soil moisture threshold, hydraulic conductivity of the saturated zone and drainage time constant; while the MIKE 11 calibration parameters used are Manning's coefficient for the channels and bed leakage coefficient within the MIKE SHE coupling. The model simulated groundwater depths with a Nash-Sutcliffe coefficient, R^2 of 0.4-0.8 for calibration and 0.5-0.95 for validation; and ditch water levels with a R^2 value of 0.8-0.95 for calibration and 0.7-0.9 for validation. Both of them showed rapid gains in levels during autumn and early winter and a gradual decline during spring and summer; while in winter and early spring the water table was at or close to the ground surface and ditch water levels exceeded the elevation of the control structures that caused the water to be discharged from the marshes. These results provided an idea of the highly seasonal nature of flooding due to high groundwater level and inundation from the ditches within the study area. The model could be later applied for climate change impact study for the marshes. This study demonstrated the need for high quality reliable data for a sufficient period of time for efficient use of the coupled MIKE SHE/MIKE 11 model for any study area.

McMichael et al. (2006) modeled streamflow with MIKE SHE for 32 years under variable climatic and wildfire conditions; and used Generalized Likelihood Uncertainty Estimation (GLUE) methodology for uncertainty estimation in the application of this model. The model was calibrated for vegetation characteristics, soil hydraulic conductivities and saturated zone components. The simulated streamflows were consistent with the observed ones with a Nash-Sutcliffe coefficient of 0.7-0.9 and the level of flow prediction error was less than 10%. One of the important limitations of this study is that the authors used Linear Reservoir Groundwater module instead of 3D groundwater module due to lack of data, which doesn't allow interactions between saturated and unsaturated zones and so may not adequately represent subsurface flow dynamics under all conditions. Moreover the model cannot represent time varying soil properties; while fire events in the study area often alter the soil physical properties. These may be the main reasons behind the model's poor performance in case of large storms and extensive wildfire. Otherwise, the model performed well in streamflow prediction, particularly for moderate and low flow conditions.

Sahoo et al. (2006) focused their study to the Manoa-Palolo watershed consisting of Waihi and Waiakeakua subwatersheds in Manoa Valley, the Palolo and Waimao subwatersheds in Palolo Valley, and the ridges separating the two valleys. The authors developed a MIKE SHE model for this area with a 15-min time step for 3 years, performing a detailed calibration and validation first for Waiakeakua subwatershed, with bypass flow constant, Manning's number, M for overland flow, vegetation parameters, drainage depth, horizontal and vertical saturated hydraulic conductivity as the calibration parameters; and later applied the information to the whole watershed. The model simulated streamflows at 15 min interval with correlation coefficients of 0.5-0.7 and it predicted the trend of measured hydrograph even though there was no measured streamflow in some parts. MIKE SHE underestimated peak flows during heavy storm events and base flows in the absence of rainfall events for a long period of time. This study was the first attempt to evaluate the performance of a physically distributed model like MIKE SHE for a tropical mountainous watershed and it illustrated a systematic procedure for calibration and validation of this model for such an area.

Shalini (2006) developed a MIKE SHE model for Canagagigue Creek watershed in South-western Ontario, Canada to simulate surface runoff and to assess the changes in surface runoff for different land use practices and climate change. The model was calibrated by adjusting the snow melt parameters and Manning's M to simulate surface runoff for 9 years. The simulated runoff was consistent with the observed ones with a Nash Sutcliffe coefficient of 0.59 for calibration and 0.40 for validation. On a daily basis, the model provided reasonable representation of other hydrologic components (evapotranspiration and base flow). The author recommended the use of a more comprehensive method for snowmelt simulation and the incorporation of frozen soil conditions. Different land use scenarios are incorporated in the model to assess the changes in surface runoff. Deforestation had the greatest impact, while urbanization had negligible impact on runoff. For climate change impact study, instead of using downscaled scenario results from climate models, the author shifted the observed precipitation data one month forward keeping the temperature data same as the observed ones. This climate change study predicted more surface runoff for wet years and less runoff for normal and dry years. Though the traditional method of climate change impact study was not applied, this study revealed the potentials of MIKE SHE model in hydrological impact assessment for alternative management scenarios and climate change in Southern Ontario.

Liu et al. (2007) applied the coupled MIKE SHE/MIKE 11 model to simulate dynamic changes in groundwater within the study area for both flood and dry seasons. They developed the model to represent the observed groundwater conditions for a period of 120 days and evaluated the sensitivity of the model to parameters like vertical and horizontal saturated hydraulic conductivity, Manning's roughness coefficient for overland flow and the empirical parameters in Kristensen-Jensen model used to calculate the actual evapotranspiration. The simulated daily groundwater depths were in close agreement with the observed ones with a Nash-Sutcliffe coefficient, R^2 value of 0.8-0.9 both for calibration and validation and for the testing period about 75% of the observed water table values fell within the 5% and 95% uncertainty bounds based on regression of simulated versus observed values. The model was also used to simulate overland flow and groundwater distribution for the whole period. The results from these study demonstrated that a coupled model might be successfully applied in such an arid area even with data for a very short period.

CHAPTER 5
METHODOLOGY

5.1 STATISTICAL DOWNSCALING MODEL (SDSM)

The key idea of downscaling with SDSM is to develop a multiple linear regression model between some selected large scale predictors and local scale predictands like temperature and precipitation. In this study, the parameters of the regression equation are estimated using *ordinary least squares* algorithm. Large scale predictors (Table 1A & 2A) for a particular perdictand are selected through correlation and partial correlation analysis and scatter plots. In modeling precipitation, the process is considered as *conditional* in which local precipitation amounts are correlated with wet-days occurrence (days with precipitation amount of 0.3 mm or more) (Khan, 2007). A *fourth root* transformation is applied to the original precipitation series to convert the skewed daily precipitation data to a normal distribution so that it can be used in regression analysis. *Unconditional* process is used to downscale temperature that assumes a direct link between the predictors and the predictand. Daily temperature data are usually normally distributed and so the original series is used directly in the model. For both precipitation and temperature, *monthly* models are developed in which different regression equations are developed for each month. This is done to obtain the best fit model. The models for daily precipitation and daily maximum and minimum temperatures are separately calibrated using twenty years' data (1961-1980) and validated with ten years' data (1981-1990). In SDSM, the calibration process usually adjusts the mean and variance of the downscaled data by bias correction and variance inflation factor to better represent the observed data. Bias correction compensates the tendency to over- or under-estimate the mean of the downscaled data and variance inflation adjusts the variance by changing the amount of *white noise* applied to the regression model to better accord with observations. The *stochastic* component of SDSM develops multiple ensembles of downscaled variables for each regression model (Khan, 2007). In this study, twenty ensembles of the downscaled precipitation and temperature are generated, but only the first ensemble is used for uncertainty analysis. The downscaled data for the validation period (1981-1990) is used for uncertainty analysis at 95% confidence level. Wilcoxon rank sum method (Conover, 1980; Lehmann, 1975) and Levene's test (Levene, 1960) are used to test the difference of the means and variances of the observed and the downscaled predictand, respectively. The final model setups for SDSM are detailed in Table 5.

Table 5: SDSM model setups for downscaling precipitation and temperature

PRECDICTAND	PREDICTORS	MODEL TRANSFORMATION	CONDITIONAL SELECTION	STEPWISE REGRESSION	VARIANCE INFLATION	BIAS CORRECTION
Daily precipitation at Hamilton Airport	**NCEP:** pmsl, p_u, p_v, p850, s500, s850 **RCM:** hfs, phi850, pcp, pmsl, sq, stmn, stmx, su, sv	Fourth root	Stochastic	AIC criteria	13 15	1 0.9
Daily precipitation at Hamilton RBG	**NCEP:** p_u, p_v, temp, s500, s850 **RCM:** hfs, phi850, pcp, pmsl, sq, stmn, stmx, su, sv	Fourth root	Stochastic	AIC criteria	12 15	1 0.9
Daily maximum temperature at Hamilton Airport	**NCEP:** p_u, p5_u,p8_v, p850,sphu,temp **RCM:** hfs, pcp, pmsl, stmx, su, sv, swmx	None	Stochastic	AIC criteria	12 12	1 1
Daily minimum temperature at Hamilton Airport	**NCEP:** p_u, p5_u,p8_v, p850,sphu,temp **RCM:** hfs, sq,stmn,stmx, st, su, sv	None	Stochastic	AIC criteria	12 13	1 1
Daily maximum temperature at Hamilton RBG	**NCEP:** p_u, p5_u,p8_v, p850,sphu,temp **RCM:** hfs, phi500,rhum1000,sq,stmx,st, su, sv	None	Stochastic	AIC criteria	12 12	1 1.2
Daily minimum temperature at Hamilton RBG	**NCEP:** p_u, p5_u,p8_v, p850,sphu,temp **RCM:** hfs, sq,stmn,stmx, st, su, sv	None	Stochastic	AIC criteria	12 13	1 1

** Predictors are described in table 1A and 2A

5.2 TIME-LAGGED-FEEDFORWARD NEURAL NETWORKS (TLFN)

TLFN is a non-linear regression type model that establishes a relationship between some selected large scale predictors (Table 1A & 2A) and the local scale predictands like temperature or precipitation. The calibration and the validation periods are the same as those in SDSM. First a sensitivity analysis is performed to select the most relevant predictors for a particular predictand by training the network with all the available predictors as inputs. The basic idea of this analysis is to shift the inputs of the neural networks slightly and monitor the corresponding change in the output (Khan, 2007). The most sensitive or relevant predictors are selected by calculating the sensitivity of each input which is the standard deviation of the output divided by that of the input which was varied to create the output (Khan, 2007). The neural network is then trained with the selected predictors independently for precipitation, maximum and minimum temperature until acceptable validation performance is achieved. Unlike SDSM, precipitation is downscaled in TLFN as an 'unconditional' process by establishing a direct link between the predictors and precipitation; and TLFN simulates only one time series of the downscaled variables. The final model setups for TLFN are detailed in Table 6.

5.3 MIKE SHE AND MIKE 11 MODELS

5.3.1 MIKE SHE model setup

The MIKE SHE model in this study represented an area of approximately 291 km^2 and is constructed with 50×50 m^2 grid squares. Though finer resolution gives better results, it also increases the computational time and there is also a limitation in the number of model calculation cells; so all the distributed files in this study are based on 50 meter cell size. The whole area is divided into 18 sub-watersheds and used in the model as the 'Subcatchment' file. The 50 meter DEM file provided by HCA is converted to a grid file and later used in the model to represent the topographic features of the study area.

Three types of meteorological data are used in the model: precipitation, temperature, potential evapotranspiration. The watershed is divided into two parts, the upper part covered by Hamilton RBG and the lower part by Hamilton Airport; and time-series files are used for the daily total precipitation. As hourly temperature data are not available from these stations, daily maximum (at 3 PM) and minimum (at 3AM) temperatures are used in this study as time-series files. Kristensen and Jensen (1975) model is used to calculate actual evapotranspiration from the potential evapotranspiration calculated by the Blaney-Criddle method (Tollner, 2002; Brouwer & Heibloem, 1986). The snow melt is also simulated in this study and the snow melt parameters are calibrated.

Table 6: TLFN model setups for downscaling precipitation and temperature

PRECDICTAND	PREDICTORS	MEMORY TYPE	TRANSFER FUNCTION	LEARNING RULE	PROCESSING ELEMENT	MAXIMUM EPOCHS
Daily precipitation at Hamilton Airport	**NCEP:** p_u, p_v, p8_v, p500,s850, Temp	TDNNAxon	Linear TanhAxon	Delta Bar Delta	8	2852
	RCM:hsf,pcp,phi850,pmsl,sq,stmn, stmx,su,sv,swmx	LanguarreAxon	TanhAxon	Delta Bar Delta	4	2999
Daily precipitation at Hamilton RBG	**NCEP:** p_u, p_v, p8_v, s850, temp	TDNNAxon	Linear TanhAxon	Delta Bar Delta	10	2998
	RCM:hsf,pcp,phi850,pmsl,sq,stmn, stmx,su,sv,swmx	TDNNAxon	TanhAxon	Delta Bar Delta	4	3000
Daily maximum temperature at Hamilton Airport	**NCEP:** p8_u, p_u, p8_v, p500,p850,s850,sphu,temp	TDNNAxon	TanhAxon	Delta Bar Delta	12	2000
	RCM:hsf,phi500,rhum1000,sq,stmx ,su,sv,st	GammaAxon	TanhAxon	Delta Bar Delta	4	1308
Daily minimum temperature at Hamilton Airport	**NCEP:** p8_u, p_u, p500,s850,temp	TDNNAxon	TanhAxon	Delta Bar Delta	8	3000
	RCM:hsf, sq,stmn,stmx,su,sv,st	GammaAxon	TanhAxon	Delta Bar Delta	4	1550
Daily maximum temperature at Hamilton RBG	**NCEP:** p8_u, p_u, p_v, p500,p850,temp	TDNNAxon	TanhAxon	Delta Bar Delta	9	3000
	RCM:hsf,phi500,rhum1000,sq,stmx ,su,sv,st	GammaAxon	TanhAxon	Delta Bar Delta	4	977
Daily minimum temperature at Hamilton RBG	**NCEP:** p8_u, p_u, p500,s850,temp	TDNNAxon	TanhAxon	Delta Bar Delta	8	3000
	RCM:hsf, sq,stmn,stmx,su,sv,st	GammaAxon	TanhAxon	Delta Bar Delta	4	1990

** Predictors are described in table 1A and 2A

The land use distribution map represented in Chapter 2 is converted into a grid file and used in the *land use* component of the model. The properties of each of the six vegetation types are specified by the vegetation property file provided by the Danish Hydraulic Institute (DHI).

In this study, the Finite Difference method is used to simulate the overland flow, which needs three inputs: the overland flow Manning's M (inverse of Manning's n), detention storage and initial water depth. The Manning's M value for six types of vegetations are obtained from literature and calibrated a little bit. A distributed grid file for Manning's M is used in the study. The initial water depth is assumed to be 0. Detention storage, which represents the amount of water retained in the surface depressions, is kept uniform and calibrated based on the values from literature.

The two layer water balance method is used to represent the unsaturated zone flow component as it requires less computational time and the main concern of this study is the surface runoff, not the groundwater flow. To represent the 2-layer UZ soil properties, the soil distribution map with 5 types of soil (figure 4) is used. The hydraulic conductivities of each type of soils are calibrated. The groundwater table used as the lower boundary of the unsaturated zone comprises of 8 wells' data discussed in Chapter 2.

The semi-distributed Linear Reservoir groundwater module, with one interflow reservoir and two base flow reservoirs, is used to represent the saturated zone flow component.

5.3.2 MIKE 11 model setup

The river channels in the study area are represented with a hydrodynamic MIKE 11 model. A simplified river network with 18 river channels is delineated from the river network image file provided by HCA. A uniform Manning's roughness coefficient, M is applied throughout the river network and is calibrated later. Valens dam is added as a regulating structure to the network including 18 culverts.

174 cross sections' data are provided by HCA, located at the starting and end of the branches, at the channels where there are significant elevation changes in the river bed, and also the immediate upstream and downstream of the hydraulic structures. Some cross-sections are added by interpolation and some are added based on the 1 m DEM file provided by HCA. The raw point elevation data from the 1 m DEM file is directly used to define the shape of the cross-sections.

Boundary conditions provided boundary data at every end of the branches. The boundary is set as 'Closed' at the upstream end of all the branches and 'Open' at the final outlet where a constant water level of 82.5 meter is specified. The daily flow data of Valens reservoirs specified in the network is added into the boundary file. Some of the water level and discharge data particularly at the flow stations are used as the initial conditions in MIKE 11.

Finally, the MIKE SHE and MIKE 11 models are coupled with all the branches in MIKE 11 river model specified as coupled reaches so that they can exchange water with adjacent MIKE SHE grid squares.

5.3.3 Model calibration and validation

MIKE SHE and MIKE 11 models should be calibrated simultaneously as modifications to a calibration parameter in one model can influence results in the other (Thompson et al., 2004). In this study, the coupled model is calibrated manually against the observed daily flows at the four stations: Westover, Highway5, Dundas and Ancaster.

The first 12 years' data (1989-2000) are used for calibration and the remaining 8 years' data (2001-2008) are used for validation. The model is calibrated in two steps: first for peak flow and then for base flow. Peak flows are calibrated by adjusting the snow melt parameters, detention storage and Manning's M for both overland and channel flow. The saturated soil hydraulic conductivities in the unsaturated zone are calibrated to adjust the base flow.

Higher value of Manning's M increases the total amount of water flowing as the surface runoff and results in a higher peak. Detention storage indicates the water retained in the surface depressions during runoff and is lowered in this study to allow more water to flow over the surface.

In the 'Snow melt' component of the model, the melting temperature is set at 0^{o}C and the simulation period of the model is set from September, 1989 so that the initial snow storage can be set as 0. The degree day coefficient indicates how much snow will melt for unit increase in temperature above the melting temperature. If the snow storage exceeds the 'minimum snow storage', then the extra snow will melt. 'Maximum wet snow fraction' indicates the amount of melting water retained in the snow before release. All these parameters are adjusted to calibrate the peak flows.

The saturated hydraulic conductivities of the unsaturated zone soils affect the infiltration capacity of the soils, which in turn affects the base flow. Lower hydraulic conductivities result in higher surface runoff and vice-versa.

The final values of the calibration parameters are listed in table 7.

Table 7: Final calibration parameter values of the coupled flow model

MODEL	PARAMETER	CALIBRATED VALUE
MIKE SHE	Manning's M for overland flow:	
	Built Up	67
	Crops	25
	Forest	7
	Open water	29
	Marsh	33
	Bare fields	40
	Detention storage (mm)	2
	Snow melt parameters:	
	Degree day coefficient (mm/oC/day)	5
	Minimum snow storage (mm)	5.5
	Maximum wet snow fraction	0.04
	Saturated hydraulic conductivities (m/s):	
	Gravel	1.52E-06
	Sand	2.51E-07
	Silt	3.00E-09
	Topsoil	2.51E-08
	Limestone	3.00E-07
MIKE 11	Manning's M for channel flow	32

All initial conditions of the validation period are specified as the conditions at the end of the calibration period and the final calibration parameter values are used to simulate the validation period flows. The Nash-Sutcliffe efficiency coefficient, R^2 (Nash & Sutcliffe, 1970) is evaluated for both calibration and validation period flow results for each of the stations and this is considered as the main performance criteria for the model.

CHAPTER 6

RESULTS AND DISCUSSIONS

6.1 DOWNSCALING RESULTS

6.1.1 Current period results

Daily precipitation, maximum and minimum temperatures for 30 years (1961-1990) are downscaled for Hamilton Airport and Hamilton RBG. The results are assessed using residuals plots (difference between the simulated and observed monthly means); bias statistics tables, statistical tests (Wilcoxon's rank sum and Levene's tests) and standard model performance statistics (mean absolute error, root mean square error, relative error, correlation coefficient). For each station, downscaling is done using two climate models (CGCM3.1/T63 and CRCM 4.2) with two downscaling techniques: SDSM and TLFN. Bias statistics tables (table 1B-6B) and statistical test results (table 9-10 and table 7B-10B) for the two stations are explained in the following sections.

From the bias plots for downscaled precipitation (figures 15-18 and 1B-4B in Appendix B) for both the stations, it appears that downscaled RCM provides better results compared to the raw RCM as the former provides lower residuals for both mean and variance of daily precipitation. Therefore there is clear benefit of downscaling the RCM simulations. For both the stations, regardless of the climate model, mean daily precipitation is overestimated in the fall. RCM overestimated mean daily precipitation in the spring and underestimated the same in summer while downscaled with SDSM; but it overestimated precipitation in winter while downscaled with TLFN. In terms of variability, TLFN largely underestimated the variance for both the stations for the two climate models, with the largest residuals in the summer months particularly in August. SDSM better captured the variability, but is consistent with TLFN in the regard that SDSM also underestimated the variability in summer. From table 8, it is observed that downscaled GCM always provided a lower root mean square error (RMSE) and mean absolute error (MAE) compared to the downscaled RCM. TLFN provided larger bias values for mean daily precipitation as it is unable to properly account for the days without precipitation. The relative error (RE) values for both the stations indicated an over estimation (except for TLFN with GCM for Hamilton RBG) of mean annual cumulative precipitation regardless of the downscaling technique and climate models.

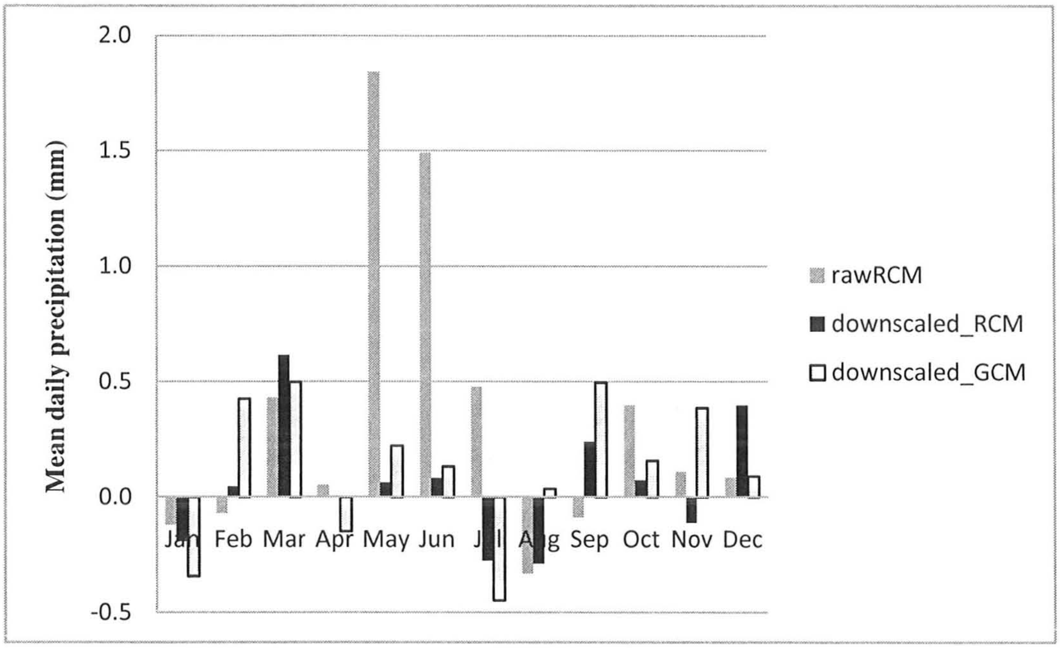

Fig 15: Residual plot for SDSM downscaled precipitation at Hamilton Airport: comparing monthly mean

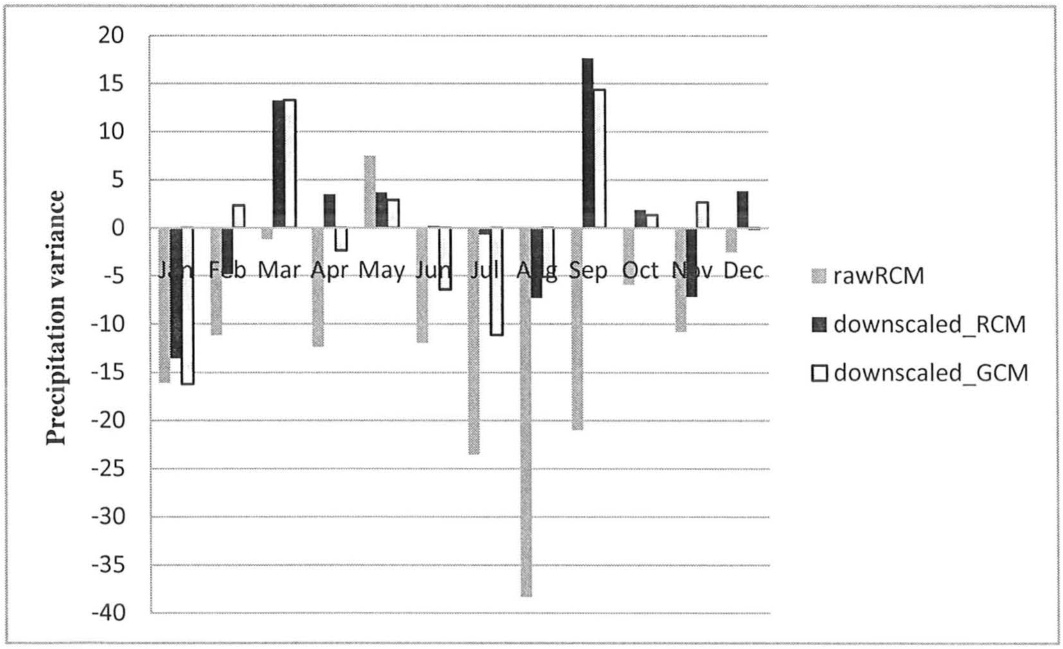

Fig 16: Residual plot for SDSM downscaled precipitation at Hamilton Airport: comparing monthly variability

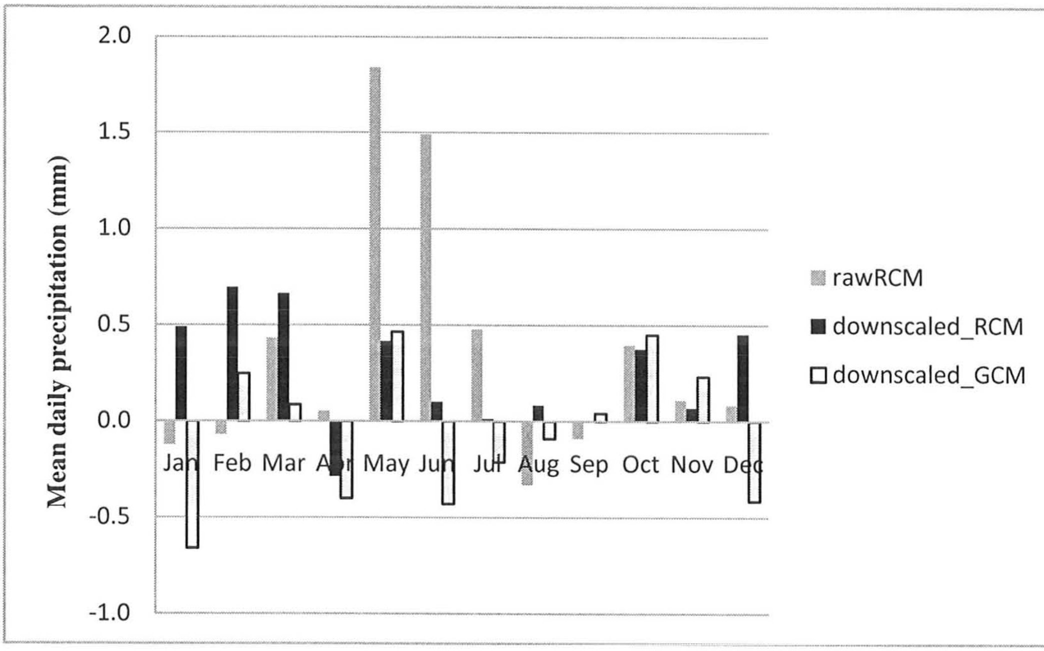

Fig 17: Residual plot for TLFN downscaled precipitation at Hamilton Airport: comparing monthly mean

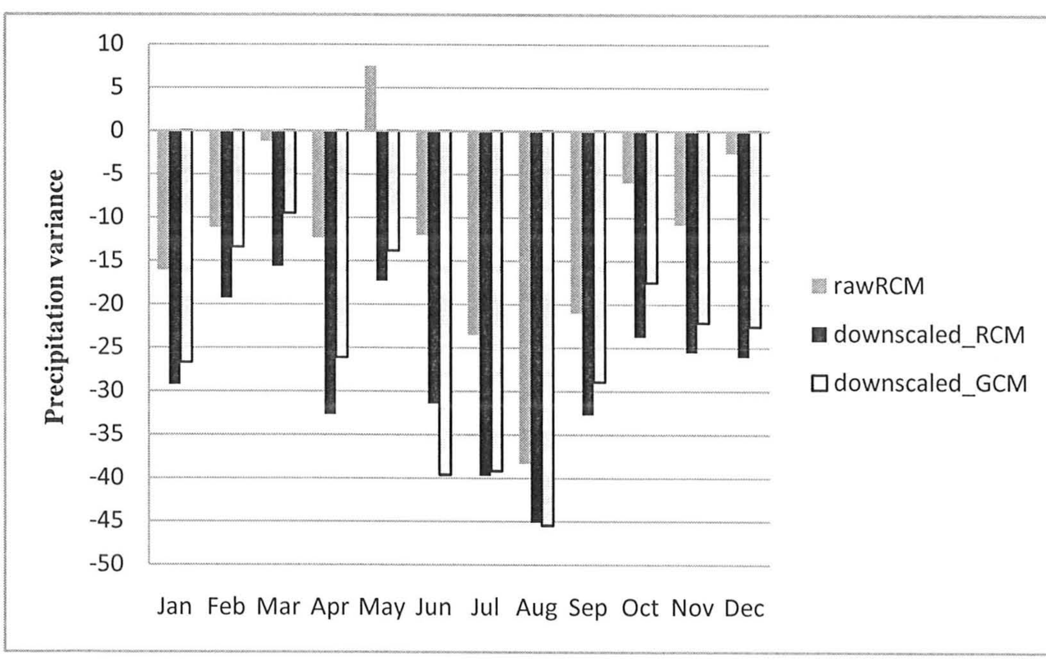

Fig 18: Residual plot for TLFN downscaled precipitation at Hamilton Airport: comparing monthly variability

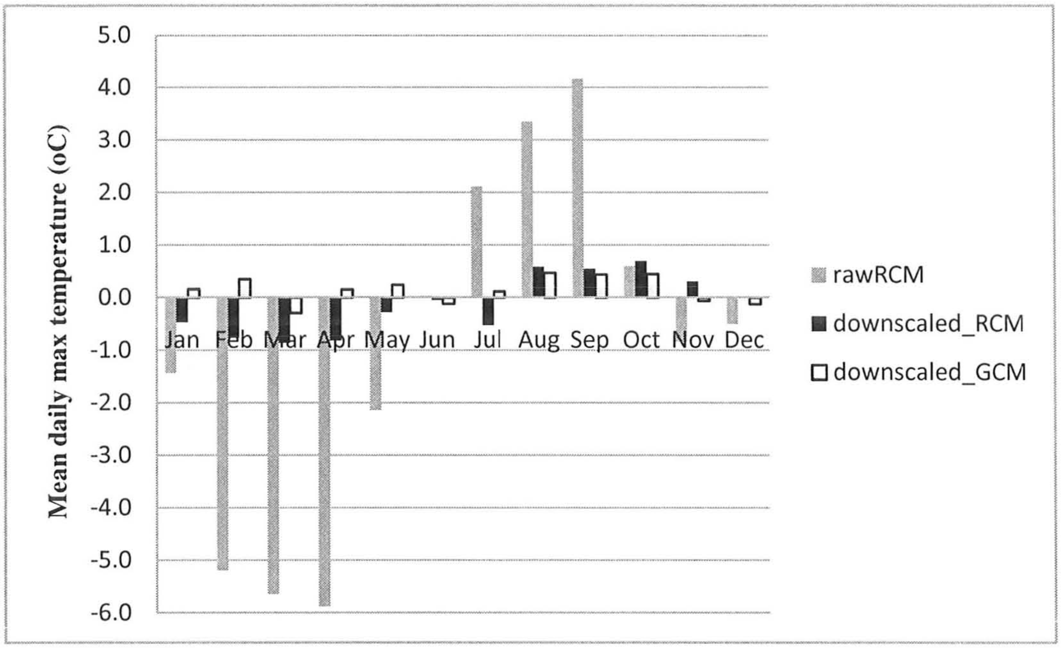

Fig 19: Residual plot for SDSM downscaled maximum temperature at Hamilton Airport: comparing monthly mean

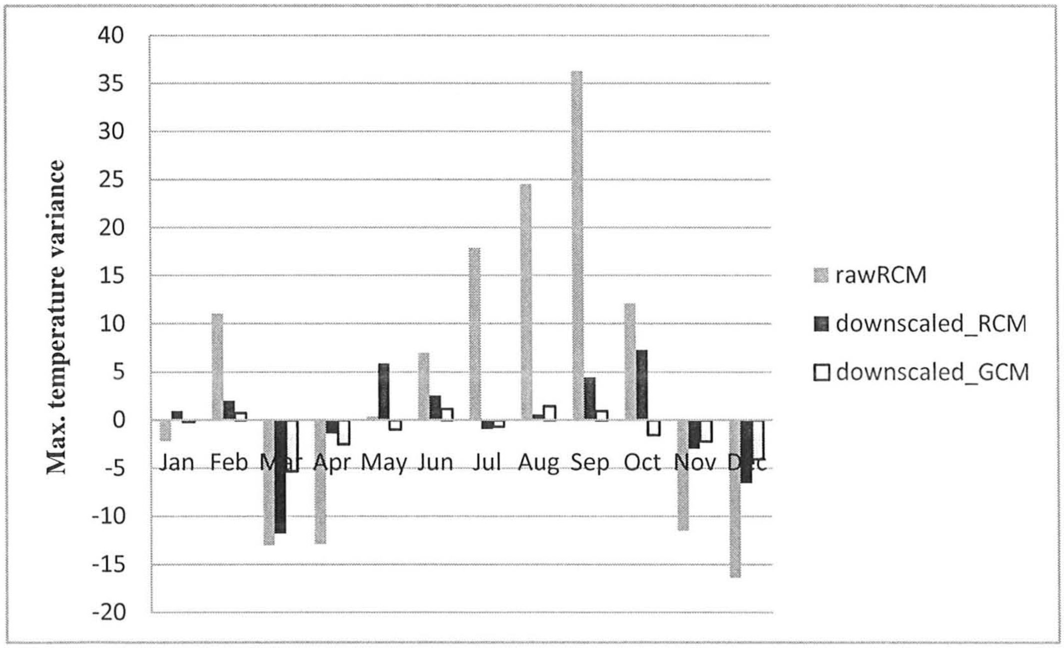

Fig 20: Residual plot for SDSM downscaled maximum temperature at Hamilton Airport: comparing monthly variability

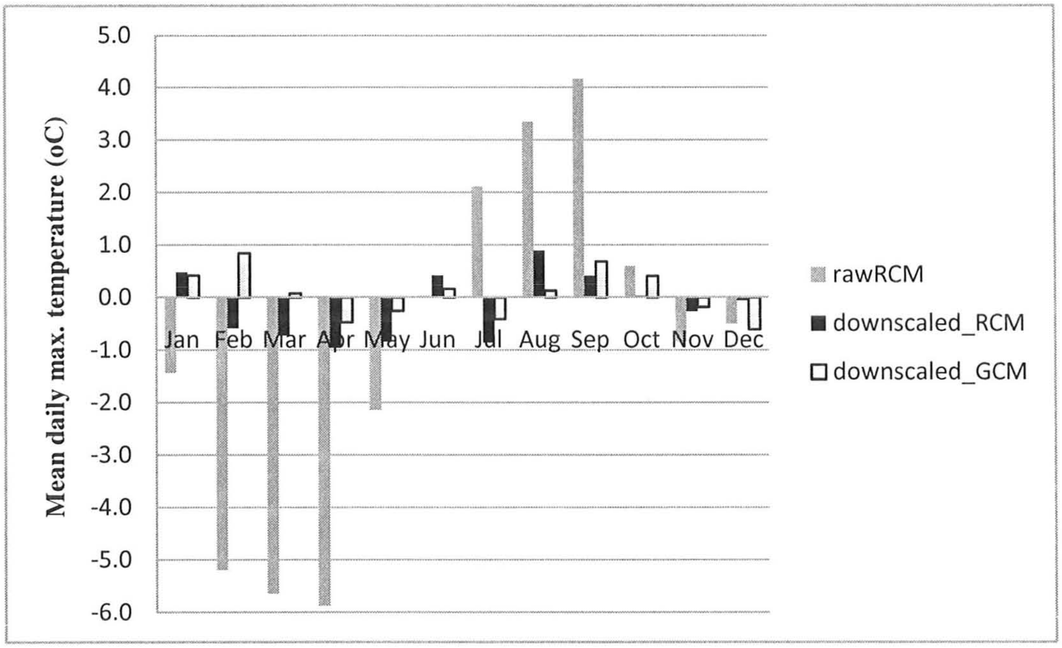

Fig 21: Residual plot for TLFN downscaled maximum temperature at Hamilton Airport: comparing monthly mean

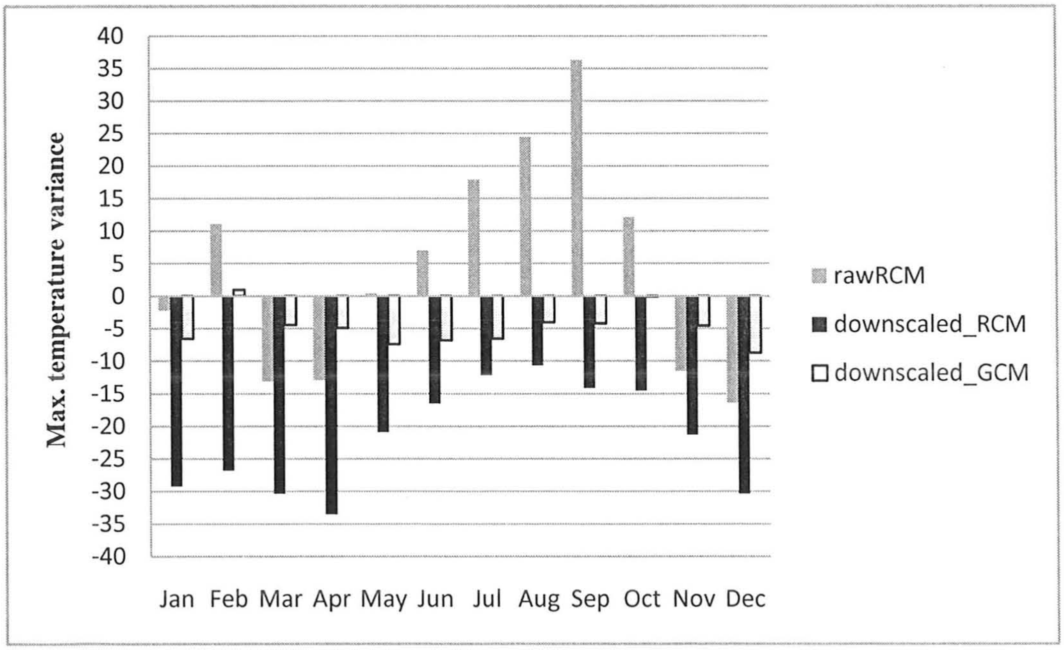

Fig 22: Residual plot for TLFN downscaled maximum temperature at Hamilton Airport: comparing monthly variability

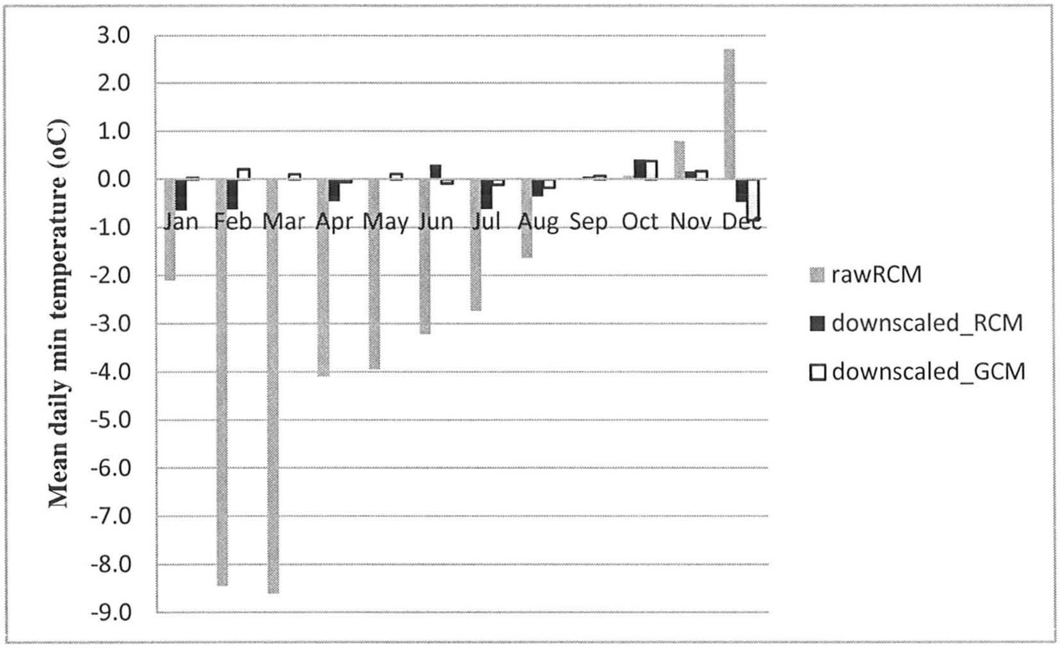

Fig 23: Residual plot for SDSM downscaled minimum temperature at Hamilton Airport: comparing monthly mean

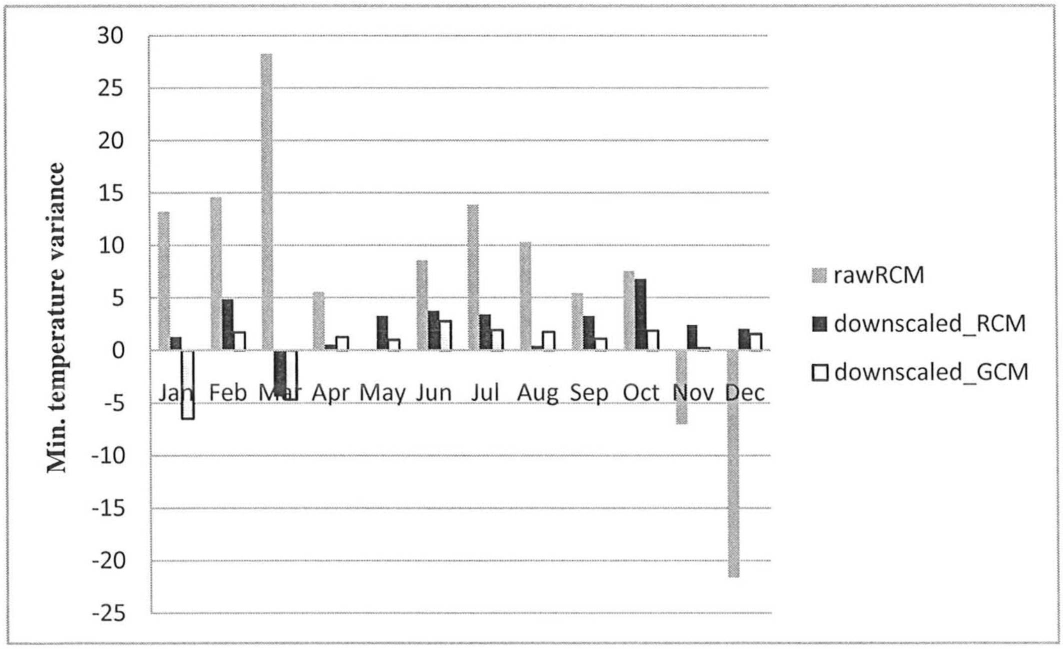

Fig 24: Residual plot for SDSM downscaled minimum temperature at Hamilton Airport: comparing monthly variability

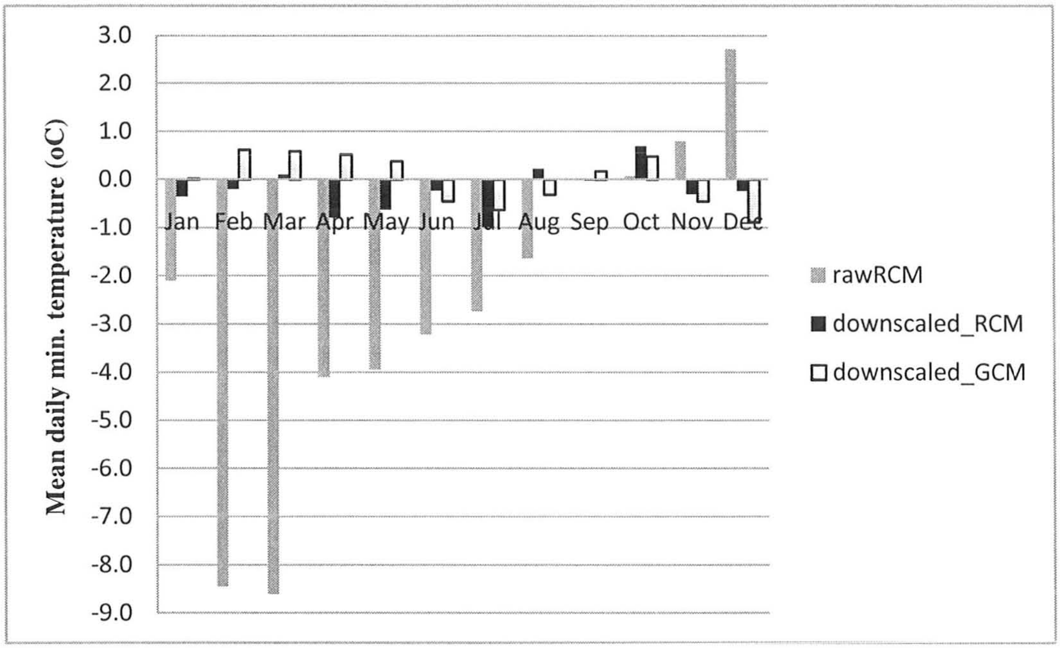

Fig 25: Residual plot for TLFN downscaled minimum temperature at Hamilton Airport: comparing monthly mean

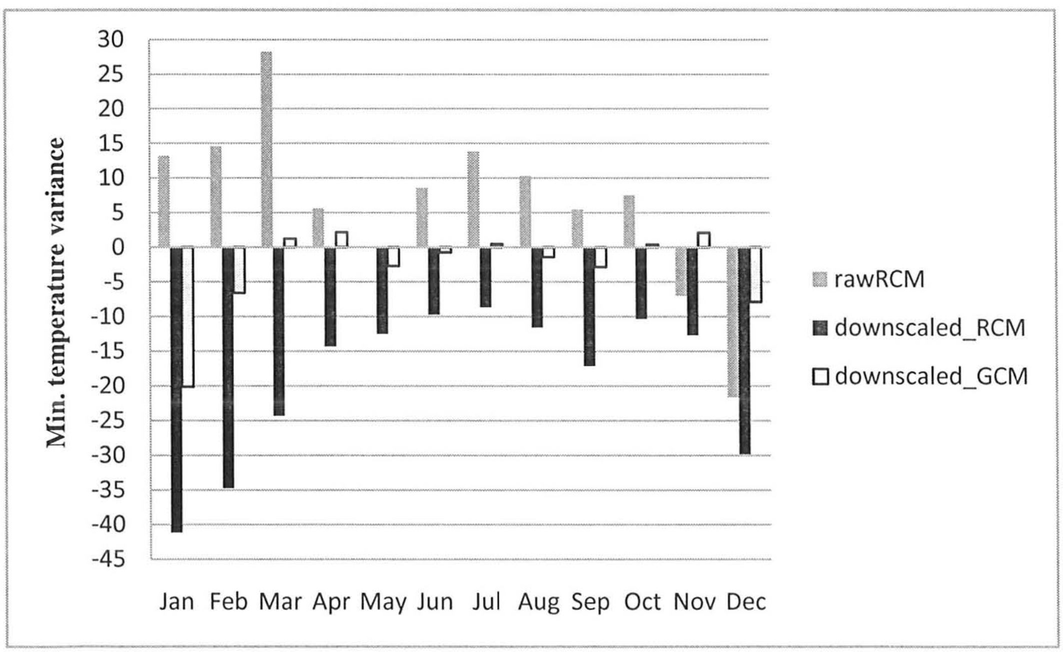

Fig 26: Residual plot for TLFN downscaled minimum temperature at Hamilton Airport: comparing monthly variability

The residual plots for downscaled maximum temperature for both the stations are provided in figures 19-22 and 5B-8B in Appendix B. From the figures, it can be observed that downscaling RCM outputs provides significantly more accurate results compared to the raw RCM data. The mean daily maximum temperatures are very close to the observed ones particularly for the spring and summer months. Downscaled GCM results appear to better capture the variability in maximum temperature than the downscaled RCM results. For both the climate models, SDSM and TLFN effectively captured the mean maximum temperature. While TLFN slightly overestimated the mean temperature in the fall, SDSM showed no clear trend. In terms of variability, SDSM overestimated the variance for some months and underestimated for others, but the results are consistent for both GCM and RCM. TLFN underestimated the variance for both the climate models, but downscaled GCM captured the variability better than the downscaled RCM. TLFN largely underestimated the variance with RCM with the largest bias values in the winter and early spring months. From table 8, it can be seen that GCM provided a lower root mean square error (RMSE) and mean absolute error (MAE) compared to RCM for both the stations regardless of the downscaling techniques. Compared to SDSM, TLFN gave lower RMSE values for both GCM and RCM; and lower MAE values for RCM, slightly higher MAE values for GCM. Moreover, TLFN also provided higher correlation (r) than SDSM for both the climate models. So, it appears that TLFN is a better downscaling technique for maximum temperature. The RE values indicate that both the downscaling techniques estimated the annual mean maximum temperature accurately.

The residual plots for downscaled minimum temperature for both the stations are provided in figures 23-26 and 9B-12B in Appendix B. The figures show it clearly that downscaled RCM significantly improved the results compared to the raw RCM, as the mean daily minimum temperatures are very close to the observed ones particularly for the spring and summer months. Downscaled GCM provided better results than downscaled RCM especially in terms of variability. For both the climate models, SDSM and TLFN effectively captured the mean minimum temperature. Both RCM and GCM models overestimated the mean minimum temperature in the fall and underestimated in the summer regardless of the downscaling technique. In terms of variability, SDSM overestimated the variance for some months and underestimated for others, but the results are consistent for both GCM and RCM. TLFN underestimated the variance for both the climate models, but downscaled GCM captured the variability better than the downscaled RCM. TLFN largely underestimated the variance with RCM with the largest bias values in winter. From table 8, it can be seen that GCM provided a lower root mean square error (RMSE) and mean absolute error (MAE) compared to RCM for both the stations regardless of the downscaling technique. Compared to SDSM, TLFN gave lower

Table 8: Validation statistics for the downscaling models (1981-1990)

Hamilton Airport												
	Precipitation				Max. Temperature				Min. Temperature			
	SDSM		TLFN		SDSM		TLFN		SDSM		TLFN	
	GCM	RCM	GCM	RCM	GCM	RCM	GCM	RCM	GCM	RCM	GCM	RCM
RE	0.137	0.179	0.226	0.110	-0.013	0.010	-0.005	0.009	0.023	0.080	0.001	0.077
MAE	2.433	4.051	2.757	3.660	1.825	5.812	1.870	4.109	1.506	5.265	1.902	3.804
RMSE	6.788	8.595	6.118	6.970	3.561	7.354	2.418	5.259	3.197	6.761	2.458	4.842
r	0.590	0.042	0.427	-0.021	0.950	0.792	0.977	0.884	0.947	0.769	0.968	0.871

Hamilton RBG												
	Precipitation				Max. Temperature				Min. Temperature			
	SDSM		TLFN		SDSM		TLFN		SDSM		TLFN	
	GCM	RCM	GCM	RCM	GCM	RCM	GCM	RCM	GCM	RCM	GCM	RCM
RE	0.044	0.057	-0.059	0.046	-0.007	0.008	-0.018	0.018	0.024	0.089	-0.016	0.092
MAE	2.486	4.090	2.977	3.418	1.958	5.808	2.152	4.171	1.444	5.324	1.777	3.810
RMSE	6.382	8.367	6.718	6.063	3.799	7.330	2.737	5.276	3.106	6.810	2.276	4.822
r	0.550	-0.023	0.391	0.040	0.941	0.789	0.970	0.882	0.951	0.773	0.973	0.874

** RE, MAE and RMS values are in 'millimetres' for precipitation and 'degree Celsius' for temperatures.

RMSE values for both GCM and RCM; and lower MAE values for RCM, slightly higher MAE values for GCM. TLFN provided higher correlation (r) than SDSM for both the climate models, which reveals that TLFN is also a better downscaling technique for minimum temperature. The RE values indicate that both the downscaling techniques estimated the annual mean minimum temperature almost accurately.

The uncertainty assessment is done for the downscaling results at 95% confidence level. As daily temperature data usually follows a normal distribution, the uncertainty in this case however can be assessed by comparing the means and variances. But in case of precipitation, this comparison is not enough as the assumption of normality may not be valid. Thus, two non-parametric tests: Wilcoxon's Rank-Sum test and Levene's test are used to assess the uncertainty of the downscaling results.

The Levene's test assesses the null hypothesis at the desired confidence level by comparing the variances for different samples. Wilcoxon's Rank-sum test does the same thing for means of different samples. If the resulting p-value from the tests is less than the critical value (in this case 0.05 for 95% confidence level), then the null hypothesis is rejected and it's concluded that there is a difference of mean or variance between the two samples.

Table 9: Wilcoxon Rank Sum and Levene Test p-values for precipitation at Hamilton Airport

Wilcoxon test results for HA precipitation				
	SDSM		TLFN	
Month	GCM	RCM	GCM	RCM
Jan	0.769	0.881	0.472	0.324
Feb	0.308	0.203	0.251	0.257
Mar	0.727	0.574	0.371	0.969
Apr	0.514	0.919	0.506	0.679
May	0.098	0.177	0.157	0.061
Jun	0.544	0.06	0.089	0.292
Jul	0.738	0.604	0.316	0.416
Aug	0.077	0.198	0.081	0.091
Sep	0.065	0.085	0.077	0.068
Oct	0.103	0.052	0.191	0.129
Nov	0.318	0.107	0.323	0.12
Dec	0.101	0.181	0.201	0.061

Levene test results for HA precipitation				
	SDSM		TLFN	
Month	GCM	RCM	GCM	RCM
Jan	0.793	0.705	0.706	0.846
Feb	0.973	0.496	0.933	0.393
Mar	0.097	0.788	0.865	0.781
Apr	0.08	0.06	0.056	0.051
May	0.302	0.864	0.468	0.858
Jun	0.07	0.9	0.121	0.993
Jul	0.901	0.976	0.657	0.954
Aug	0.561	0.116	0.661	0.107
Sep	0.591	0.885	0.647	0.894
Oct	0.107	0.875	0.148	0.893
Nov	0.646	0.832	0.07	0.899
Dec	0.664	0.53	0.234	0.74

Table 10: Wilcoxon Rank Sum and Levene Test p-values for precipitation at Hamilton RBG

Wilcoxon test results for HR precipitation				
	SDSM		TLFN	
Month	GCM	RCM	GCM	RCM
Jan	0.428	0.357	0.256	0.157
Feb	0.734	0.343	0.102	0.248
Mar	0.951	0.392	0.415	0.493
Apr	0.74	0.553	0.119	0.443
May	0.096	0.201	0.29	0.198
Jun	0.124	0.875	0.275	0.768
Jul	0.739	0.669	0.545	0.558
Aug	0.534	0.101	0.237	0.096
Sep	0.379	0.08	0.09	0.056
Oct	0.532	0.769	0.36	0.562
Nov	0.131	0.119	0.13	0.106
Dec	0.557	0.507	0.341	0.228

Levene test results for HR precipitation				
	SDSM		TLFN	
Month	GCM	RCM	GCM	RCM
Jan	0.891	0.927	0.959	0.807
Feb	0.15	0.958	0.439	0.564
Mar	0.09	0.746	0.688	0.68
Apr	0.824	0.247	0.717	0.334
May	0.108	0.21	0.266	0.603
Jun	0.608	0.616	0.818	0.901
Jul	0.665	0.281	0.437	0.443
Aug	0.941	0.182	0.676	0.916
Sep	0.87	0.54	0.803	0.496
Oct	0.263	0.878	0.96	0.89
Nov	0.134	0.397	0.094	0.776
Dec	0.194	0.739	0.668	0.465

Table 9 and 10 shows that the Wilcoxon Rank Sum p-values for precipitation are low for May and August compared to the other months and Levene test p-values for Hamilton Airport are low in April. These results suggest that the downscaling models captured the precipitation reasonably well for both the stations except for those months. The p-values for all the months are above 0.05 for both stations in case of daily maximum and minimum temperatures revealing the fact that downscaled results for temperature are statistically significant.

6.1.2 Future period predictions

After calibrating and validating the models for current period (1961-1990), they are used to project the future conditions using the SRES A2 scenario. In this study, future predictions for precipitation, maximum and minimum temperatures are made for 2050s (2046-2065) with SDSM and TLFN for both the climate models so that the predictions by different models and downscaling techniques can be compared to get a reliable simulation of future hydrologic conditions later. The monthly means of these variables are compared for the current and future periods (figures 27-29 and 13B-15B in Appendix B). The mean annual change as well as the seasonal changes between current and future periods are also calculated for these variables and listed in table 11 and 12 respectively. From the figures, it can be seen that for both the stations downscaled GCM results show a larger increasing trend in mean precipitation, maximum and minimum temperatures for the 2050s compared to the downscaled RCM projections.

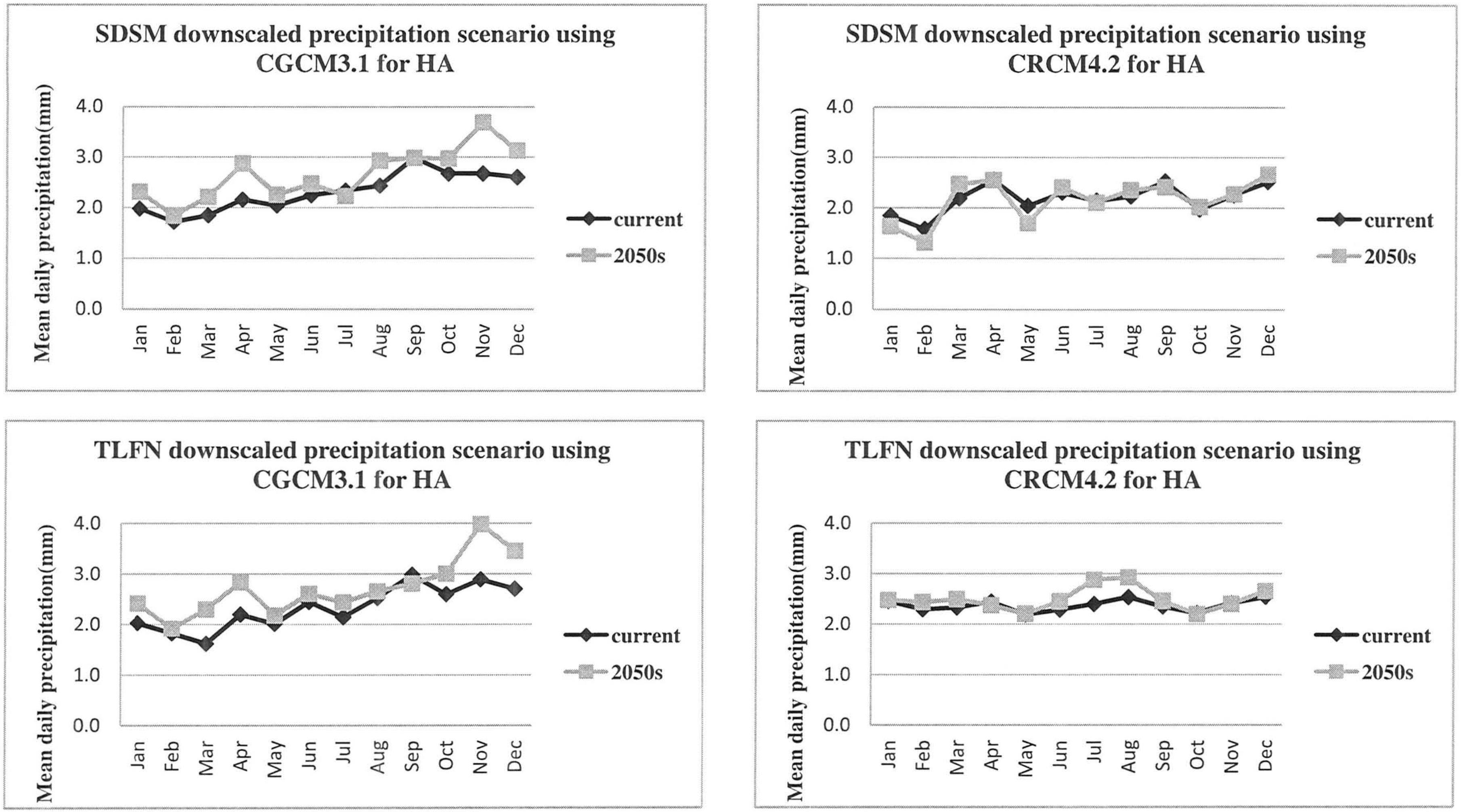

Fig 27: SDSM and TLFN downscaled monthly mean precipitation at Hamilton Airport for current (1961-1990) and future period (2050s)

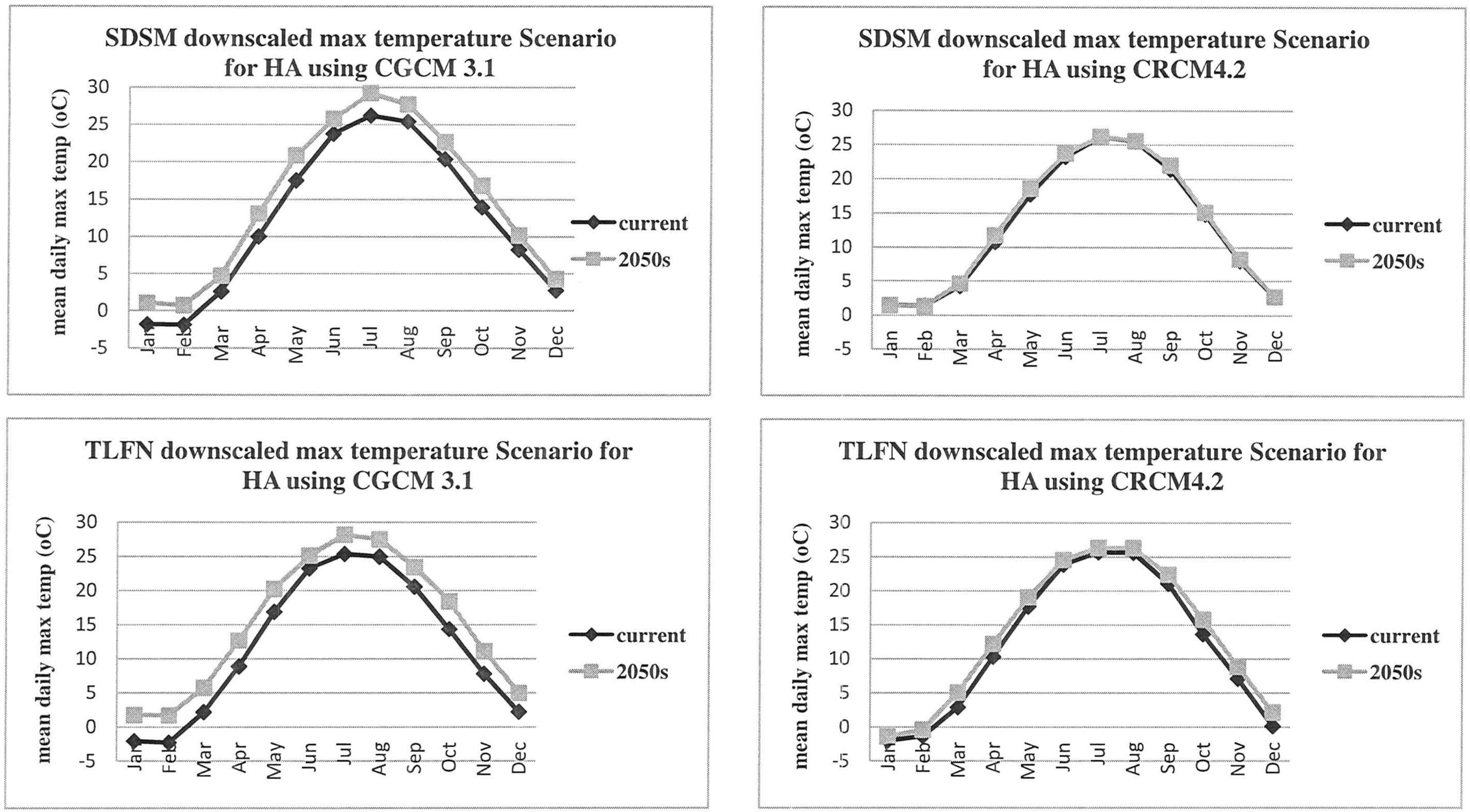

Fig 28: SDSM and TLFN downscaled monthly mean maximum temperature at Hamilton Airport for current (1961-1990) and future period (2050s)

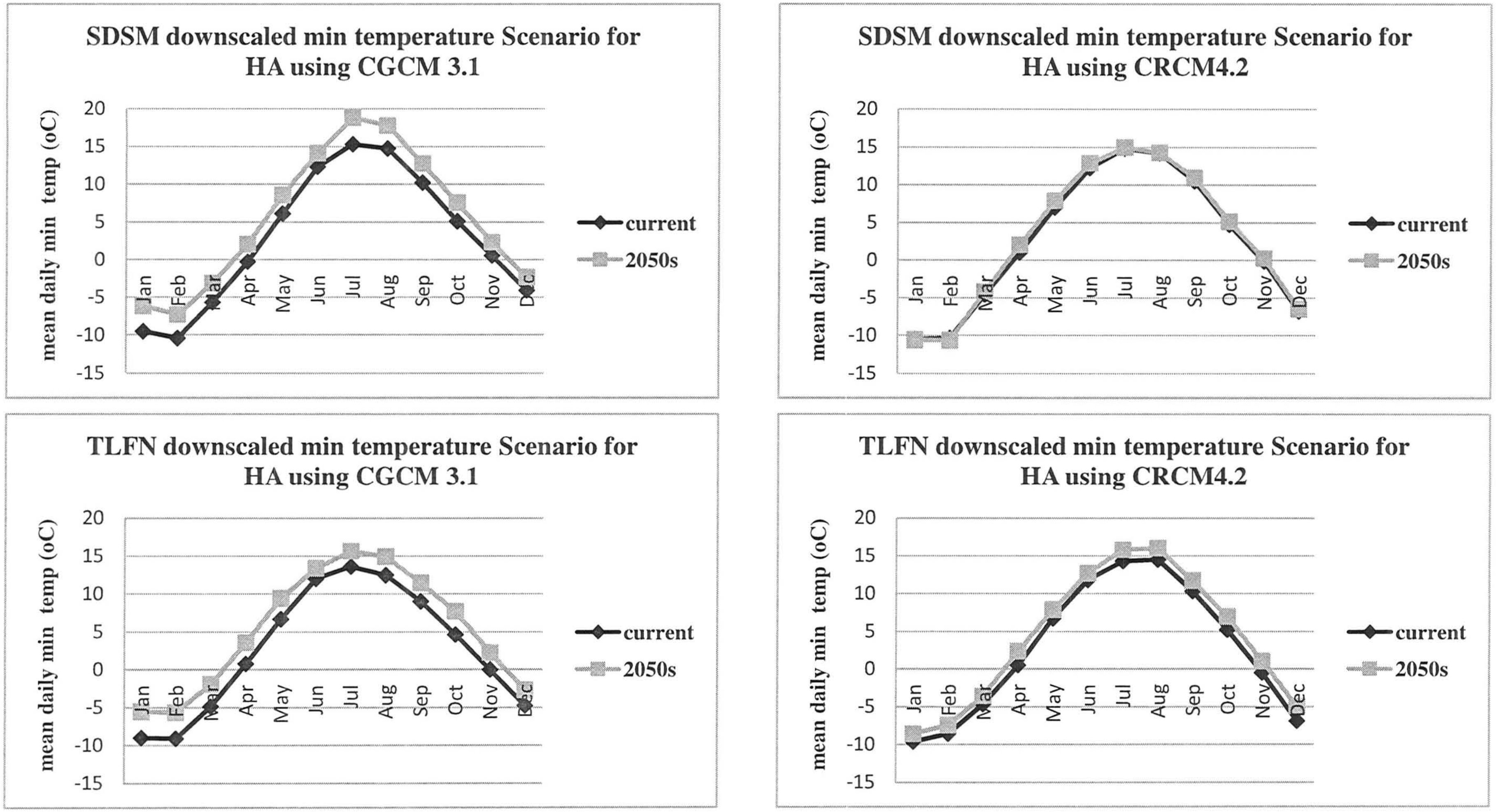

Fig 29: SDSM and TLFN downscaled monthly mean minimum temperature at Hamilton Airport for current (1961-1990) and future period (2050s)

Table 11: Changes in annual average values for 2050s (2046-2065) at Hamilton Airport and Hamilton RBG from current conditions (1961-1990) as predicted by the SDSM and TLFN downscaling models

	Average Increase/Decrease														
Station HR	Precipitation (%)					Tmax (oC)					Tmin (oC)				
	Raw_RCM	GCM		RCM		Raw_RCM	GCM		RCM		Raw_RCM	GCM		RCM	
		SDSM	TLFN	SDSM	TLFN		SDSM	TLFN	SDSM	TLFN		SDSM	TLFN	SDSM	TLFN
2050s	3.98	15.15	16.63	-0.91	5.34	3.10	2.50	3.25	0.34	1.34	3.62	2.56	2.60	0.36	1.40

	Average Increase/Decrease														
Station HA	Precipitation (%)					Tmax (oC)					Tmin (oC)				
	Raw_RCM	GCM		RCM		Raw_RCM	GCM		RCM		Raw_RCM	GCM		RCM	
		SDSM	TLFN	SDSM	TLFN		SDSM	TLFN	SDSM	TLFN		SDSM	TLFN	SDSM	TLFN
2050s	3.98	14.71	15.42	-0.61	7.03	3.10	2.42	2.85	0.36	1.35	3.62	2.58	2.17	0.43	1.56

Table 12: Changes in average seasonal values for 2050s (2046-2065) at Hamilton Airport and Hamilton RBG from current conditions (1961-1990) as predicted by the SDSM and TLFN downscaling models

Hamilton Airport						
			SEASONS			
			Winter	Spring	Summer	Fall
Precipitation (%)	RAW_RCM		21.33	16.32	-11.60	-5.52
	GCM	SDSM	15.53	21.44	8.72	15.70
		TLFN	18.95	25.67	8.23	15.73
	RCM	SDSM	-5.44	-0.98	2.91	-0.62
		TLFN	3.89	1.62	14.45	1.14
Max. temp(oC)	RAW_RCM		2.07	3.02	4.13	3.18
	GCM	SDSM	2.34	2.86	2.44	2.37
		TLFN	3.53	3.60	2.41	3.46
	RCM	SDSM	0.00	0.76	0.22	0.37
		TLFN	1.15	1.80	0.65	1.75
Min. temp (oC)	RAW_RCM		2.99	6.03	4.14	1.32
	GCM	SDSM	2.76	2.45	2.79	2.24
		TLFN	2.99	2.83	1.95	2.59
	RCM	SDSM	-0.01	0.76	0.28	0.40
		TLFN	1.38	1.36	1.31	1.55

Hamilton RBG						
			SEASONS			
			Winter	Spring	Summer	Fall
Precipitation (%)	RAW_RCM		21.33	16.32	-11.60	-5.52
	GCM	SDSM	13.25	21.30	8.19	16.34
		TLFN	17.58	23.04	7.82	13.47
	RCM	SDSM	-6.69	-1.48	4.49	0.45
		TLFN	7.16	3.94	13.17	3.28
Max. temp(oC)	RAW_RCM		2.07	3.02	4.13	3.18
	GCM	SDSM	2.29	2.71	2.34	2.31
		TLFN	2.78	3.21	2.52	2.92
	RCM	SDSM	-0.08	0.57	0.16	0.79
		TLFN	1.01	1.83	0.87	1.67
Min. temp (oC)	RAW_RCM		2.99	6.03	4.14	1.32
	GCM	SDSM	2.87	2.42	2.78	2.27
		TLFN	2.37	2.67	1.27	2.38
	RCM	SDSM	-0.05	0.71	0.40	0.64
		TLFN	1.56	1.60	1.30	1.79

For downscaled GCM, both SDSM and TLFN showed an increasing trend for monthly mean precipitation in 2050s, with significant increase in winter, spring and fall. For maximum temperature, GCM showed a gradual increasing trend throughout the year with the largest increase in spring. Monthly mean minimum temperature for 2050s also showed a gradual increasing trend with GCM with significant increase in winter. Regardless of the downscaling techniques employed, GCM predicted 14 to 17% increase in annual mean precipitation and 2-3°C increase in annual mean maximum and minimum temperatures for both the stations.

While GCM showed an overall increasing trend in precipitation for both the stations in 2050s, both raw RCM and downscaled RCM showed decrease for some months. Raw RCM showed only 4% increase in mean annual precipitation with a decreasing trend in summer and fall; and SDSM downscaled RCM predicted around 1% decrease in mean annual precipitation. RCM predicted an increasing trend in precipitation with TLFN (5-7% annual increase), with the largest increase in summer (around 15%). For maximum and minimum temperatures, RCM predicted almost no change in annual mean temperatures (only 0.4-0.5°C increase) when downscaled with SDSM; while raw RCM showed an overall increasing trend with 3-4°C annual increase. But it showed 1-2°C increase in mean annual maximum and minimum temperatures with TLFN, the seasonal changes are also in good agreement with the GCM results. The limitation of downscaling with SDSM may be due to the model calibration with RCM predictors instead of reanalysis data (e.g. North American Regional Reanalysis (NARR) data) from the National Oceanic and Atmospheric Administration (NOAA). It is anticipated that the use of NARR data for calibrating SDSM model would have improved the model performance, but the NARR data was unavailable at the time of this study.

Regardless of the climate models used, TLFN showed a larger increase in mean annual precipitation than SDSM because of its inability to accurately predict the days without precipitation. For maximum temperature, TLFN also predicted a slightly larger increase in annual mean values than SDSM. Overall, downscaling results indicated 1% decrease to around 20% increase in annual precipitation; and 0.5-3°C increase in annual temperatures for the 2050s.

These results will later be used in the distributed coupled model to project the future hydrologic conditions for the Spencer Creek watershed.

6.2 MIKE SHE AND MIKE 11 COUPLED MODEL RESULTS

6.2.1 Current Period Results

The coupled hydrological model is mainly used to simulate streamflows. But to assess the accuracy of the streamflow results, the snow storage and evapotranspiration at the desired flow stations are also predicted. Distributed flow simulation is performed at locations other than the flow stations in the watershed to assess the distributed modeling potential of the model. The model performance is assessed by computing the mean absolute error (MAE), root mean square error (RMSE), correlation (r) and the Nash-Sutcliffe coefficient (R^2). The hydrologic modeling results are presented and discussed in the following sections.

Snow Storage Simulation

The total snow storage at three stations: Christie, Valens and Dundas, are modeled as snow-water equivalent for both the calibration (1989-2000) and validation (2001-2008) period. The model results are compared with the observed data obtained from HCA. To better represent the results, the monthly values of snow storage are compared (Figure 30) for November-April, as there is usually no snowfall in the other months. The model performance statistics (RMSE, MAE values are in 'millimetres') for snow storage simulation are provided in table 13.

Table 13: Model performance statistics for snow storage simulation

Snow stations	Calibration			Validation		
	RMSE	MAE	r	RMSE	MAE	r
Christie	20.76	13.73	0.80	18.91	10.89	0.65
Valens	22.13	12.86	0.72	16.74	9.36	0.50
Dundas	20.07	13.34	0.81	18.89	11.28	0.66

The model produced reasonable results for snow storage for all the stations. From the table, it can be seen that the model results are reasonable for the calibration period and for all the stations the correlation is above 0.7 and MAE values are below 15. For the validation period, the MAE values are better than those for the calibration period which indicates better reproduction of observed mean snow storage for validation period. But correlation for validation period is lower than for calibration which reveals that the model captured the variability in snow storage better for the calibration period.

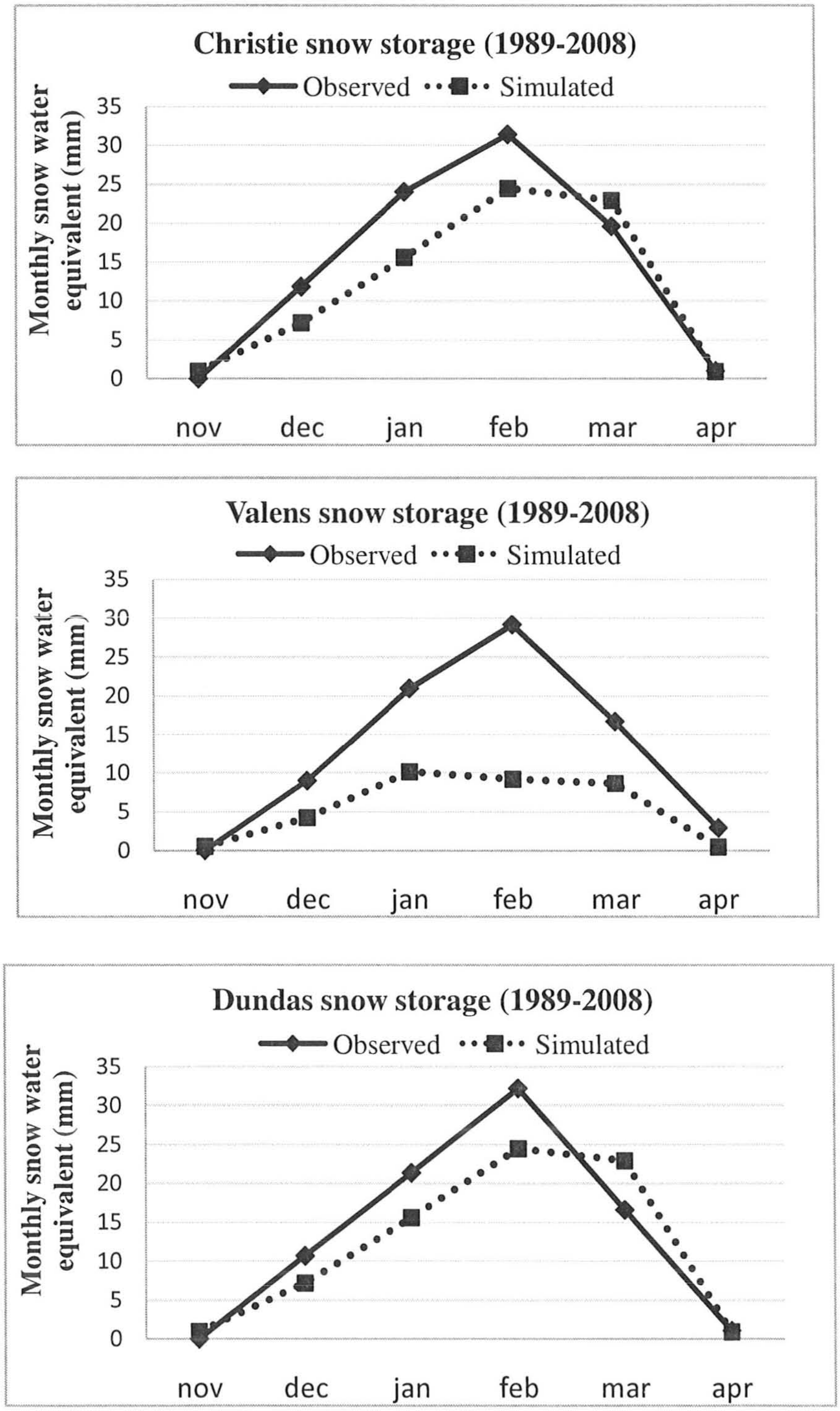

Fig 30: Total snow storage at three stations in Spencer Creek Watershed

Various reasons limited the model's performance in simulating the snow storage. The observed data obtained from HCA is not continuous, HCA measured the accumulated snow depth for just 15 days every year in the winter and early spring and the accuracy of these data is questionable as their flow data was found to have some major discrepancies when compared to the WSC data (Chapter 2). Instead of using hourly temperature data, daily maximum (at 3PM) and minimum temperature (at 3AM) are used in the model; and so the model couldn't capture the diurnal variations in temperature accurately. As a result, the model might be unable to properly partition precipitation into rainfall or snowfall in winter/spring season (Shalini, 2006). Again, for minimum snow storage and maximum wet snow fraction in the model, uniform values are used instead of distributed ones due to of lack of data. The melting temperature is kept uniform at $0^{o}C$ for the entire watershed; whereas it should be lower in the mountainous or escarpment areas.

From figure 30, it is evident that the simulated snow storage in the winter is always lower than the observed ones but follows almost the same pattern except for Valens in February. This may be due to the model's inability to capture extreme events such as freezing rain (at temperature below $0^{o}C$) or snow pellets. The model gave slightly higher snow storage in March for Christie and Dundas but lower for Valens. Valens is covered by the Hamilton RBG station that has a lower precipitation compared to Hamilton Airport that covers Christie and Dundas; may be for this reason it's having lower snow storage than the other two stations. The limited performance of the model may be essentially due to the lack of accurate continuous long records from the meteorological stations inside the watershed. Due to this reason, data from the outside stations are used in the model; moreover Hamilton RBG and Hamilton Airport are assumed to cover the upper and lower parts of the watershed respectively, but in fact both stations are closer to the lower part of the watershed.

Evapotranspiration results

The actual evapotranspiration (ET) are computed for all the flow stations for 1989-2008. The monthly plots of the ET values for the stations are provided in figure 31. Dundas has the relatively low ET for all the months and Ancaster has the higher ones compared to the other stations. The ET values are higher for late spring and early summer months.

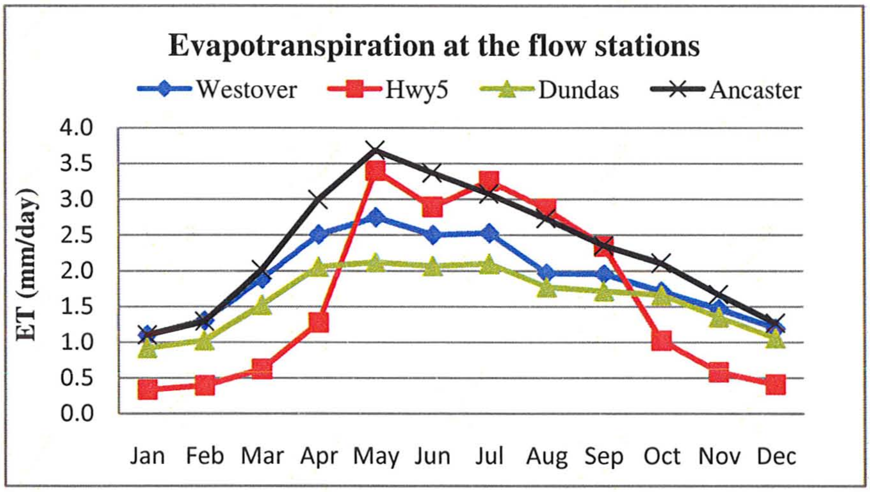

Fig 31: Evapotranspiration in Spencer Creek Watershed for 1989-2008

<u>Streamflow simulation</u>

The monthly simulated flows are compared with the observed ones for both the calibration and validation period and presented in figures 1C and 2C in the Appendix. The daily flows for the validation period are shown only for the years 2006-2008 (figure 32) for a clear presentation and scatter plots along with the black line representing the perfect model output (figure 33) for this period are also provided. Table 14 represents the model calibration and validation statistics for streamflows at each hydrometric station.

Table 14: Model performance statistics for streamflow simulation

Flow stations	Calibration			Validation		
	RMSE	r	Nash	RMSE	r	Nash
Westover	0.483	0.66	0.43	0.549	0.72	0.38
HWY5	1.574	0.73	0.44	1.55	0.76	0.43
Dundas	1.872	0.76	0.46	1.843	0.77	0.42
Ancaster	0.089	0.59	0.07	0.093	0.68	0.15

*** RMSE values are in 'cubic metre per seconds'.

Westover is the most upstream station in the watershed and the simulated flows are in good agreement with the observed ones. The correlation is above 0.65 and R^2 value is around 0.4 for both calibration and validation. Figure 32 shows that the model captures the base flows well for the validation period. The scatter plot in figure 33 also shows that the low flows are close to the perfect model line; whereas the higher flows are away from the line. The model overestimated the peak flows for some years and underestimated for the others. The spring flows are underestimated for all the years (figure 1C & 2C) which is consistent with the snow results discussed above. Given that the model underestimated the snow storage in winter, therefore the spring snowmelt is also lower resulting in underestimation of spring flows. The lower streamflows occurred in the summer mainly due to higher evapotranspiration discussed above.

The streamflow results for Highway 5 are slightly better than Westover with a higher correlation (>0.7) and R^2 values (>0.4). The base flows are simulated almost accurately. The scatter plot is same as that for Westover, but the model usually underestimated the peak flows in validation period. The spring flows are underestimated same as for Westover. For Hwy5, the model underestimated the flows also in the winter. The lower streamflows occurred in the summer due to high evapotranspiration.

The model simulated the Dundas flows efficiently with a correlation above 0.75 and R^2 value above 0.4. The peak flows are mostly underestimated. The streamflows in the spring and winter months are lower than the observed ones same as Hwy5.

For Ancaster, the correlation is very low and R^2 value is only around 0.1-0.2. Both the base flows and peak flows are not captured well by the model. The scatter plot in figure 33 shows that the higher flows are always below the perfect model line for the validation period. For both the calibration and validation period, the model underestimated the flows for all seasons but it followed almost the same pattern as the observed ones. This may be due to limited cross-section data for the Ancaster river.

Two facts limited the model's capability to simulate streamflows for all the seasons. Firstly, for each type of soil the hydraulic conductivity is kept uniform throughout the year; while it can be altered by cultivation operations (Shalini, 2006). Secondly, the frozen soil conditions are not incorporated in the model which affects the infiltration as well as surface runoff (Shalini, 2006).

Distributed flow simulation

The coupled model is a fully distributed hydrologic model; it can be used to simulate the flows at any location within the watershed. The simulated river flows for the validation period from two locations at Upper Spencer Creek are presented in figure 34.

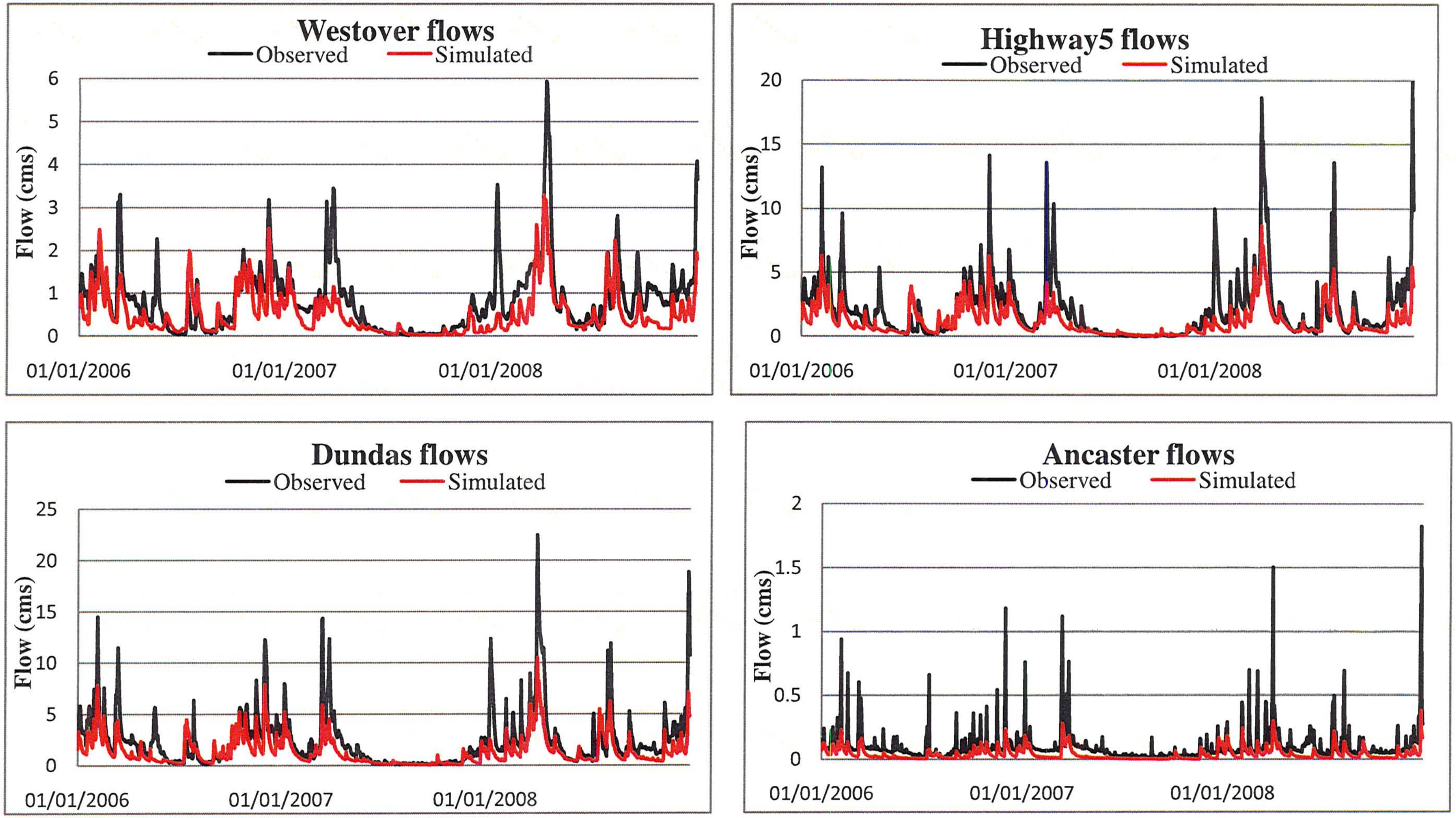

Fig 32: Streamflows for the validation period

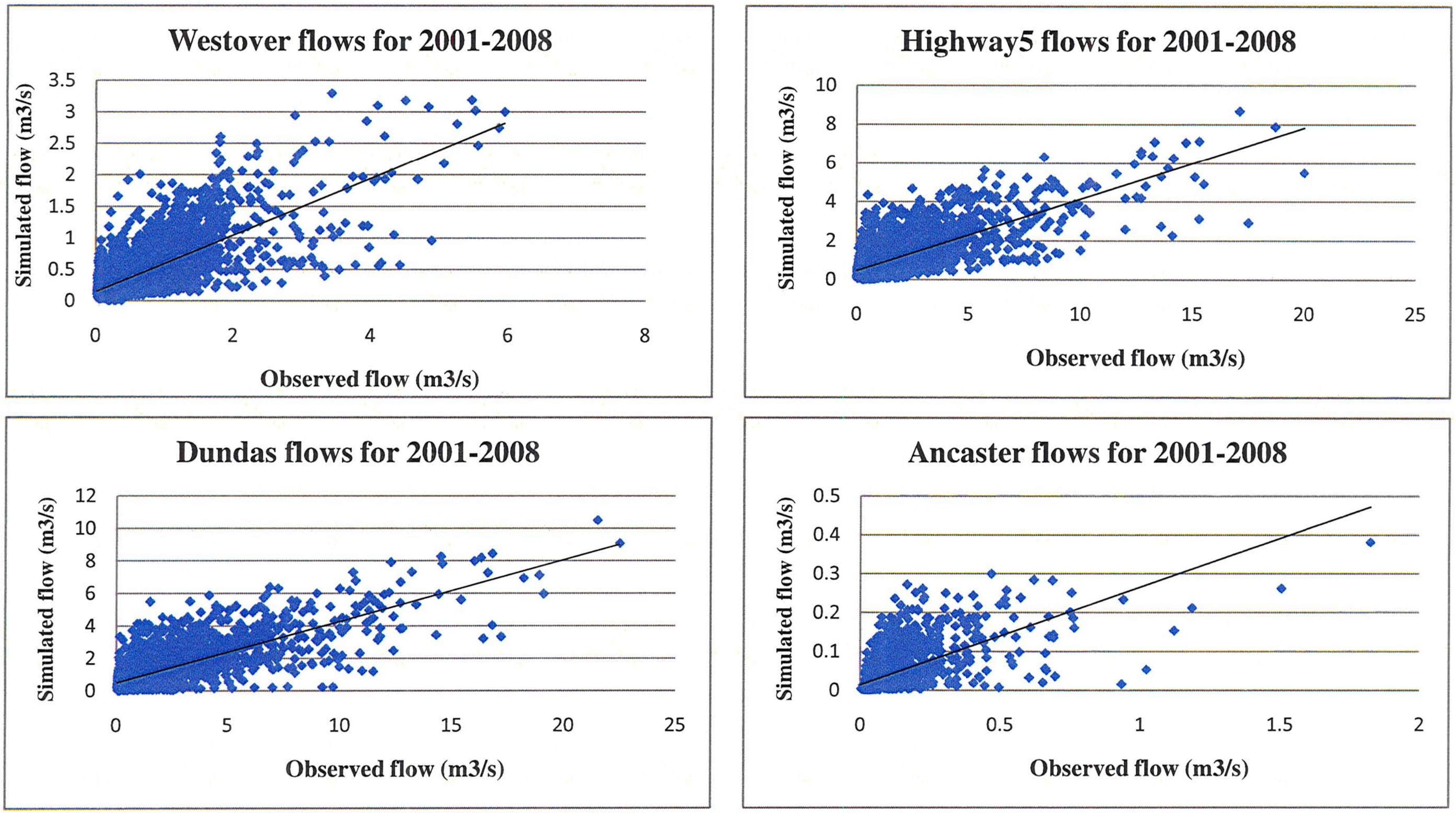

Fig 33: Scatter plots of observed and simulated streamflows for validation period

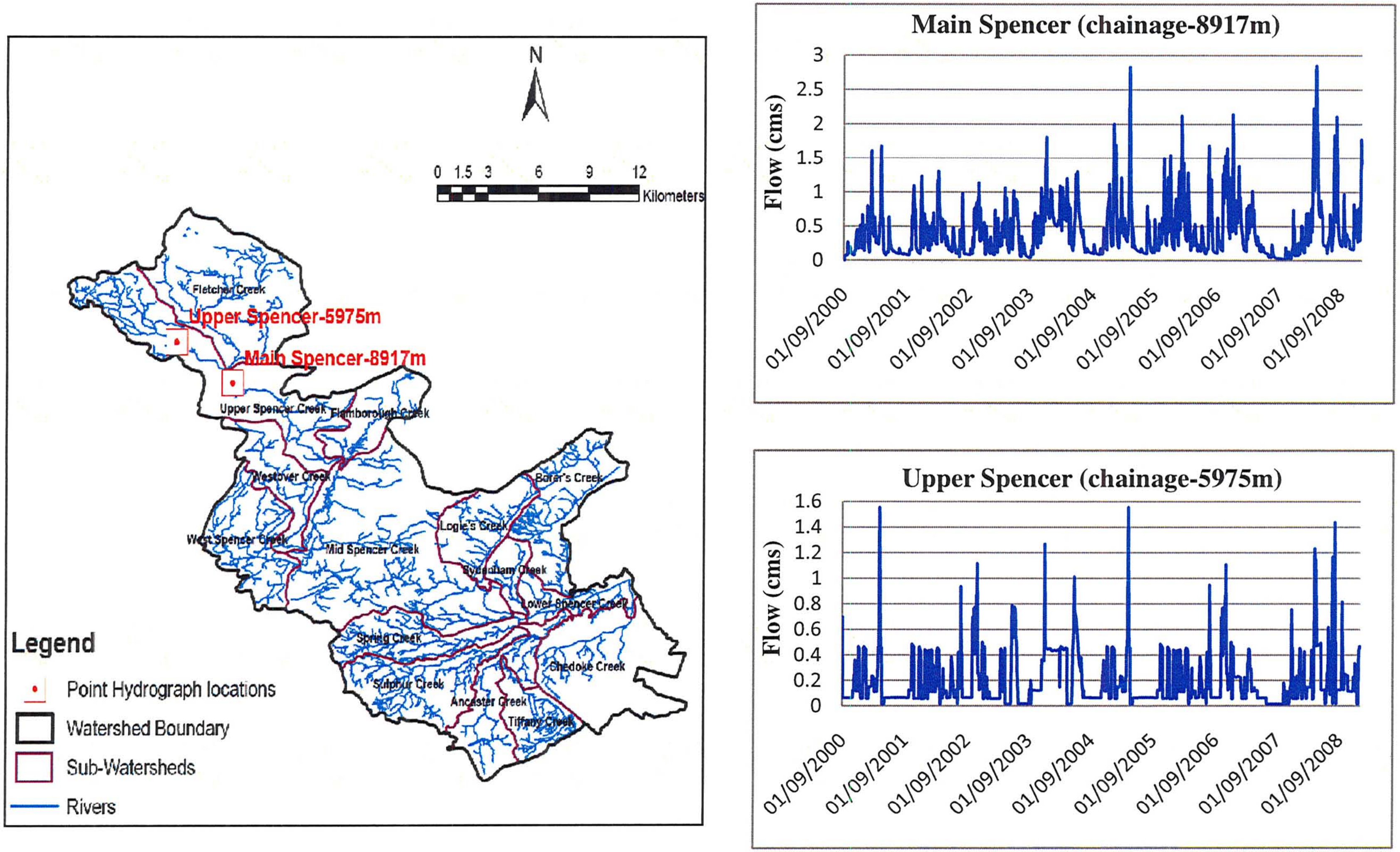

Fig 34: Point hydrographs at two locations in Spencer Creek Watershed

6.2.2 Future changes in hydrologic processes

SDSM and TLFN downscaled future scenario results using CGCM 3.1 and CRCM 4.2 are used in the flow model to predict the changes in streamflow for 2050s. The changes in snow storage and evapotranspiration are also monitored to better understand the changes in the streamflow. In all the cases, the future results are compared with the current period results (1989-2008) discussed above. Normally, the future results are supposed to be compared with the downscaled current period results, which are for 1961-1990. But the streamflow data starts from 1989 and due to lack of data, the results for 1989-2008 are used as current period in this study for the comparison.

<u>Snow storage for 2050s</u>

Using the downscaled future scenario, the snow storage for the three stations are simulated. The snow results for Christie are presented in figure 35 and for the other stations in the Appendix (figure 3C). The annual average change for 2050s is calculated for all the stations (table 15) and seasonal changes (table 1C) are also presented.

For all the stations, the hydrologic model with GCM scenario results predicted a decrease in snow storage throughout the year regardless of the downscaling techniques. SDSM downscaled scenario results provided lower snow-water equivalent for 2050s compared to TLFN as TLFN always overestimated precipitation. From table 1C and figure 35 and 3C, it appears that the 2050s' winter and spring are having around 5-10% decreased snow compared to the current period. These results are consistent with the downscaled results. Table 12 showed that GCM predicted an overall increase in maximum and minimum temperature for 2050s with the highest increase in winter and spring. Due to higher temperature at 2050s, most of the precipitation will occur as rainfall even in winter and earlier snow melt will take place resulting in lower snow storage.

The coupled model with raw RCM and downscaled RCM scenario results predicted an increase in snow storage both in winter and spring except for Christie and Dundas with SDSM downscaled scenario (table 15). Regardless of the downscaling techniques, RCM predicted very slight increase in temperature compared to GCM (table 11 and 12). Though SDSM presented a decrease in 2050s' precipitation, TLFN predicted higher precipitation same as the raw RCM. The insignificant change in temperature combined with an increased precipitation for 2050s (table 11 and 12) are supposed to create a higher snow storage. Compared to the other scenarios, TLFN downscaled RCM scenario provided much higher increase in snow storage. While the model predicted an overall decrease (1-5%) in annual snow storage for 2050s with GCM; with RCM it indicated 5-22% increase.

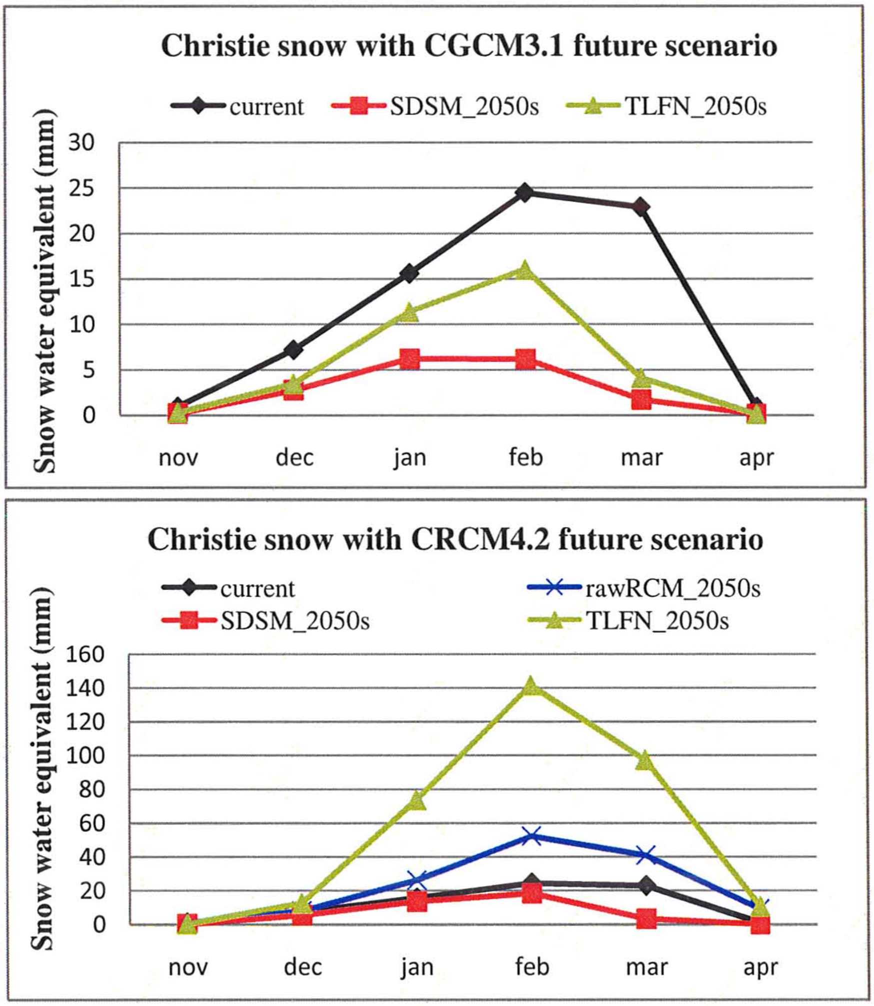

Fig 35: Snow storage at Christie for current period and 2050s

Table 15: Changes in annual average snow storage for 2050s (2046-2065) at the snow stations from current conditions (1989-2008)

Average annual increase/decrease (mm)					
Station	**GCM**		**Raw RCM**	**RCM**	
	SDSM	**TLFN**		**SDSM**	**TLFN**
Christie	-4.56	-3.04	5.35	-2.52	21.97
Valens	-1.82	-1.60	8.59	2.26	13.51
Dundas	-4.56	-3.04	5.35	-2.52	21.97

Evapotranspiration for 2050s

Evapotranspiration at the flow stations are also monitored to have a better idea of the streamflow results for 2050s. The 2050s ET for the stations are presented in figure 36 and 4C-5C in Appendix. The annual and seasonal changes in ET are also calculated and listed in table 16 and 2C respectively.

The hydrologic model with GCM scenario results predicted higher annual evapotranspiration for 2050s regardless of the downscaling techniques due to increasing temperature (table 11 and 12). Same as the case with raw RCM and TLFN downscaled RCM. But for HWY5, Dundas and Ancaster, SDSM scenario results for RCM indicated an annual decrease in ET that may be due to SDSM's limitation in downscaling RCM data as discussed earlier.

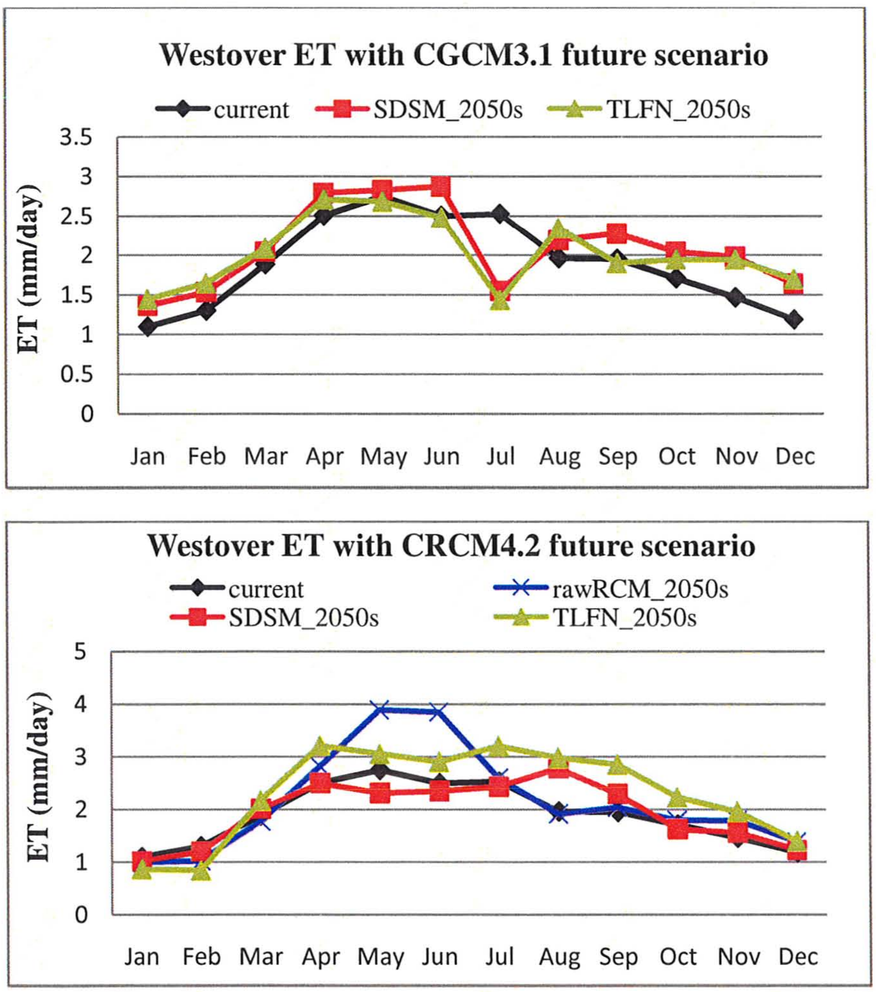

Fig 36: Evapotranspiration results for Westover for current period and 2050s

Table 16: Changes in annual average evapotranspiration for 2050s (2046-2065) from current conditions (1989-2008)

Average annual increase/decrease (%)					
Station	GCM		Raw RCM	RCM	
	SDSM	TLFN		SDSM	TLFN
Westover	10.01	6.52	12.96	2.17	21.01
Highway5	5.37	1.54	4.19	-11.12	1.99
Dundas	5.24	5.41	17.00	-8.57	21.19
Ancaster	4.87	4.33	7.27	-9.44	8.75

With GCM, the coupled model predicted 1-10% annual increase in ET for 2050s with the highest increase in winter and fall. With raw RCM and downscaled RCM, it estimated 2-22% increase in annual ET with TLFN with highest increase in spring and fall.

Streamflow for 2050s

The future streamflow results for all the four stations are presented in figures 37 and 6C-7C. The annual and seasonal changes in streamflow are calculated and listed in table 17 and table 3C.

When downscaled GCM scenarios are used, the coupled hydrologic model predicted an overall increase in streamflows for all the stations with the highest increase in winter and fall (15-50%). These results are consistent with the downscaling results and snow results discussed earlier. Both SDSM and TLFN showed the highest temperature increase in winter that will result in lower snow storage and earlier snow melts increasing the streamflow in winter. From table 12, it can be seen that downscaled GCM predicted 15-25% increase in precipitation for the spring and fall. The high flows in the fall may be attributed to this fact.

Using the raw RCM data, the coupled hydrologic model predicted an annual increase of 5-12% in streamflow, while downscaled RCM scenarios are used, the model predicted decrease in streamflow for 2050s for all the stations. Those results are consistent in the sense that the flow patterns for 2050s are almost same for both SDSM and TLFN. While the model predicted the highest flow increase in winter and fall with GCM scenarios, it estimated significant decrease in flow with RCM scenarios for the same period. With the TLFN, the model showed increase in flow only in spring which is consistent with the higher temperature and precipitation in winter and spring (table 12) resulting in more flow due to accelerated snow melt. With the SDSM, the model predicted an overall decreasing trend in streamflow for all the stations as SDSM predicted lower precipitation for 2050s. Overall, using GCM scenarios, the coupled model predicted 10-30% flow increase, while with RCM, the model estimated 3-30% decrease in annual streamflows for 2050s.

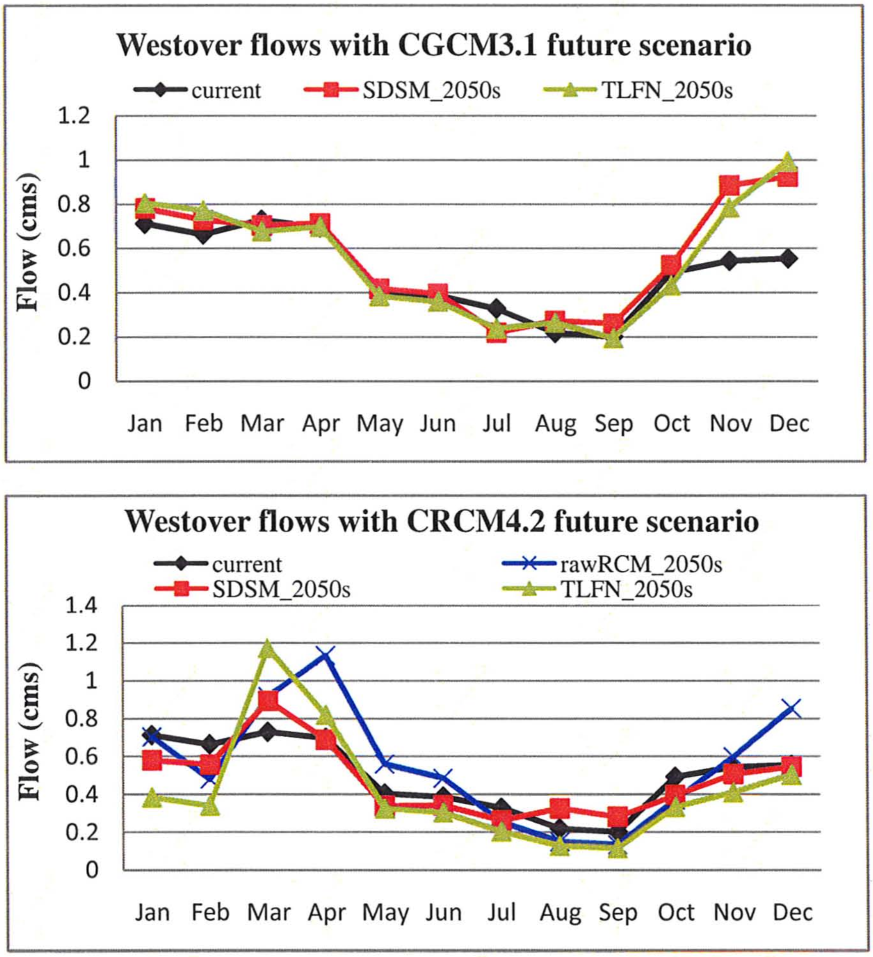

Fig 37: Westover flows for current period and 2050s

Table 17: Changes in annual average streamflows for 2050s (2046-2065) from current conditions (1989-2008)

Average annual increase/decrease (%)					
Station	**GCM**		**Raw RCM**	**RCM**	
	SDSM	**TLFN**		**SDSM**	**TLFN**
Westover	15.28	11.40	11.73	-3.51	-15.01
Highway5	17.76	14.74	11.55	-8.48	-24.92
Dundas	16.99	15.96	10.45	-11.17	-24.91
Ancaster	15.79	26.51	5.81	-25.90	-26.01

CHAPTER 7

CONCLUSIONS AND RECOMMENDATIONS

7.1 CONCLUSIONS

MIKE SHE is a physically distributed model that integrates surface, subsurface and groundwater flow. Its flexible nature makes it an efficient technique for modeling complex hydrologic conditions resulting from a wide range of soil types and land cover and uses. When coupled with MIKE 11, it can provide a fully integrated model capable of simulating most hydrologic processes. In this study, a coupled MIKE SHE/MIKE 11 model is implemented for the Spencer Creek watershed. It is shown that the coupled model can be effectively used to simulate the present hydrologic conditions as well as to evaluate anticipated climate change effects on key hydrologic processes in the Spencer Creek watershed.

The coupled MIKE SHE/MIKE 11 model captured the snow storage well with a correlation coefficient of 0.5-0.8 and mean absolute error of 9-15. The model efficiency in snow storage simulation was limited in this study due to the use of daily maximum and minimum temperature data instead of hourly data and the use of uniform snow melt parameters. The model provided reasonable results for evapotranspiration with higher values in late spring and early summer months. The simulated streamflows are in good agreement with the observed flow at different stations with a correlation coefficient of 0.6-0.8 and Nash-Sutcliffe coefficient of around 0.4-0.5. The flow results showed consistency with the snow storage and evapotranspiration results. The patterns of high flows obtained for the snowmelt period (March/April) and the minimum flows in summer (June/July/August) are consistent with those of the observed streamflows. Some of the model limitations can be attributed to the fact that temporal variability of soil hydraulic conductivity cannot be incorporated in the model. Similarly, frozen soil properties were not included in the model. Nevertheless, the model represented the hydrologic conditions in the watershed quite well. It also simulated streamflows at some internal locations other than the calibration sites, which reveals its potential for representing spatial variability in hydrologic characteristics.

The current period (1961-1990) downscaling results for daily precipitation and temperature indicated the importance of downscaling raw RCM data, as downscaled RCM results are closer to the observed values. For both the climate models (CGCM and

CRCM), SDSM is better for downscaling precipitation and TLFN is better for temperature. Under the 'business as usual climate change scenario' (SRES A2), downscaled GCM showed a larger increasing trend in mean precipitation, maximum and minimum temperatures for 2050s compared to the downscaled RCM. Downscaled GCM predicted 14 to 17% increase in annual mean precipitation and 2-3°C increase in annual mean maximum and minimum temperatures for 2050s. While GCM showed an overall increasing trend in precipitation for the 2050s, both the raw RCM and downscaled RCM showed decrease for some months. Raw RCM estimated only 4% increase in mean annual precipitation; and SDSM downscaled RCM predicted around 1% decrease in mean annual precipitation. But RCM predicted 5-7% annual increase in precipitation with TLFN. For maximum and minimum temperatures, RCM predicted only 0.4-0.5°C annual increase when downscaled with SDSM; while raw RCM showed 3-4°C annual increase. RCM estimated 1-2°C increase in mean annual maximum and minimum temperatures with TLFN. Regardless of the climate models used, TLFN showed a larger increase in mean annual precipitation than SDSM because of its inability to accurately predict the days without precipitation. For maximum temperature, TLFN also predicted a slightly larger increase in annual mean values than SDSM. Overall, the downscaling results indicated 1% decrease to around 20% increase in annual precipitation; and 0.5-3°C increase in annual temperatures for 2050s.

The coupled hydrologic model predicted 1-5% annual decrease in snow storage for the 2050s when downscaled GCM scenarios for 2050s are used. When downscaled RCM scenarios are used, the coupled model predicted 5-22% increase in annual snow storage. SDSM downscaled scenario results provided lower snow-water equivalents compared to TLFN as TLFN always overestimated precipitation. The future snow storage results are consistent with the downscaled scenario results for precipitation and temperature. The coupled model predicted 1-10% annual increase in ET for 2050s when GCM scenarios are used, and it estimated 2-22% increase while downscaled RCM with TLFN is used. But the model predicted around 10% decrease in annual ET when downscaled RCM with SDSM is used. The simulated streamflows for 2050s using the downscaled scenarios revealed a wide range of changes in mean annual and seasonal flows. When GCM scenarios are used, the model predicted 10-25% increase in annual streamflows for all the stations with the highest increase in winter and fall, which is in good agreement with the predicted changes in snowmelt and ET. Using the raw RCM data, the coupled model predicted an annual increase of 5-12% in streamflow, and predicted 3-30% decrease in streamflow for 2050s while downscaled RCM scenarios are used. Those results are consistent in the sense that the flow patterns for 2050s are almost same for both SDSM and TLFN. While the model predicted the highest increase in winter and fall with GCM, it estimated significant decrease in flow for the same period with RCM. Those results are consistent with the downscaled scenarios and suggest that further investigation is required to refine specially the RCM downscaling results. This could be achieved by using the North American Regional Reanalysis (NARR) data for calibrating the SDSM and TLFN models. In general, the study reveals a wide range of predicted changes in the hydrologic processes (ET, snow storage, and flow) – which clearly highlights the importance of distributed hydrologic model in assessing climate change impact at the catchment scale. Despite of all the limitations, this is the first attempt to use a physically distributed model for conventional climate change impact study in such a complex watershed. Temporally and spatially distributed hydro-meteorological data for a longer period is required for improving the coupled hydrologic model. Reliable local scale meteorological data and further improvement of this hydrologic model will provide better climate change impact assessment that can be used for decision making in watershed and water resources management.

7.2 SIGNIFICANCE OF THE STUDY

i) This is the first attempt to implement a physically distributed hydrologic model (MIKE SHE/MIKE 11) for the Spencer Creek watershed and to assess its efficiency for simulating the major hydrologic processes such as evapotranspiration, snowmelt and surface runoff in such complex watershed.

ii) To our best knowledge, this may be the first time when a physically distributed hydrologic model is used for climate change impact study incorporating downscaled scenario results from both CGCM and CRCM.

iii) Despite the data limitation in the study area, it is shown that the coupled model can be an appropriate tool for assessing future changes in hydrologic processes at the catchment scale – which cannot be achieved with common conceptual and statistical hydrologic models.

7.3 RECOMMENDATIONS FOR FUTURE WORK

i) Reliable and long term continuous meteorological data from stations within the watershed will improve the efficiency of the hydrologic model in simulating current hydrologic conditions.

ii) Temporally and spatially distributed groundwater data will help the model to better capture the base flows.

iii) Vertical discretization and macropore flow within the soils are not considered in this study as it increases the computational time.

iv) Christie dam located at the Main Spencer Creek in the watershed is not included in the hydrologic model due to lack of data concerning discharge regulation of the dam. The incorporation of this dam may improve the flow simulation results.

v) Real cross-section data collected from field measurements should be used in the model for better results.

vi) RCM should be downscaled with NARR data from National Oceanic and Atmospheric Administration (NOAA) to verify whether the results improve or not.

REFERENCES

Abbott, M.B., Bathurst, J.C., Cunge, J.A., O'Connell, P.E., Rasmussen, J. (1986), *An introduction to the European hydrological system-Système Hydrologique Europèen "SHE", 1: History and philosophy of a physically based distributed modeling system,* Journal of Hydrology, 87, 45-59.

Andersen, J., Refsgaard, J.C., Jensen, K.H. (2001), *Distributed hydrological modeling of the Senegal River Basin-model construction and validation*, Journal of Hydrology, 247, 200-214.

Bardossy, A., Plate, E.J. (1992), *Space-time model for daily rainfall using atmospheric circulation patterns,* Water Resources Research, 28, 1247-1259.

Brouwer, C., Heibloem, M. (1986), *Irrigation Water Management: Irrigation water need-Training manual 3*, National Resources management and Environment Department, FAO.

Canadian Centre for Climate Modeling and Analysis, Environment Canada. http://www.cccma.ec.gc.ca/eng_index.shtml. Date Accessed: 2007-2009.

Cannon, A.J., Whitfield, P.H. (2002), *Downscaling recent streamflow conditions in British Columbia, Canada using ensemble neural network models,* Journal of Hydrology, 259, 136-151.

Caron, F. (2007), *Methodology for Implementing MIKE Basin: Case Study of Spencer Creek Watershed,* Research Project, McMaster University.

Caya, D., Laprise, R. (1999), *A Semi-Implicit Semi-Lagrangian Regional Climate Model: The Canadian RCM, Mon. Wea. Rev.*, 127, 341-362.

Christiaens, K., Feyen, J. (2001), *Analysis of uncertainties associated with different methods to determine soil hydraulic properties and their propagation in the distributed hydrological MIKE SHE model*, Journal of Hydrology, 246, 63-81.

Conover, W.J. (1980), *Practical Nonparametric Statistics,* 2nd ed. Wiley, New York.

Coulibaly P., Anctil F., Bobee B. (2001), *Multivariate Reservoir Inflow Forecasting using Temporal Neural Networks,* Journal of Hydrologic Engineering, 6(5), 367-376.

Coulibaly, P., Dibike, Y.B., Anctil, F. (2005), *Downscaling precipitation and temperature with Temporal Neural Networks,* Journal of Hydrometeorology, 6, 483-496.

Crane, R.G., Hewitson, B.C. (1998), *Doubled CO_2 precipitation changes for the Susquehanna basin: Downscaling from the GENESIS general circulation model,* International Journal of Climatology, 18, 65-76.

Crawford, N.H., Linsey, R.K. (1966), *Digital simulation in hydrology, Stanford Watershed Model IV,* Technical Report 39, Department of Civil Engineering, Stanford University, California, USA.

DHI (2005), *MIKE 11: A Modeling System for Rivers and Channels-Short Introduction and Tutorial*, Danish Hydraulic Institute, Denmark.

DHI (2007), *MIKE SHE User Manual, Volume 2: Reference Guide*, Danish Hydraulic Institute, Denmark.

Dibike Y. B., Coulibaly P. (2005), *Hydrologic Impact of Climate Change in the Saguenay Watershed: Comparison of Downscaling Methods and Hydrologic Models,* Journal of Hydrology, 307, 145-163.

Dibike, Y.B., Coulibaly P. (2006), *Temporal neural networks for downscaling climate variability and extremes*, Neural Networks, 19, 135-144.

Dibike, Y.B., Coulibaly, P. (2007), *Validation of hydrological models for climate scenario simulation: the case of Saguenay watershed in Quebec,* Hydrological Processes, 21, 3123-3135.

Ewen, J., Parkin, G., O'Connell, P.E., SHETRAN (2000), *Distributed river basin flow and transport modeling system,* In: Proceedings of the American Society of Civil Engineering, Journal of Hydrologic Engineering, 5, 250-258.

Feyen, L., Vázquez, R., Christiaens, K., Sels, O., Feyen, J. (2000), *Application of a distributed physically-based hydrological model to a medium size catchment*, Hydrology and Earth System Sciences, 4(1), 47-63.

Giles, C.L., Lawrence, S., Tsoi, A.C. (1997), *Rule inference for financial prediction using recurrent neural networks,* Proc., IEEE/IAFE Conf. on computational Intelligence for Financial Engrg., IEEE Press, Piscataway, N.J., 263-259.

Giogri, F., Mearns, L.O. (1999), *Introduction to special section: Regional climate modeling revisited,* J. Geophys. Res-Atmos., 104, 6335-6352.

Hamilton Region Conservation Authority (1983), *Watershed Plan-Vol. 1 and 2.*

Hamilton Region Conservation Authority-MacLaren Plansearch Lavalin (1990), *Volume 1-Technical Report: Canada/Ontario Flood Damage Reduction Program.*

Hay, L.E., McCabe, G.J., Willock, D.M., Ayers, M.A. (1991), *Simulation of precipitation by weather type analysis*, Water Resources Research, 27, 493-501.

Hay, L.E., Clark, M.P. (2003), *Use of statistically and dynamically downscaled atmospheric model output for hydrologic simulations in three mountainous basins in the western United States,* Journal of Hydrology, 282, 56-75.

Haykin, S. (1999), *Neural Networks – A Comprehensive Foundation (2nd Edition),* Prentice Hall. New Jersey.

Huth, R., Kysely, J., Dubrovsky, M. (2002), *Simulation of surface air temperature by GCMs, statistical downscaling and weather generator: higher order statistical moments,* Institute of Atmospheric Physics, Acad. Sci. Czech Republic, Bocni II/1401, 141 31 Prague 4, Czech Republic.

James, W. (1994), *Current Practices in Modeling the Management of Stormwater Impacts,* CRC press, p-91.

Jasper, K., Gurtz, J., Lang, H. (2002), *Advanced flood forecasting in Alpine watersheds by coupling meteorological observations and forecasts with a distributed hydrological model*, Journal of Hydrology, 267, 40-52.

Johnson, M.S., Coon, W.F., Mehta, V.K., Steenhuis, T.S., Brooks, E.S., Boll, J. (2003), *Application of two hydrologic models with different runoff mechanisms to a hillslope dominated watershed in the northern US: a comparison of HSPF and SMR*, Journal of Hydrology, 284, 57-76.

Jayatilaka, C.J., Storm, B., Mudgway, L.B. (1998), *Simulation of water flow on irrigation bay scale with MIKE SHE*, Journal of Hydrology, 208, 108-130.

Karunanithini, N., Grenney, W.J., Whitley, D., Bovee, K. (1994), *Neural networks for river flow prediction,* J. Comp. Civ. Engrg., ASCE, 8(2), 201-220.

Khan, M. S. (2007), *Climate Change Impact Study on Water resources with Uncertainty Estimates using Bayesian Neural Network*, PhD Thesis, Dept. of Civil Engineering, McMaster University, Hamilton, Ontario, Canada.

Kristensen, K.J., Jensen, S.E. (1975), *A model for estimating actual evapotranspiration from potential Evapotranspiration,* Nordic Hydrology, 6, 170-188.

Larson N. (2005), *Implementation of Coupled MIKE SHE and MIKE 11 Dynamic Hydrological Models for the Grand River Watershed and Mill Creek Sub Basin*, Research Project, McMaster University.

Lehmann, E.L. (1975), *Nonparametrics: Statistical Methods Based on Ranks*, Holden and Day, San Francisco.

Levene, H. (1960), *Contributions to Probability and Statistics,* Stanford University press.

Linden R, Harlin J. (2000), *Analysis of conceptual rainfall–runoff modeling performance in different climate,* Journal of Hydrology, 238, 231–247.

Liu, H., Chen, X., Bao, A., Wang, L. (2007), *Investigation of groundwater response to overland flow and topography using a coupled MIKE SHE/MIKE 11 modeling system for an arid watershed*, Journal of Hydrology, 347, 448-459.

Liu, X. (2007), *Downscaling Meteorological Predictions for Short-term Hydrologic Forecasting,* M.A.Sc Thesis, Dept. of Civil Engineering, McMaster University, Hamilton, Ontario, Canada.

Mareuil, A., Leconte, R., Brissette, F., Minville, M. (2007), *Impacts of climate change on the frequency and severity of floods in the Châteauguay River basin, Canada,* Can. J. Civ. Eng., 34, 1048-1060.

McGregor, J.J. (1997), *Regional climate modeling*, Meteorological Atmospheric Physics, 63, 105-117.

McMichael, C.E., Hope, A.S., Loaiciga, H. A. (2006), *Distributed hydrological modeling in California semi-arid shrublands: MIKE SHE model calibration and uncertainty estimation,* Journal of Hydrology, 317, 307-324.

Minville M., Brissette F., Leconte R. (2008), *Uncertainty of the impact of climate change on the hydrology of a Nordic watershed*, Journal of Hydrology, 358, 70-83.

Murphy, J.M. (2000), *Predictions of climate change over Europe using statistical and dynamical downscaling techniques*, Int. J. Climatol., 20, 489– 501.

Music, B., Caya, D (2007), *Evaluation of the Hydrological Cycle over the Mississippi River Basin as simulated by the Canadian Regional Climate Model (CRCM)*, J. Hydromet., 8(5), 969-988.

Nash, I.E., Sutcliffe, I.V. (1970), *River flow forecasting through conceptual models,* Journal of Hydrology, 10, 282-290.

Nguyen, V.T.V. (2005), *Downscaling methods for evaluating the impacts of climate change and variability on hydrological regime at basin scale,* Role of Water Sciences in Transboundary River Basin Management, Thailand.

Ontario Department of Lands and Forests, Conservation Authorities Branch (1962), *Spencer Creek Conservation Report.*

Refsgaard, J.C. (1997), *Parameterization, calibration and validation of distributed hydrological models,* Journal of Hydrology, 198, 69-97.

Refsgaard, J.C., Storm, B. (1995), *Computer Models of Watershed Hydrology,* Water Resources Publications, Eaglewood, USA, 809-846.

Refsgaard, J.C., Thorsen, M., Jensen, J.B., Kleeschulte, S., Hansen, S. (1999), *Large scale modeling of groundwater contamination from nitrate leaching*, Journal of Hydrology, 221, 117-140.

Regonada, S.K., Rajagolapan, B., Clark, M., Pitlick, J. (2005), *Seasonal cycle shifts in hydroclimatology over the western Unites States,* Journal of Climate, 18 (2), 372-384.

Romano, N., Palladino, M. (2002), *Prediction of soil water retention using soil physical data and terrain attributes*, Journal of Hydrology, 265, 56-75.

Sahoo, G.B., Ray, C., De Carlo, E.H. (2006), *Calibration and validation of a physically distributed hydrological model, MIKE SHE, to predict streamflow at high frequency in a flashy mountainous Hawaii stream,* Journal of Hydrology, 327, 94-109.

Salathé Jr, E.P. (2005), *Downscaling simulations of future global climate with application to hydrologic modeling,* In. J. Climatol., 25, 419-436.

Schubert, S. (1998), *Downscaling local extreme temperature changes in south-eastern Australian from the CSIRO Mark2 GCM,* Int. J. Climatol., 18, 1419-1438.

Semenov, M.A., barrow, E.M. (1997), *Use of a stochastic weather generator in the development of climate change scenarios,* Climatic Change, 35, 397-414.

Shalini, O. (2006), *Runoff simulation in the Canagagigue creek watershed using the MIKE SHE model,* M.A.Sc Thesis, Dept. of Bioresource Engineering, McGill University, Montreal, Canada.

Sharma, M. (2009), *Comparison of Downscaled RCM and GCM data for hydrologic impact assessment,* M.A.Sc Thesis, Dept. of Civil Engineering, McMaster University, Hamilton, Ontario, Canada.

Simnovic S. , Li, L. (2004), *Sensitivity of the Red River Basin Flood Protection System to Climate Variability and Change,* Water Resources Management 18, 89-110.

Singh, R., Subramanian, K., Refsgaard, J.C. (1999), *Hydrological modeling of a small watershed using MIKE SHE for irrigation planning,* Agricultural Water Management, 41, 149-166.

Smith, J., Eli, R.N. (1995), *Neural-network models of rainfall-runoff process,* J. Water Resour. Plng. And Mgmt., ASCE, 121 (6), 499-508.

Thompson, J.R., Sørenson, H.R., Gavin, H., Refsgaard, A. (2004), *Application of the coupled MIKE SHE/MIKE 11 modeling system to a lowland wet grassland in southeast England,* Journal of Hydrology, 293, 151-179.

Tollner, E.W. (2002), *Natural Resources Engineering,* Wiley Blackwell, p-85.

Water Survey Canada (2009), *Data products and services: Archived Hydrometric data.*

Weichert, A., Burger, G. (1998), *Linear versus nonlinear techniques in downscaling,* Climate Res., 10, 83-93.

Wetterhall, F., Bardossy, A., Chen, D., Halldin, S., Xu, C.-Y. (2006), *Daily precipitation-downscaling techniques in three Chinese Regions,* Water Resources Research, 42, W11423, doi: 10.1029/2005WR004573.

Wetterhall, F., Halldin, S., Xu, C.-Y. (2007), *Seasonality properties of four statistical-downscaling methods in central Sweden,* Theor. Appl. Climatol., 87, 123-137.

Whitfield, P.H., Cannon, A.J. (2000), *Recent variation in climate and hydrology in Canada,* Canadian Water Resources Journal, 25 (1), 19-65.

Wilby, R.L., Dawson C.W., Barrow E.M. (2002), *SDSM- a decision support tool for the assessment of regional climate change impacts*, Environmental Modeling and Software, 17, 145-157.

Wilby, R.L., Dawson, C.W. (2007), *SDSM 4.2- A decision support tool for the assessment of regional climate change impacts.*

Wilks, D.S. (1999), *Multisite downscaling of daily precipitation with a stochastic weather generator*, Climate Research, 11, 125-136.

Woo, Ming-Ko (1978), *Impact of Ontario Hydro Transmission Line Construction Activities upon the Hydrology of an area of Beverly Swamp,* prepared for Ontario Hydro.

Xevi, E., Christiaens, K., Espino, A., Sewnandan, W., Mallants, D., Sørensen, H., Feyen, J. (1997), *Calibration, validation and sensitivity analysis of the MIKE SHE model using the Neuenkirchen Catchment as case study,* Water Resources Management, 11, 219-242.

Xu, C. Y. (1999), *From GCM to River flow: A review of downscaling methods and hydrologic modeling approaches,* Prog. Phys. Geogr. , 23, 229-249.

APPENDIX A

Table 1A: Large scale predictor variables from NCEP and CGCM3.1/T63

Daily variable	Description
temp	Mean temperature
mslp	Mean Sea level pressure
p500	500 hPa geopotential height
p850	850 hPa geopotential height
shum	Near surface specific humidity
s500	Specific humidity at 500hPa height
s850	Specific humidity at 850 hPa height
**_u	Zonal velocity component
**_v	Meriodional velocity component

**indicates p_, p% or p* which represent the variable values near surface, at 500 hPa height or 850 hPa height, respectively.

Table 2A: The CRCM4.2 predictors

Daily variable	Description
hsf	surface upward sensible heat flux (W/m2)
pcp	precipitation (mm)
phi500	geopotential height at 500 hPa (m^2/s^2)
phi850	geopotential height at 850 hPa (m^2/s^2)
pmsl	mean sea level pressure (Pa)
sq	screen specific humidity at 2m (kg/kg)
stmn	minimum temperature (°C)
stmx	maximum temperature (°C)
su	eastward surface wind (m/s)
sv	northward surface wind (m/s)
swmx	mean amplitude of sustained wind at 10 m (m/s)
rhum1000	Relative humidity at 1000 hpa

Table 3A: Mean daily percentage (p) of annual daytime hours for different latitudes (Brouwer & Heibloem, 1986)

Latitude	North	Jan	Feb	Mar	Apr	May	June	July	Aug	Sept	Oct	Nov	Dec
	South	July	Aug	Sept	Oct	Nov	Dec	Jan	Feb	Mar	Apr	May	June
60°		.15	.20	.26	.32	.38	.41	.40	.34	.28	.22	.17	.13
55		.17	.21	.26	.32	.36	.39	.38	.33	.28	.23	.18	.16
50		.19	.23	.27	.31	.34	.36	.35	.32	.28	.24	.20	.18
45		.20	.23	.27	.30	.34	.35	.34	.32	.28	.24	.21	.20
40		.22	.24	.27	.30	.32	.34	.33	.31	.28	.25	.22	.21
35		.23	.25	.27	.29	.31	.32	.32	.30	.28	.25	.23	.22
30		.24	.25	.27	.29	.31	.32	.31	.30	.28	.26	.24	.23
25		.24	.26	.27	.29	.30	.31	.31	.29	.28	.26	.25	.24
20		.25	.26	.27	.28	.29	.30	.30	.29	.28	.26	.25	.25
15		.26	.26	.27	.28	.29	.29	.29	.28	.28	.27	.26	.25
10		.26	.27	.27	.28	.28	.29	.29	.28	.28	.27	.26	.26
5		.27	.27	.27	.28	.28	.28	.28	.28	.28	.27	.27	.27
0		.27	.27	.27	.27	.27	.27	.27	.27	.27	.27	.27	.27

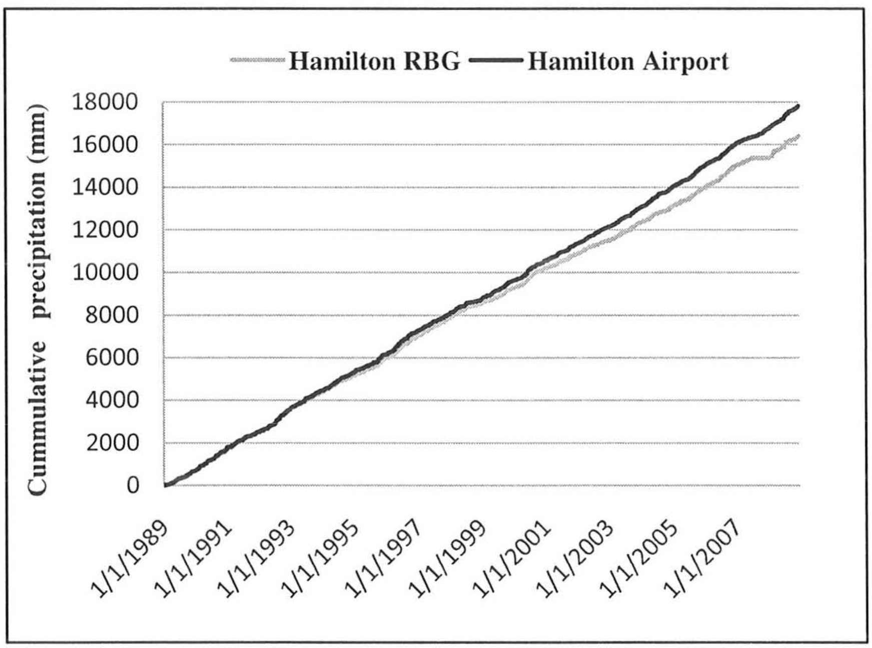

Fig 1A: Precipitation at the meteorological stations for 1989-2008

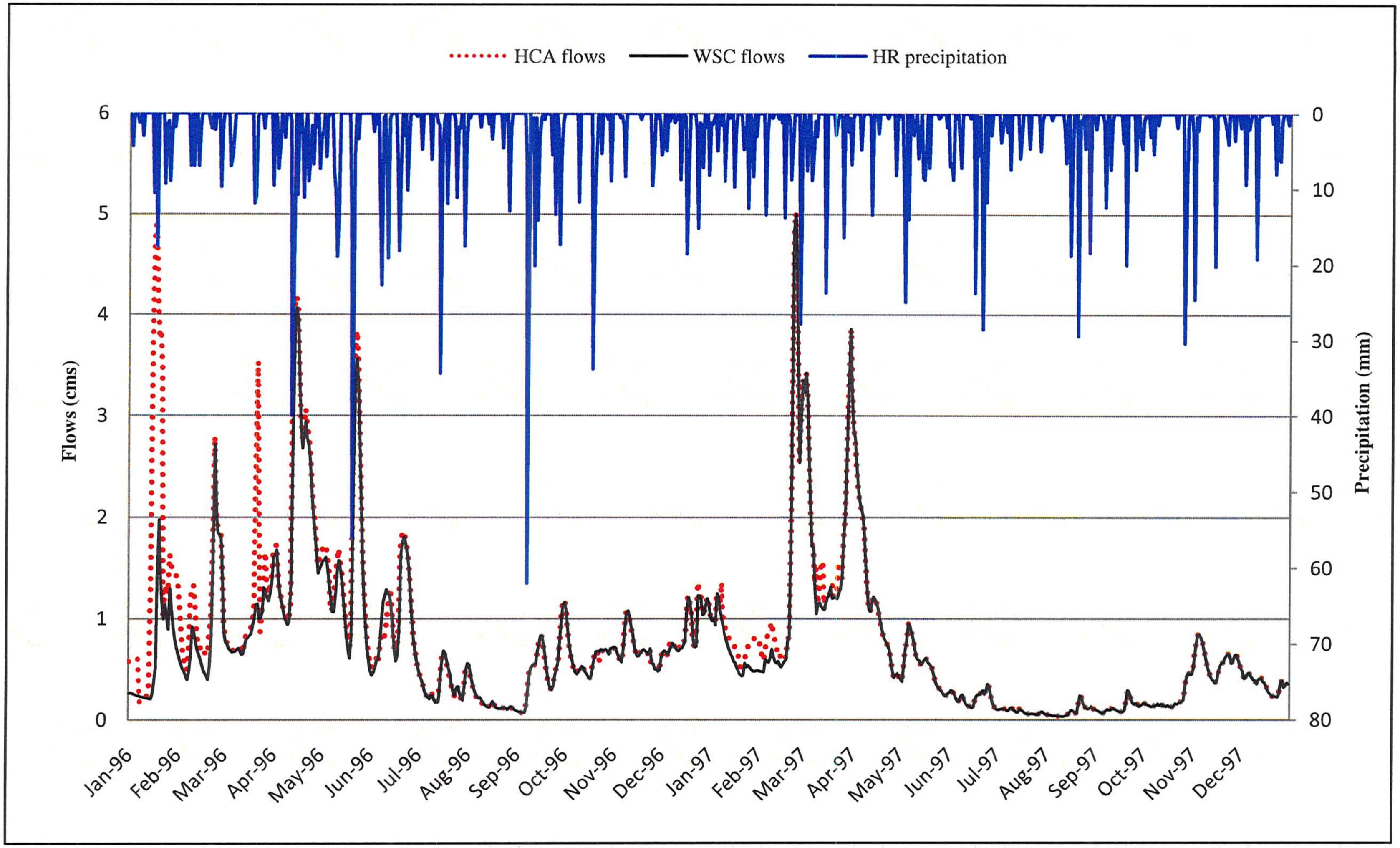

Fig 2A: Comparison of WSC and HCA flows for Westover with the precipitation at Hamilton RBG

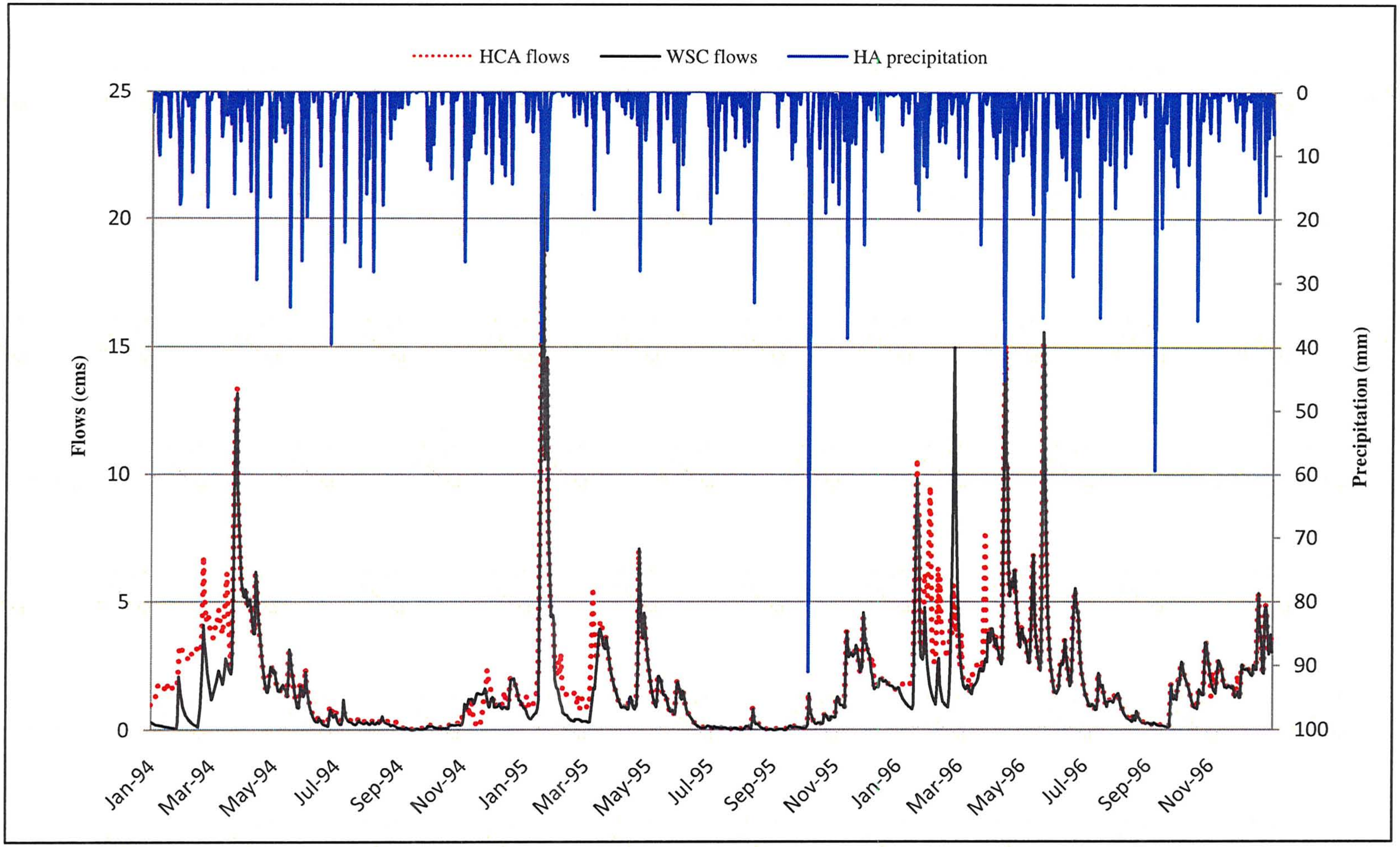

Fig 3A: Comparison of WSC and HCA flows for Highway5 with the precipitation at Hamilton Airport

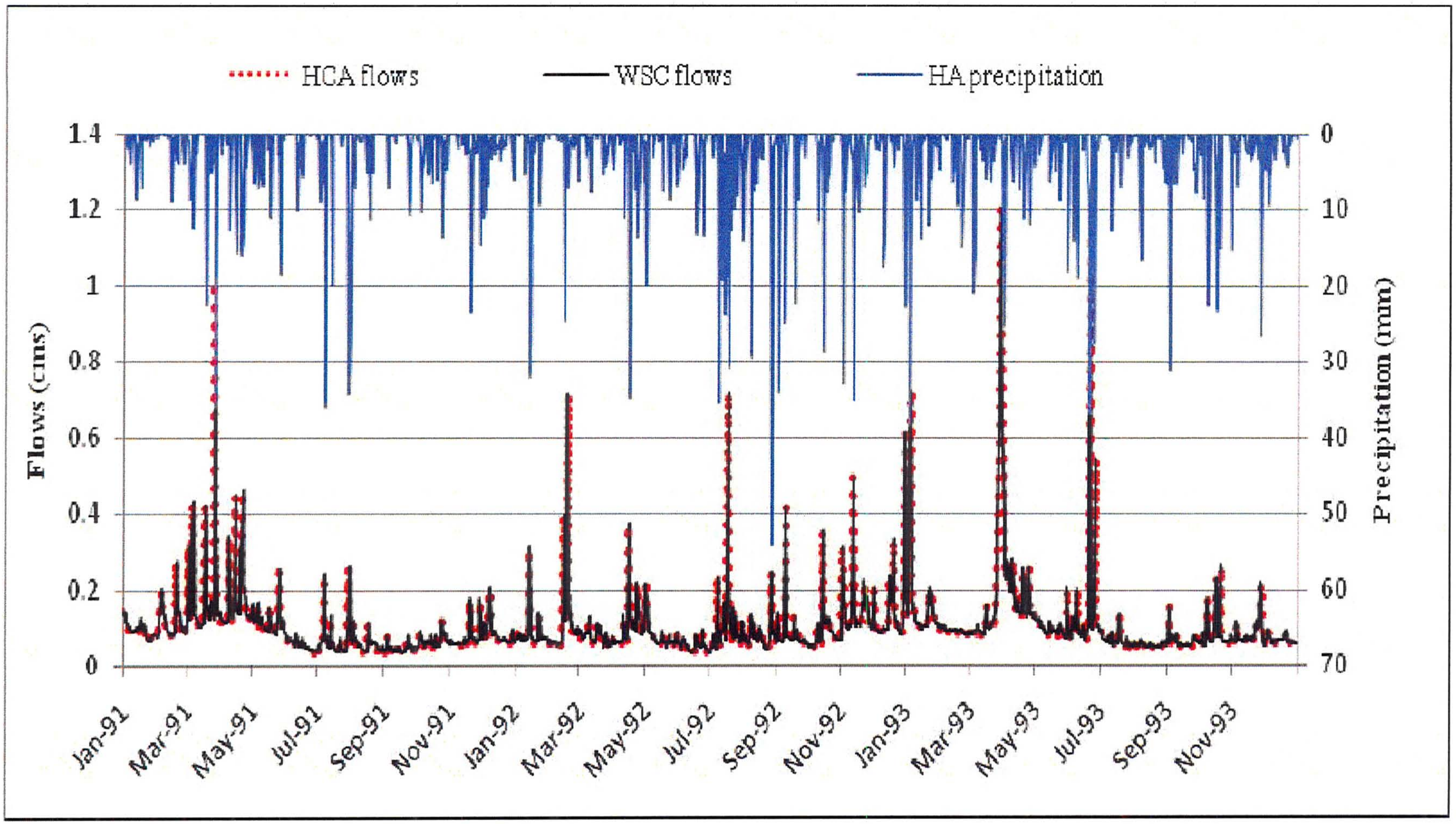

Fig 4A: Comparison of WSC and HCA flows for Ancaster with the precipitation at Hamilton Airport

APPENDIX B

Table 1B: Bias Statistics of monthly mean and variance of precipitation at Hamilton Airport

Bias Table-Precipitation monthly mean					
		SDSM		TLFN	
Month	Raw RCM	RCM	GCM	RCM	GCM
JAN	-0.1213	-0.1924	-0.3428	0.4900	-0.6591
FEB	-0.0706	0.0462	0.4257	0.6957	0.2477
MAR	0.4309	0.6155	0.4978	0.6643	0.0862
APR	0.0536	-0.0015	-0.1488	-0.2864	-0.3998
MAY	1.8405	0.0624	0.2218	0.4158	0.4656
JUN	1.4914	0.0829	0.1322	0.1017	-0.4290
JUL	0.4784	-0.2759	-0.4475	0.0137	-0.2121
AUG	-0.3308	-0.2882	0.0354	0.0831	-0.0899
SEP	-0.0890	0.2406	0.4961	-0.0027	0.0416
OCT	0.3968	0.0724	0.1573	0.3758	0.4500
NOV	0.1104	-0.1115	0.3860	0.0703	0.2324
DEC	0.0839	0.3969	0.0897	0.4535	-0.4141

Bias Table-Precipitation monthly variance					
		SDSM		TLFN	
Month	Raw RCM	RCM	GCM	RCM	GCM
JAN	-16.0901	-13.5735	-16.2070	-29.2496	-26.7032
FEB	-11.1803	-4.8200	2.3241	-19.2782	-13.3964
MAR	-1.2004	13.2481	13.2723	-15.6290	-9.4896
APR	-12.3604	3.4867	-2.3560	-32.6703	-26.1142
MAY	7.5006	3.6806	2.8984	-17.2928	-13.7929
JUN	-11.9711	0.1901	-6.3981	-31.4098	-39.6060
JUL	-23.5447	-0.6958	-11.1346	-39.7213	-39.1695
AUG	-38.3402	-7.2857	-5.0826	-45.1078	-45.4337
SEP	-20.9889	17.6433	14.3760	-32.6919	-28.9048
OCT	-5.9183	1.8600	1.3370	-23.7606	-17.4635
NOV	-10.7880	-7.1466	2.6838	-25.5388	-22.1219
DEC	-2.5552	3.8584	-0.0527	-26.0582	-22.5466

Table 2B: Bias Statistics of monthly mean and variance of precipitation at Hamilton RBG

Bias Table-Precipitation monthly mean

Month	RawRCM	SDSM		TLFN	
		RCM	GCM	RCM	GCM
JAN	-0.281	-0.102	-0.448	0.160	-0.673
FEB	-0.133	-0.013	0.403	0.534	0.130
MAR	0.233	0.395	0.282	0.253	0.074
APR	0.079	0.004	-0.210	-0.388	-0.426
MAY	1.821	0.227	0.281	0.325	0.485
JUN	1.346	-0.312	-0.425	-0.222	-0.482
JUL	0.352	-0.268	-0.109	0.252	0.851
AUG	-0.777	-0.243	0.112	-0.302	0.815
SEP	0.351	0.373	0.660	0.952	0.668
OCT	0.530	0.055	0.393	0.172	0.887
NOV	0.192	-0.052	0.382	-0.034	0.525
DEC	-0.042	0.200	-0.076	-0.215	-0.410

Bias Table-Precipitation monthly variance

Month	RawRCM	SDSM		TLFN	
		RCM	GCM	RCM	GCM
JAN	-14.533	-7.951	-15.394	-26.315	-24.198
FEB	-10.121	-3.386	0.428	-18.495	-11.349
MAR	-4.052	11.336	6.740	-19.161	-2.282
APR	-9.570	7.085	-1.243	-30.970	-21.749
MAY	9.208	8.807	3.772	-19.151	-4.415
JUN	-14.509	-16.780	-20.681	-45.525	-34.820
JUL	-32.355	-10.386	-10.936	-47.138	-40.144
AUG	-44.671	-0.237	5.165	-51.830	-41.873
SEP	-14.796	12.499	9.497	-23.444	-15.636
OCT	-3.451	-1.567	3.567	-44.043	-12.909
NOV	-16.811	-8.485	-5.969	-35.451	-17.448
DEC	-6.067	-3.779	-7.345	-31.261	-24.552

Table 3B: Bias Statistics of monthly mean and variance of maximum temperature at Hamilton Airport

Bias Table-Tmax monthly mean

Month	Raw RCM	SDSM RCM	SDSM GCM	TLFN RCM	TLFN GCM
JAN	-1.437	-0.466	0.159	0.482	0.418
FEB	-5.196	-0.763	0.349	-0.586	0.841
MAR	-5.647	-0.864	-0.293	-0.729	0.077
APR	-5.885	-0.818	0.154	-0.958	-0.474
MAY	-2.145	-0.277	0.244	-0.842	-0.257
JUN	0.031	-0.049	-0.120	0.422	0.161
JUL	2.110	-0.522	0.116	-0.861	-0.415
AUG	3.349	0.586	0.468	0.889	0.130
SEP	4.168	0.548	0.438	0.416	0.683
OCT	0.596	0.696	0.448	0.034	0.408
NOV	-0.836	0.312	-0.064	-0.264	-0.185
DEC	-0.500	-0.005	-0.124	-0.060	-0.609

Bias Table-Tmax monthly variance

Month	Raw RCM	SDSM RCM	SDSM GCM	TLFN RCM	TLFN GCM
JAN	-2.205	0.945	-0.199	-29.184	-6.567
FEB	11.078	1.991	0.727	-26.769	0.933
MAR	-13.057	-11.797	-5.325	-30.354	-4.447
APR	-12.906	-1.414	-2.516	-33.498	-4.924
MAY	0.376	5.866	-0.997	-20.904	-7.400
JUN	6.958	2.537	1.150	-16.484	-6.834
JUL	17.893	-0.952	-0.694	-12.128	-6.575
AUG	24.509	0.565	1.433	-10.713	-4.048
SEP	36.285	4.459	0.936	-14.130	-4.224
OCT	12.115	7.256	-1.564	-14.480	-0.076
NOV	-11.502	-2.993	-2.219	-21.279	-4.575
DEC	-16.379	-6.561	-4.061	-30.362	-8.750

Table 4B: Bias Statistics of monthly mean and variance of maximum temperature at Hamilton RBG

Bias Table-Tmax monthly mean					
		SDSM		TLFN	
Month	RawRCM	RCM	GCM	RCM	GCM
JAN	-2.666	-0.851	0.132	0.527	0.641
FEB	-6.274	-0.832	0.470	-0.529	0.863
MAR	-6.471	-0.131	-0.238	-0.667	0.447
APR	-6.267	-0.372	0.146	-0.938	-0.230
MAY	-2.560	-0.124	-0.059	-0.916	-0.331
JUN	-0.754	-0.110	-0.398	-0.104	-0.231
JUL	1.155	-0.669	0.208	-0.812	-0.636
AUG	2.379	-0.013	-0.235	0.517	-0.138
SEP	3.373	0.535	0.548	0.705	0.796
OCT	-0.157	0.691	0.217	-0.071	0.864
NOV	-1.545	0.192	-0.013	-0.059	0.523
DEC	-1.493	0.069	-0.094	-0.060	-0.041

Bias Table-Tmax monthly variance					
		SDSM		TLFN	
Month	RawRCM	RCM	GCM	RCM	GCM
JAN	-1.701	1.633	-0.248	-29.032	-5.216
FEB	11.661	-0.127	0.553	-26.756	0.824
MAR	-7.535	-7.674	-2.267	-26.470	-2.294
APR	-9.979	-1.493	-3.133	-31.791	-8.459
MAY	-3.095	1.815	-2.344	-25.514	-11.580
JUN	2.547	0.101	-0.096	-20.399	-8.806
JUL	14.167	-2.183	-0.253	-15.788	-7.804
AUG	21.542	0.722	1.064	-13.681	-4.029
SEP	33.860	3.463	-1.741	-15.611	-4.465
OCT	11.938	7.884	-1.018	-15.602	-1.474
NOV	-9.798	-2.041	-1.855	-17.812	-4.777
DEC	-13.337	-5.035	-4.208	-27.766	-4.221

Table 5B: Bias Statistics of monthly mean and variance of minimum temperature at Hamilton Airport

Bias Table-Tmin monthly mean					
		SDSM		TLFN	
Month	Raw RCM	RCM	GCM	RCM	GCM
JAN	-2.103	-0.649	0.030	-0.354	0.012
FEB	-8.453	-0.626	0.207	-0.197	0.615
MAR	-8.610	0.004	0.103	0.101	0.583
APR	-4.107	-0.460	-0.062	-0.792	0.513
MAY	-3.951	0.023	0.110	-0.627	0.376
JUN	-3.223	0.303	-0.088	-0.228	-0.455
JUL	-2.738	-0.620	-0.114	-0.990	-0.633
AUG	-1.637	-0.360	-0.179	0.225	-0.319
SEP	0.010	0.055	0.071	-0.025	0.172
OCT	0.074	0.410	0.378	0.693	0.480
NOV	0.801	0.166	0.166	-0.308	-0.458
DEC	2.728	-0.471	-0.855	-0.239	-0.890

Bias Table-Tmin monthly variance					
		SDSM		TLFN	
Month	Raw RCM	RCM	GCM	RCM	GCM
JAN	13.221	1.284	-6.467	-41.132	-20.126
FEB	14.578	4.873	1.718	-34.744	-6.613
MAR	28.282	-4.388	-4.671	-24.298	1.233
APR	5.574	0.539	1.246	-14.299	2.152
MAY	-0.051	3.261	0.990	-12.533	-2.724
JUN	8.568	3.742	2.768	-9.739	-0.743
JUL	13.865	3.416	1.918	-8.654	0.472
AUG	10.308	0.405	1.738	-11.587	-1.407
SEP	5.483	3.262	1.107	-17.139	-2.844
OCT	7.559	6.795	1.858	-10.316	0.408
NOV	-7.033	2.403	0.195	-12.709	2.084
DEC	-21.615	2.047	1.538	-29.846	-7.894

Table 6B: Bias Statistics of monthly mean and variance of minimum temperature at Hamilton RBG

Bias Table-Tmin monthly mean					
		SDSM		TLFN	
Month	Raw RCM	RCM	GCM	RCM	GCM
JAN	-3.134	-0.792	0.259	-0.445	0.528
FEB	-9.672	-0.879	0.118	-0.783	0.540
MAR	-9.737	-0.113	-0.158	-0.590	0.938
APR	-5.188	-0.694	-0.459	-0.857	0.522
MAY	-4.970	-0.380	-0.265	-0.523	0.090
JUN	-4.437	0.180	-0.125	-0.204	-0.221
JUL	-4.086	-0.576	-0.002	-0.854	-0.588
AUG	-3.024	-0.216	-0.184	0.351	-0.566
SEP	-1.145	0.180	0.253	0.507	-0.169
OCT	-1.041	0.464	0.414	0.356	0.044
NOV	-0.106	0.349	0.465	0.408	-0.103
DEC	1.502	-0.443	-0.879	-0.368	-0.873

Bias Table-Tmin monthly variance					
		SDSM		TLFN	
Month	Raw RCM	RCM	GCM	RCM	GCM
JAN	14.659	2.804	-4.380	-39.595	-11.545
FEB	16.513	7.483	2.780	-33.250	-1.354
MAR	29.980	-4.913	-5.455	-21.949	2.474
APR	7.786	1.907	2.433	-12.611	0.614
MAY	0.300	2.493	-0.008	-11.537	-1.814
JUN	8.153	4.253	3.161	-9.180	0.314
JUL	12.165	1.331	0.421	-10.558	-2.849
AUG	9.061	-0.329	0.562	-13.027	-3.407
SEP	6.308	4.044	2.273	-15.463	-0.661
OCT	6.381	5.324	2.412	-12.659	-1.748
NOV	-7.350	1.163	0.339	-13.449	-1.717
DEC	-19.475	2.233	1.598	-26.753	-2.244

Table 7B: Wilcoxon Rank Sum and Levene Test p-values for maximum temperature at Hamilton Airport

Wilcoxon test results for HA max temperature				
	SDSM		TLFN	
Month	GCM	RCM	GCM	RCM
Jan	0.969	0.173	0.548	0.34
Feb	0.569	0.19	0.319	0.497
Mar	0.793	0.937	0.237	0.778
Apr	0.522	0.192	0.954	0.836
May	0.239	0.697	0.945	0.377
Jun	0.499	0.475	0.33	0.38
Jul	0.743	0.241	0.167	0.098
Aug	0.135	0.403	0.928	0.121
Sep	0.551	0.271	0.078	0.152
Oct	0.263	0.198	0.53	0.064
Nov	0.942	0.557	0.358	0.167
Dec	0.797	0.659	0.107	0.128

Levene test results for HA max temperature				
	SDSM		TLFN	
Month	GCM	RCM	GCM	RCM
Jan	0.676	0.18	0.885	0.47
Feb	0.672	0.484	0.107	0.061
Mar	0.203	0.734	0.193	0.287
Apr	0.105	0.065	0.16	0.465
May	0.824	0.601	0.414	0.456
Jun	0.882	0.332	0.938	0.838
Jul	0.736	0.66	0.065	0.345
Aug	0.992	0.908	0.097	0.175
Sep	0.718	0.59	0.147	0.828
Oct	0.693	0.929	0.835	0.387
Nov	0.993	0.994	0.485	0.629
Dec	0.73	0.989	0.171	0.249

Table 8B: Wilcoxon Rank Sum and Levene Test p-values for maximum temperature at Hamilton RBG

Wilcoxon test results for HR max temperature				
	SDSM		TLFN	
Month	GCM	RCM	GCM	RCM
Jan	0.895	0.092	0.271	0.081
Feb	0.421	0.33	0.394	0.42
Mar	0.818	0.556	0.055	0.103
Apr	0.82	0.102	0.466	0.098
May	0.918	0.631	0.793	0.656
Jun	0.285	0.682	0.664	0.998
Jul	0.353	0.26	0.154	0.099
Aug	0.303	0.54	0.748	0.305
Sep	0.33	0.48	0.426	0.316
Oct	0.51	0.071	0.08	0.201
Nov	0.917	0.167	0.262	0.086
Dec	0.608	0.742	0.663	0.358

Levene test results for HR max temperature				
	SDSM		TLFN	
Month	GCM	RCM	GCM	RCM
Jan	0.089	0.958	0.062	0.469
Feb	0.184	0.313	0.251	0.349
Mar	0.297	0.653	0.609	0.713
Apr	0.204	0.066	0.176	0.114
May	0.691	0.826	0.539	0.885
Jun	0.386	0.503	0.29	0.608
Jul	0.474	0.942	0.758	0.909
Aug	0.382	0.233	0.259	0.226
Sep	0.097	0.921	0.116	0.46
Oct	0.241	0.183	0.103	0.168
Nov	0.533	0.797	0.975	0.835
Dec	0.746	0.296	0.532	0.837

Table 9B: Wilcoxon Rank Sum and Levene Test p-values for minimum temperature at Hamilton Airport

Wilcoxon test results for HA min temperature				
	SDSM		TLFN	
Month	GCM	RCM	GCM	RCM
Jan	0.713	0.28	0.543	0.325
Feb	0.303	0.109	0.155	0.822
Mar	0.697	0.95	0.135	0.087
Apr	0.727	0.129	0.253	0.132
May	0.57	0.786	0.059	0.181
Jun	0.622	0.347	0.088	0.27
Jul	0.434	0.151	0.09	0.064
Aug	0.633	0.205	0.11	0.077
Sep	0.397	0.141	0.801	0.635
Oct	0.119	0.232	0.422	0.142
Nov	0.677	0.205	0.412	0.707
Dec	0.259	0.273	0.135	0.735

Levene test results for HA min temperature				
	SDSM		TLFN	
Month	GCM	RCM	GCM	RCM
Jan	0.499	0.444	0.774	0.111
Feb	0.358	0.669	0.398	0.203
Mar	0.987	0.851	0.35	0.856
Apr	0.752	0.501	0.864	0.72
May	0.799	0.927	0.715	0.74
Jun	0.723	0.892	0.527	0.962
Jul	0.637	0.844	0.554	0.148
Aug	0.78	0.925	0.911	0.944
Sep	0.603	0.979	0.903	0.982
Oct	0.506	0.848	0.485	0.64
Nov	0.753	0.838	0.972	0.957
Dec	0.276	0.332	0.053	0.186

Table 10B: Wilcoxon Rank Sum and Levene Test p-values for minimum temperature at Hamilton RBG

Wilcoxon test results for HR min temperature				
	SDSM		TLFN	
Month	GCM	RCM	GCM	RCM
Jan	0.978	0.092	0.542	0.083
Feb	0.892	0.109	0.386	0.37
Mar	0.635	0.383	0.075	0.089
Apr	0.147	0.084	0.082	0.102
May	0.587	0.401	0.459	0.504
Jun	0.972	0.793	0.511	0.458
Jul	0.852	0.29	0.147	0.097
Aug	0.595	0.067	0.424	0.063
Sep	0.337	0.117	0.58	0.554
Oct	0.269	0.197	0.379	0.429
Nov	0.106	0.089	0.621	0.071
Dec	0.16	0.188	0.085	0.458

Levene test results for HR min temperature				
	SDSM		TLFN	
Month	GCM	RCM	GCM	RCM
Jan	0.644	0.296	0.555	0.727
Feb	0.057	0.062	0.241	0.092
Mar	0.445	0.794	0.629	0.768
Apr	0.668	0.881	0.295	0.448
May	0.631	0.482	0.364	0.172
Jun	0.487	0.916	0.757	0.813
Jul	0.425	0.91	0.806	0.81
Aug	0.882	0.617	0.941	0.832
Sep	0.691	0.414	0.249	0.133
Oct	0.499	0.595	0.452	0.149
Nov	0.827	0.418	0.682	0.26
Dec	0.374	0.874	0.864	0.79

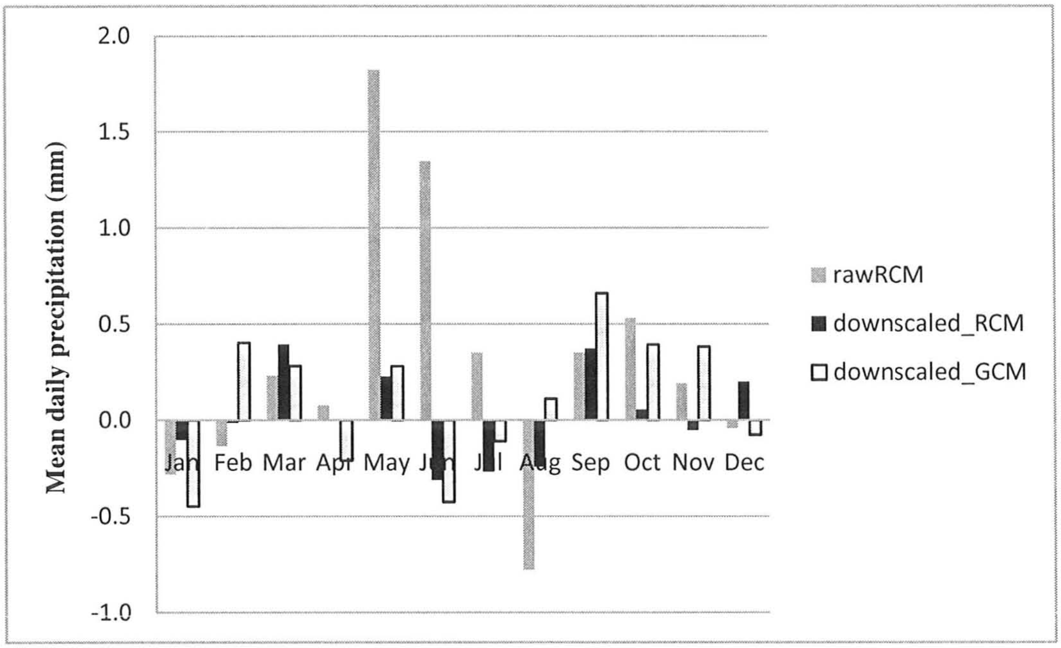

Fig 1B: Residual plot for SDSM downscaled precipitation at Hamilton RBG: comparing monthly mean

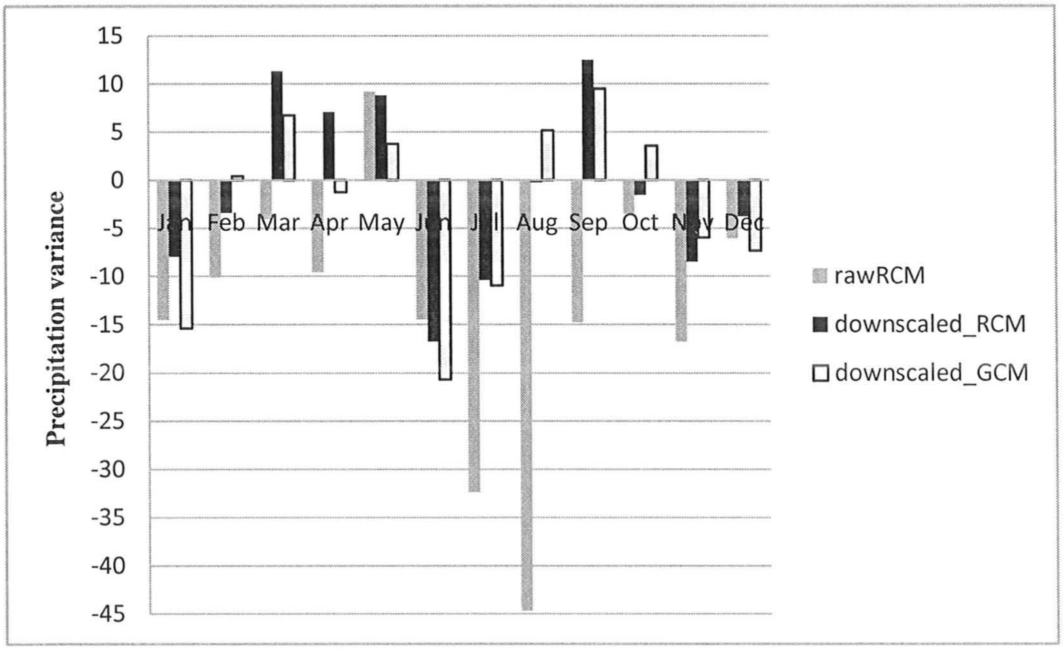

Fig 2B: Residual plot for SDSM downscaled precipitation at Hamilton RBG: comparing monthly variability

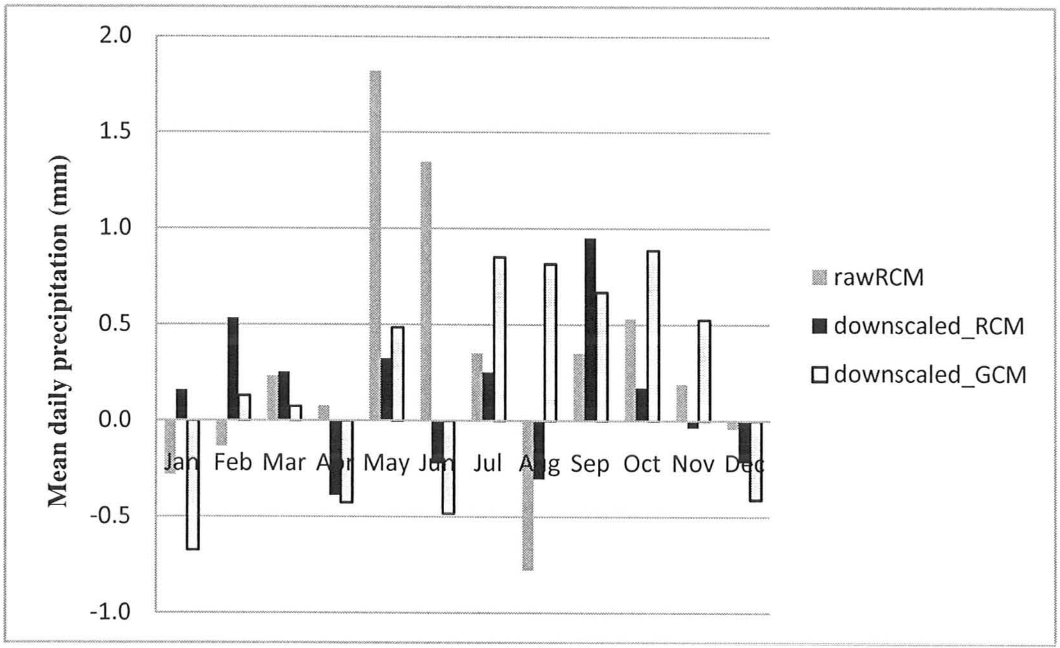

Fig 3B: Residual plot for TLFN downscaled precipitation at Hamilton RBG: comparing monthly mean

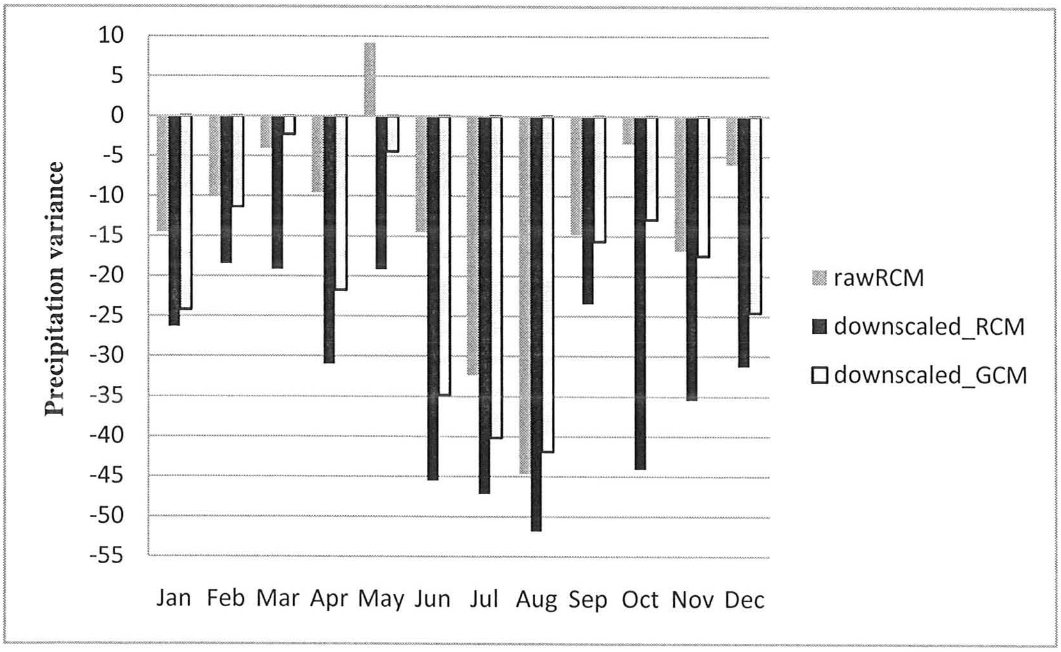

Fig 4B: Residual plot for TLFN downscaled precipitation at Hamilton RBG: comparing monthly variability

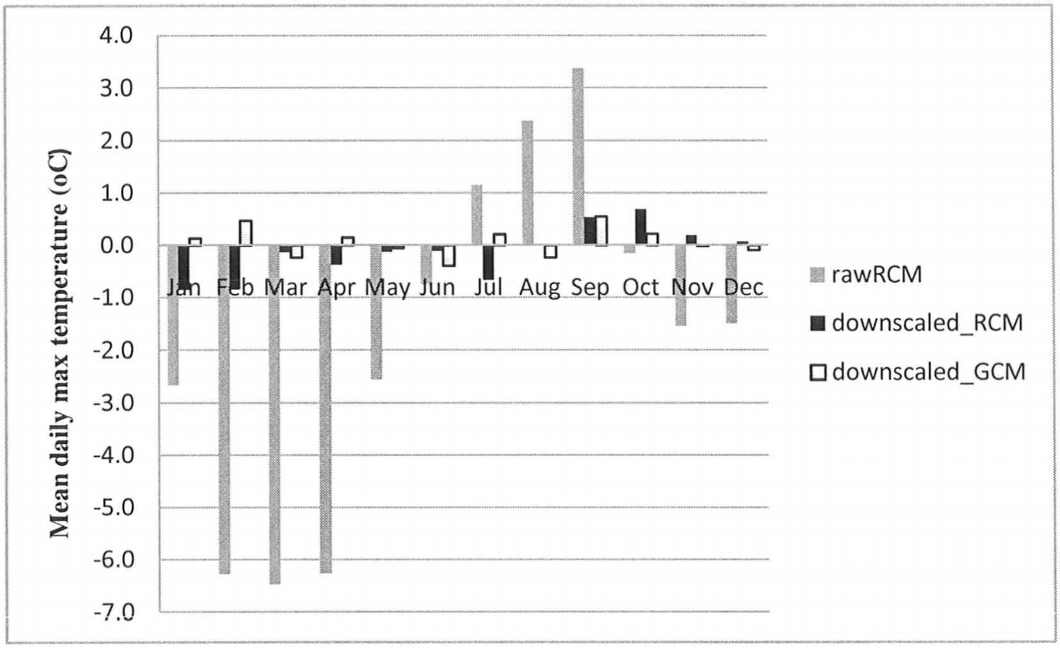

Fig 5B: Residual plot for SDSM downscaled maximum temperature at Hamilton RBG: comparing monthly mean

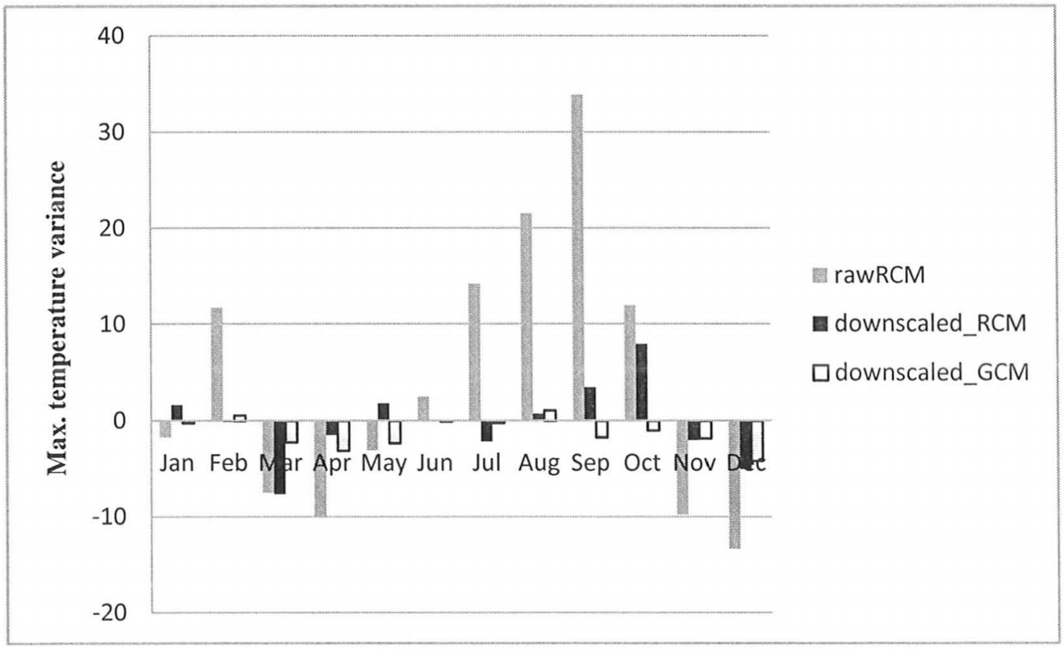

Fig 6B: Residual plot for SDSM downscaled maximum temperature at Hamilton RBG: comparing monthly variability

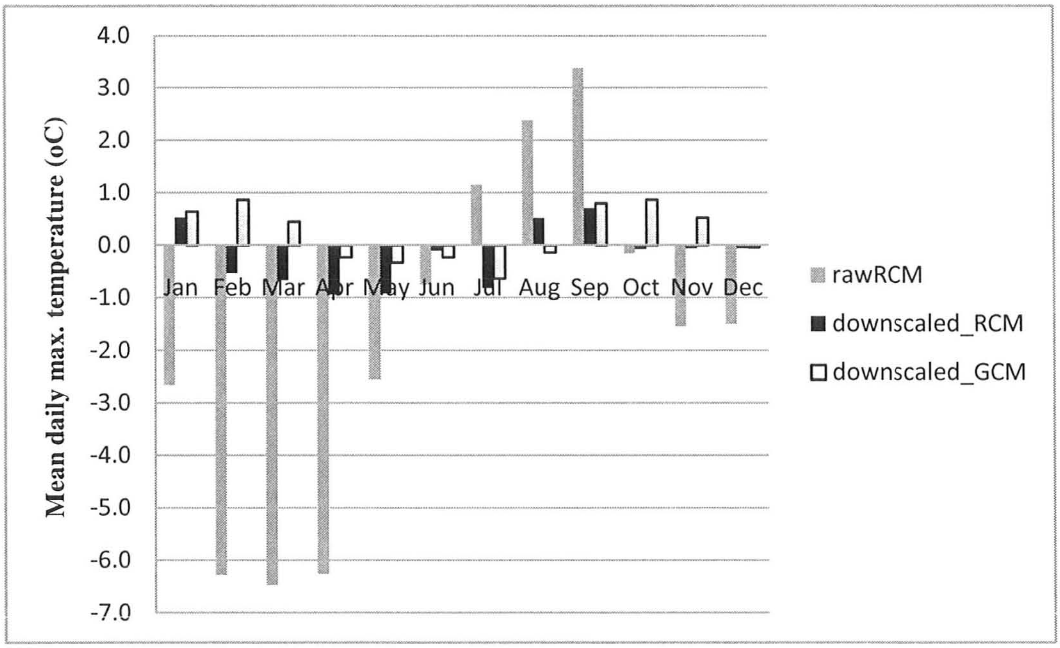

Fig 7B: Residual plot for TLFN downscaled maximum temperature at Hamilton RBG: comparing monthly mean

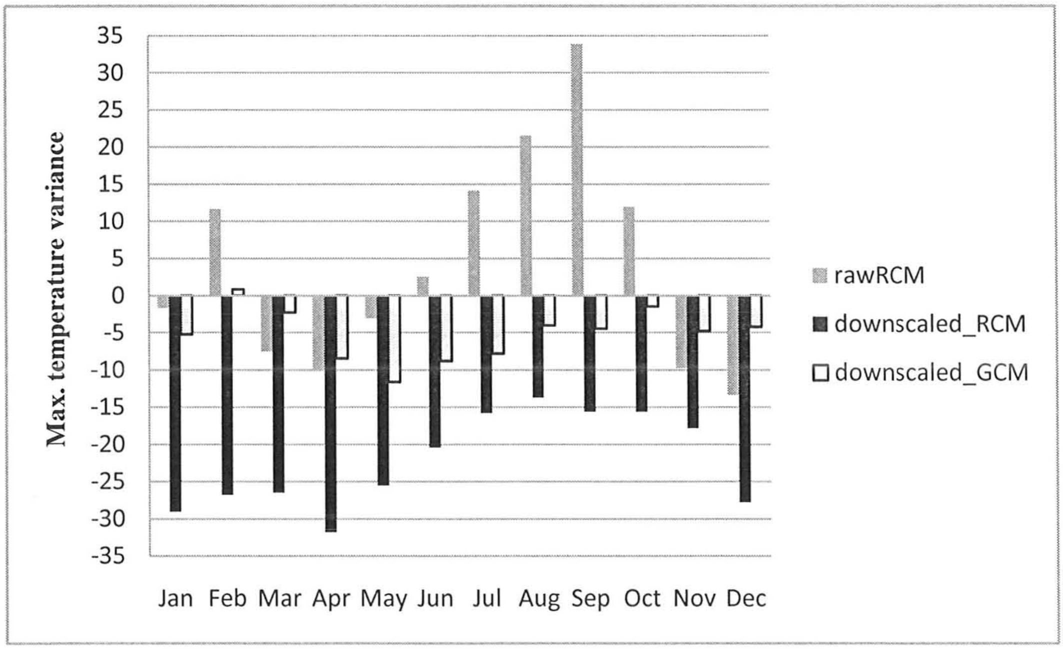

Fig 8B: Residual plot for TLFN downscaled maximum temperature at Hamilton RBG: comparing monthly variability

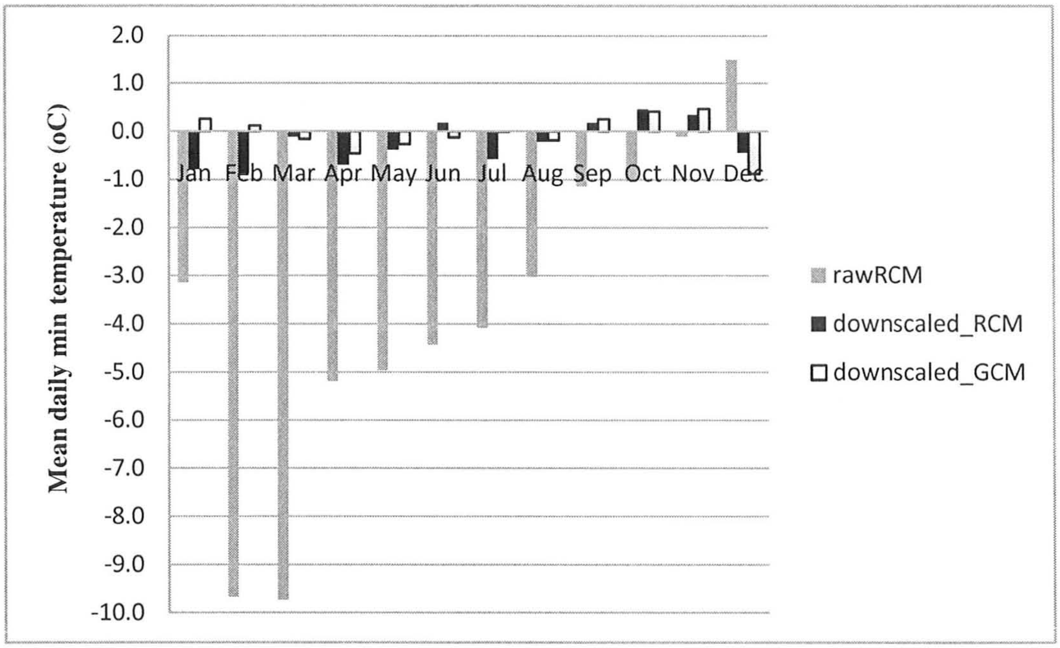

Fig 9B: Residual plot for SDSM downscaled minimum temperature at Hamilton RBG: comparing monthly mean

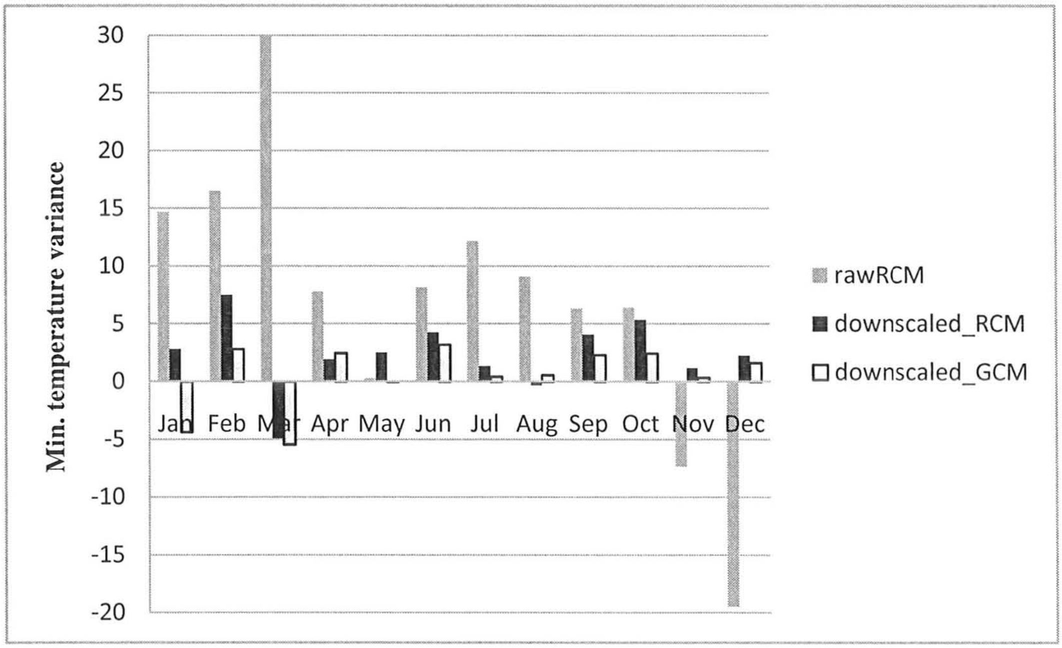

Fig 10B: Residual plot for SDSM downscaled minimum temperature at Hamilton RBG: comparing monthly variability

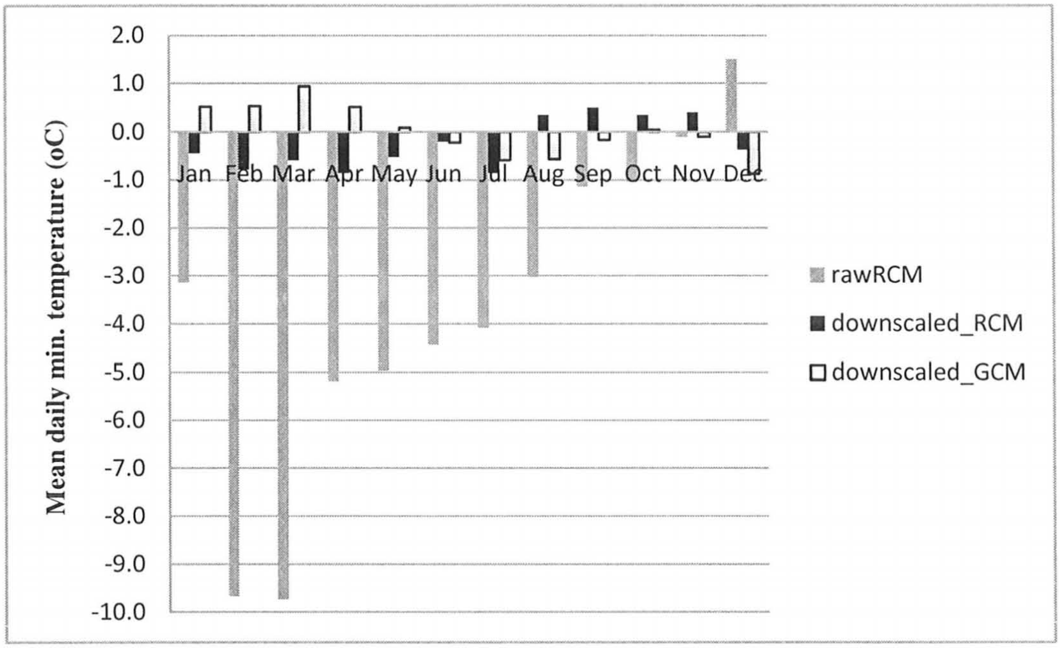

Fig 11B: Residual plot for TLFN downscaled minimum temperature at Hamilton RBG: comparing monthly mean

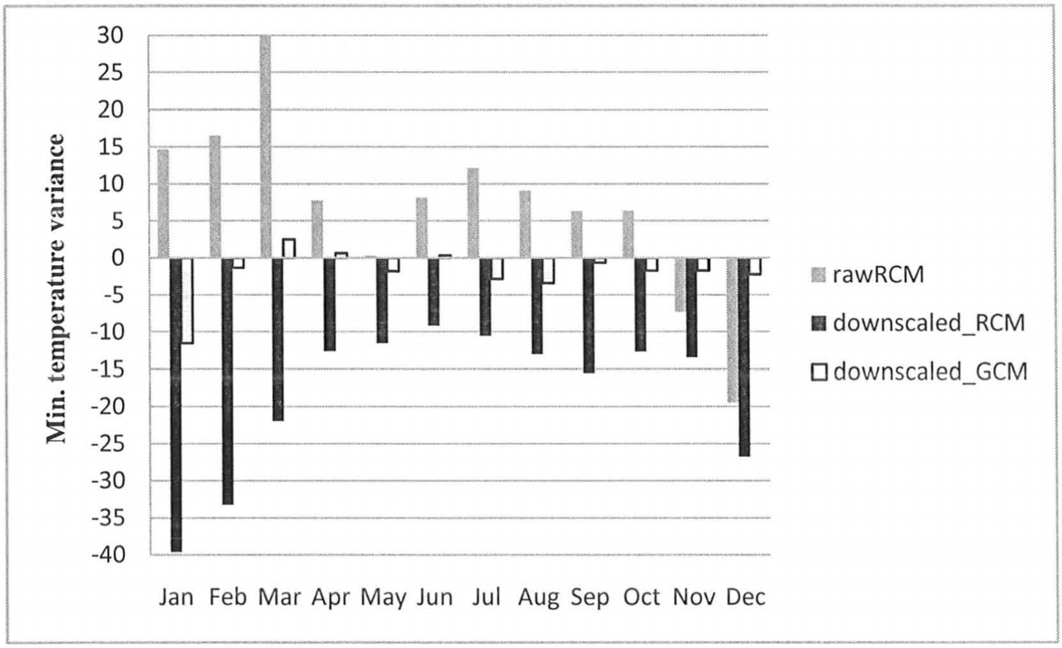

Fig 12B: Residual plot for TLFN downscaled minimum temperature at Hamilton RBG: comparing monthly variability

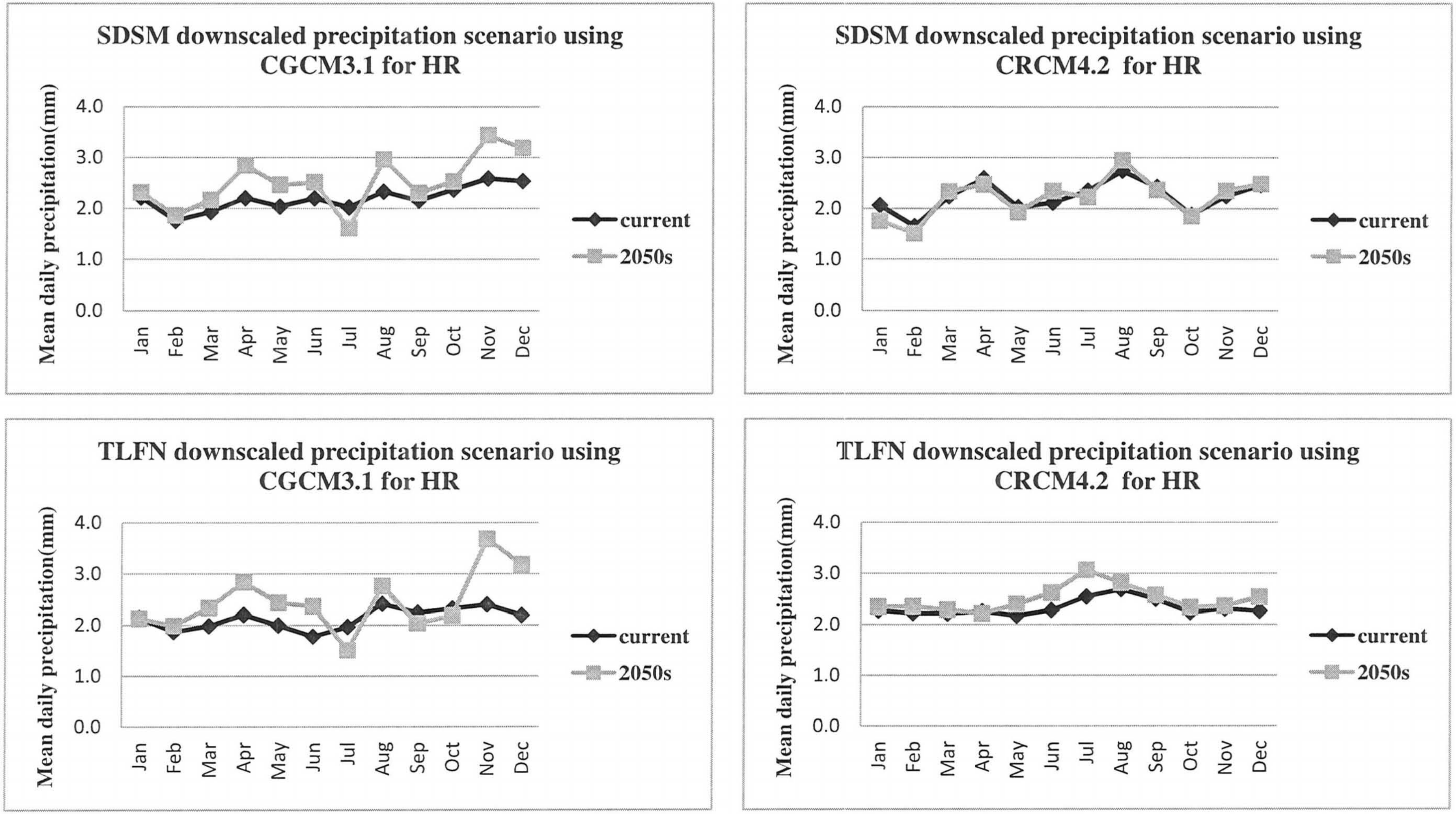

Fig 13B: SDSM and TLFN downscaled monthly mean precipitation at Hamilton RBG for current (1961-1990) and future period (2050s)

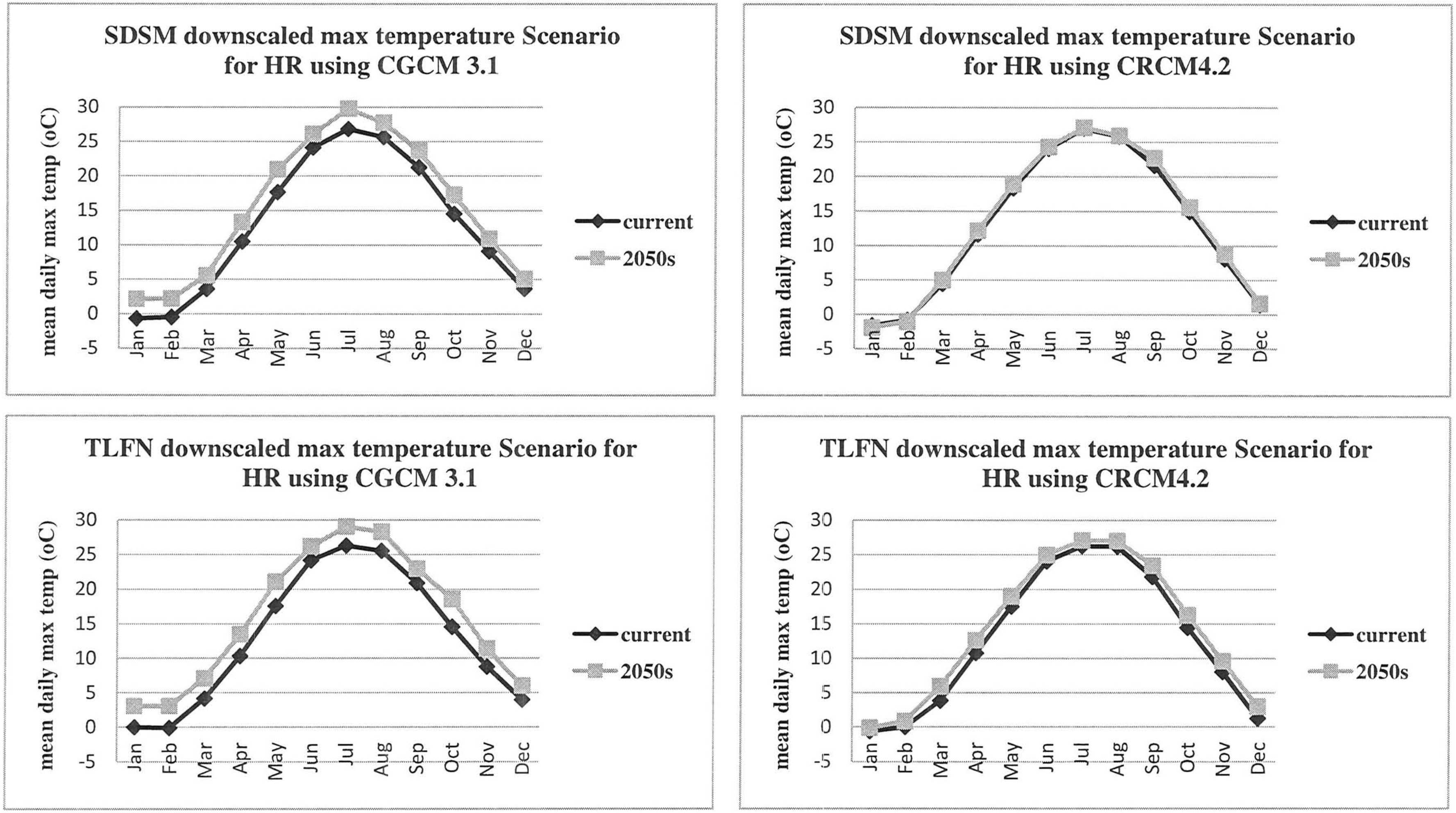

Fig 14B: SDSM and TLFN downscaled monthly mean maximum temperature at Hamilton RBG for current (1961-1990) and future period (2050s)

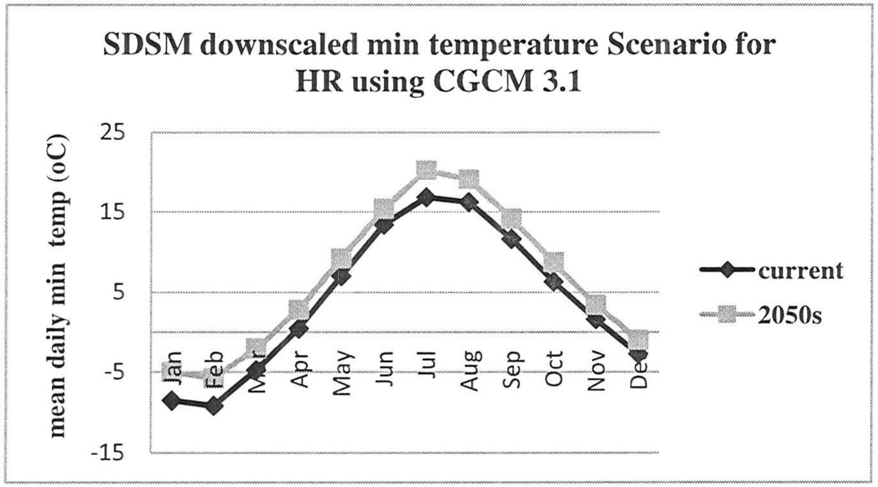

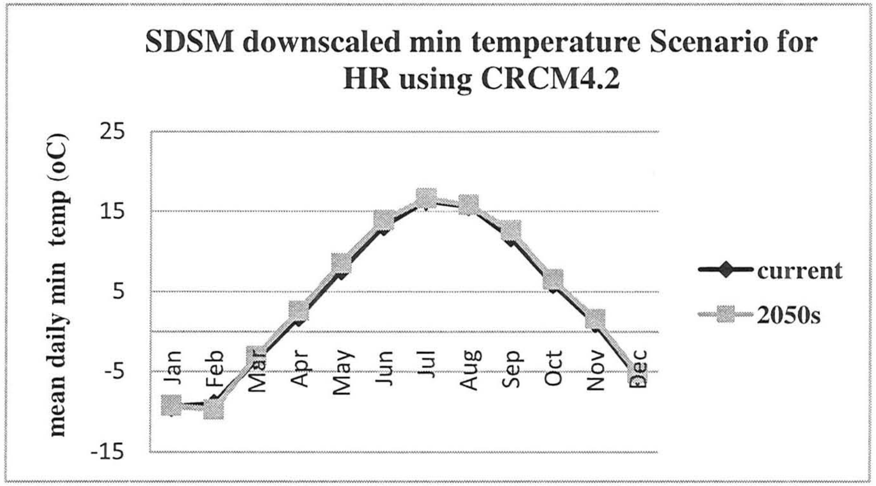

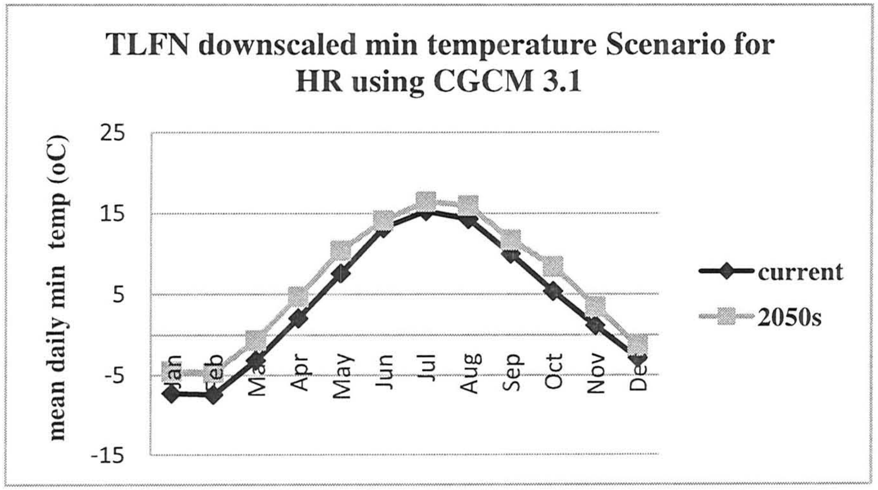

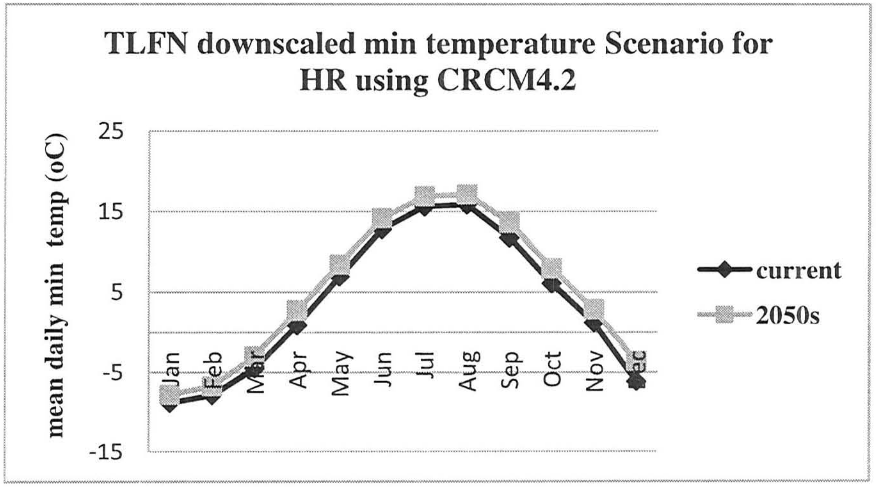

Fig 15B: SDSM and TLFN downscaled monthly mean minimum temperature at Hamilton RBG for current (1961-1990) and future period (2050s)

APPENDIX C

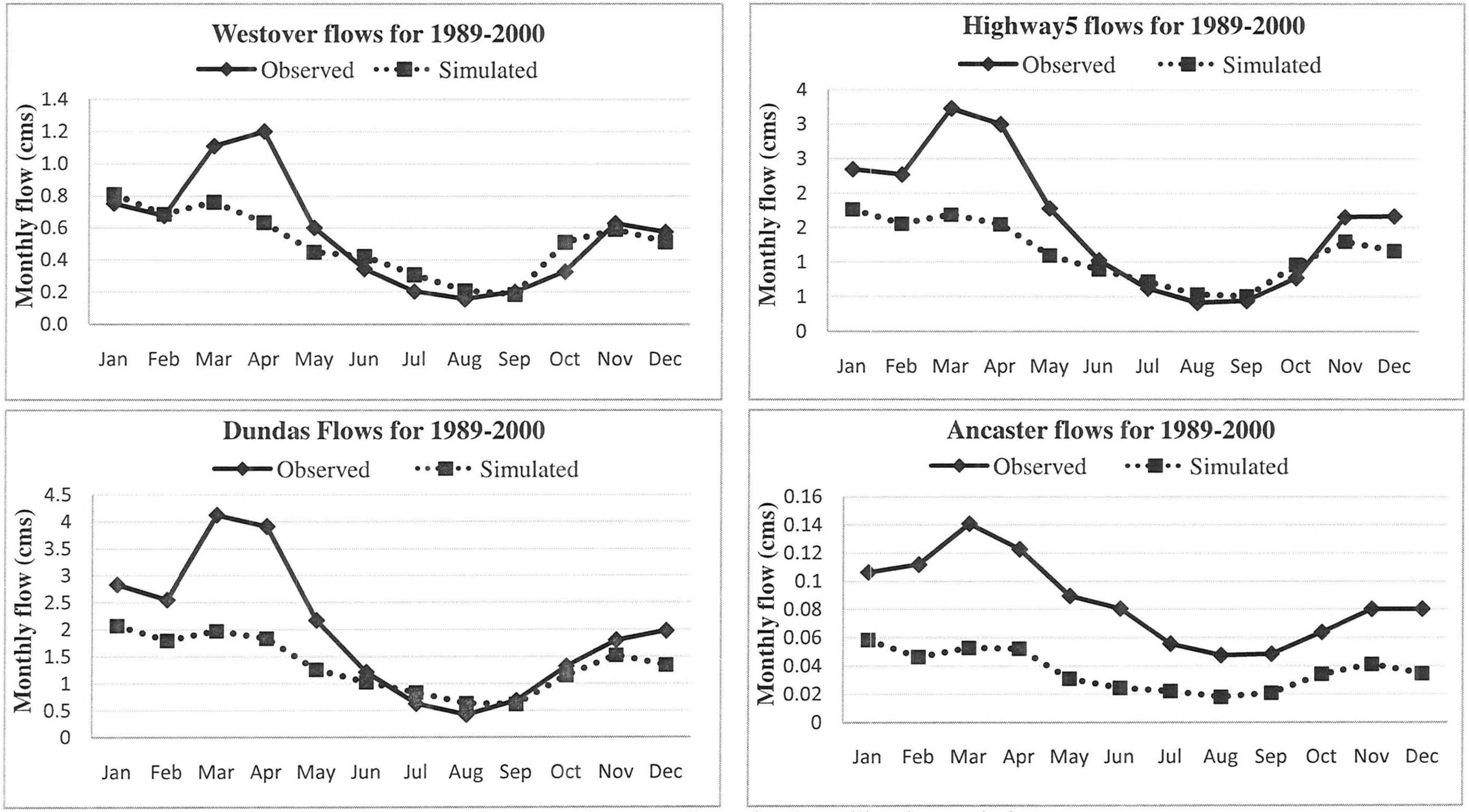

Fig 1C: Monthly streamflows for the calibration period

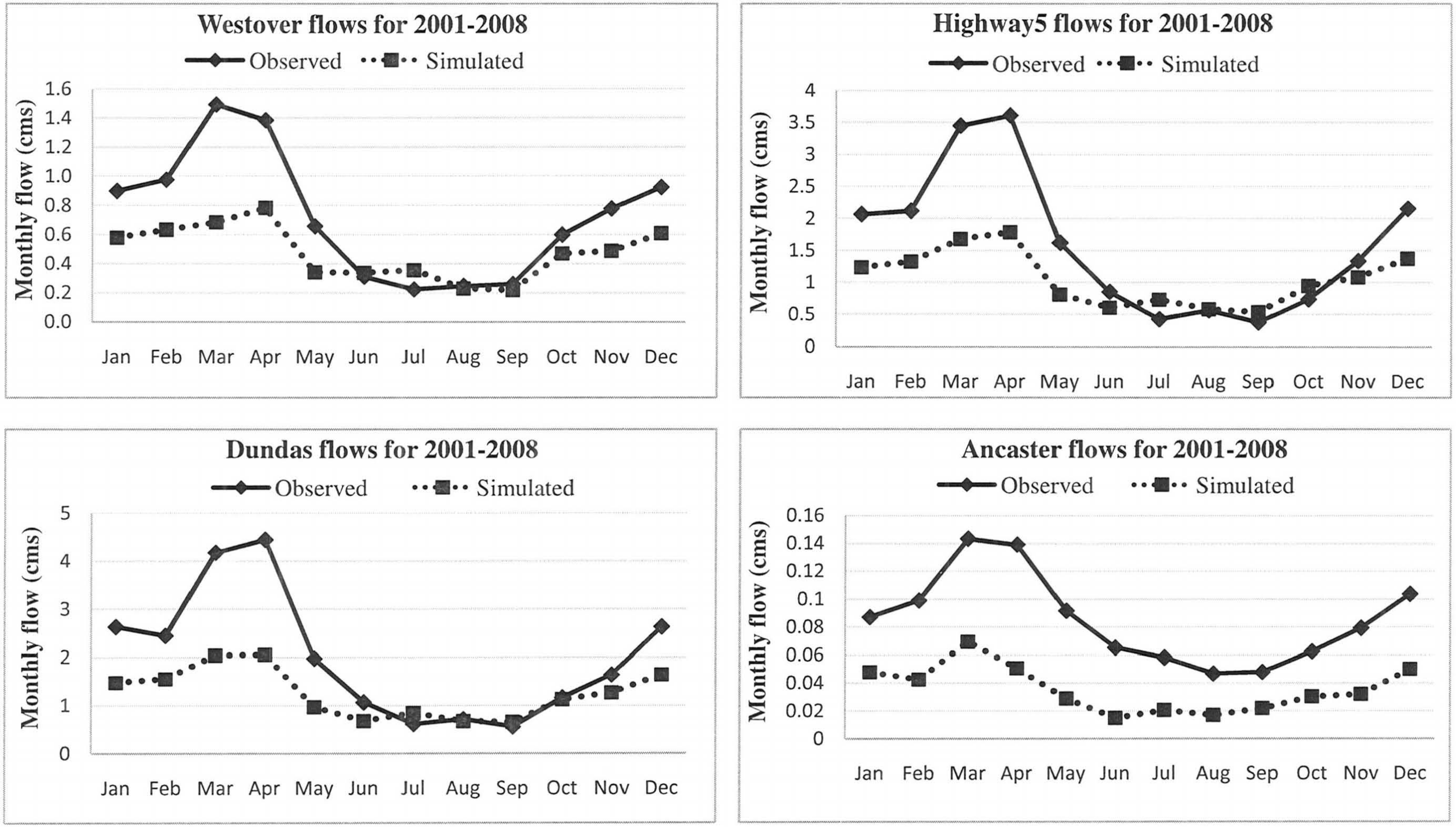

Fig 2C: Monthly streamflows for the validation period

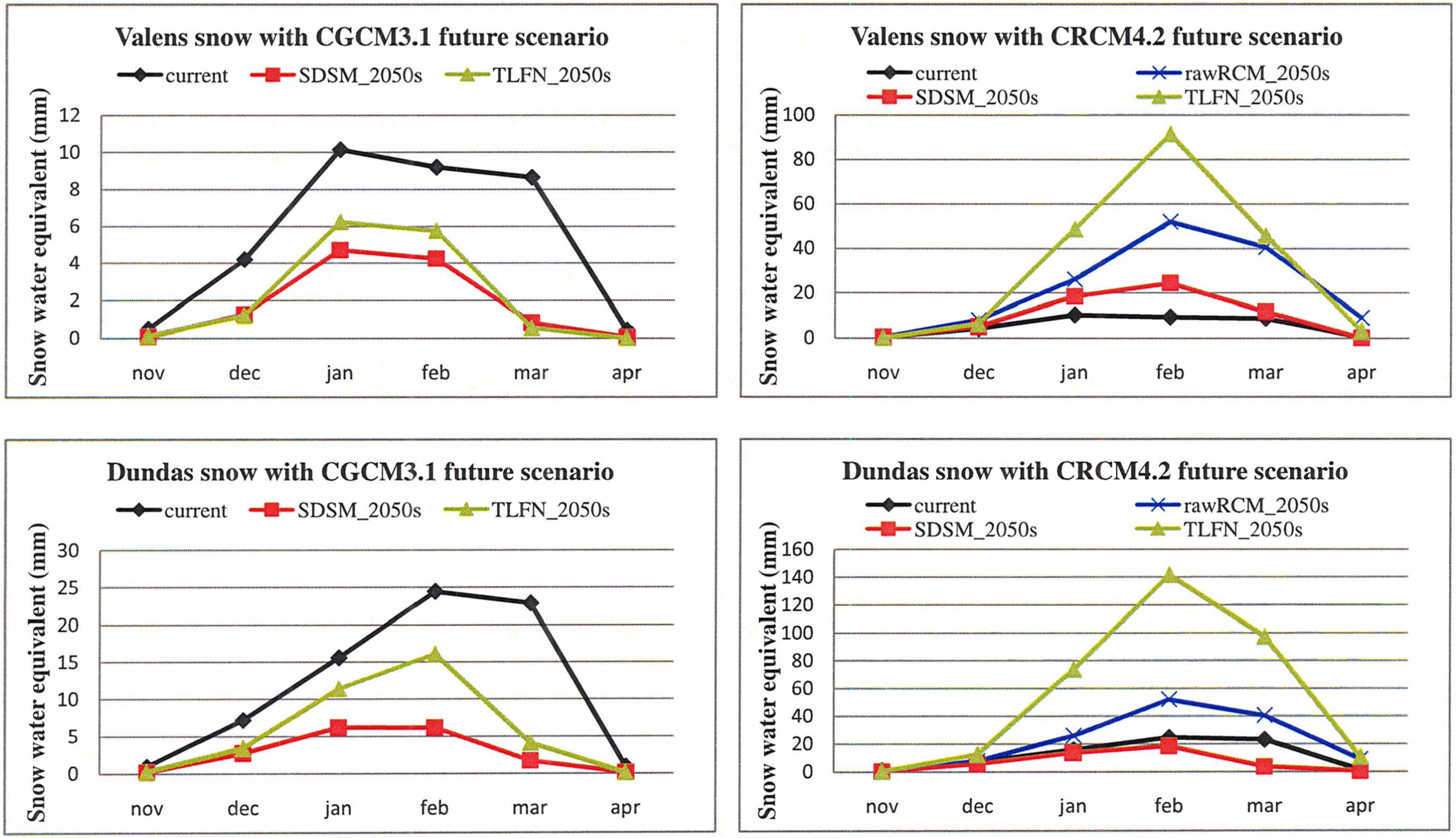

Fig 3C: Snow storage results at Valens and Dundas for 2050s

Table 1C: Changes in average seasonal values of snow storage for 2050s (2046-2065) from current conditions (1989-2008)

Average increase/decrease in total snow storage (mm)					
Snow Station			SEASONS		
			Winter	Spring	Fall
Christie	RAW_RCM		12.94	12.95	-0.53
	GCM	SDSM	-10.68	-10.96	-0.71
		TLFN	-5.43	-9.79	-0.64
	RCM	SDSM	-3.19	-10.02	-0.61
		TLFN	60.11	42.04	-0.71
Valens	RAW_RCM		20.83	20.31	-0.11
	GCM	SDSM	-4.42	-4.09	-0.40
		TLFN	-3.44	-4.25	-0.35
	RCM	SDSM	8.14	1.32	-0.03
		TLFN	40.94	19.88	-0.45
Dundas	RAW_RCM		12.94	12.95	-0.53
	GCM	SDSM	-10.68	-10.96	-0.71
		TLFN	-5.43	-9.79	-0.64
	RCM	SDSM	-3.19	-10.02	-0.61
		TLFN	60.11	42.04	-0.71

Table 2C: Changes in average seasonal values of evapotranspiration for 2050s (2046-2065) from current conditions (1989-2008)

Average increase/decrease in evapotranspiration (%)						
Flow Station			SEASONS			
			Winter	Spring	Summer	Fall
Westover	RAW_RCM		-5.69	18.68	19.40	9.27
	GCM	SDSM	26.50	7.40	-5.29	22.92
		TLFN	33.50	4.85	-10.35	12.95
	RCM	SDSM	-3.94	-4.32	8.42	6.98
		TLFN	-13.49	18.05	29.90	37.15
Highway 5	RAW_RCM		-4.61	18.05	2.44	-7.86
	GCM	SDSM	16.70	-6.85	5.13	19.04
		TLFN	22.52	-1.63	-5.15	14.97
	RCM	SDSM	0.77	-15.67	-13.75	-2.46
		TLFN	-7.00	2.02	1.62	5.38
Dundas	RAW_RCM		-0.59	27.73	21.79	9.20
	GCM	SDSM	21.19	-2.02	-0.06	10.54
		TLFN	26.00	0.84	-7.54	14.14
	RCM	SDSM	-0.91	-10.96	-12.16	-6.04
		TLFN	-35.05	25.13	33.99	36.02
Ancaster	RAW_RCM		-3.60	9.75	17.52	-5.13
	GCM	SDSM	19.01	0.60	-3.37	14.81
		TLFN	24.56	3.63	-9.91	14.58
	RCM	SDSM	0.42	-6.61	-17.25	-7.67
		TLFN	-17.07	15.13	9.36	14.21

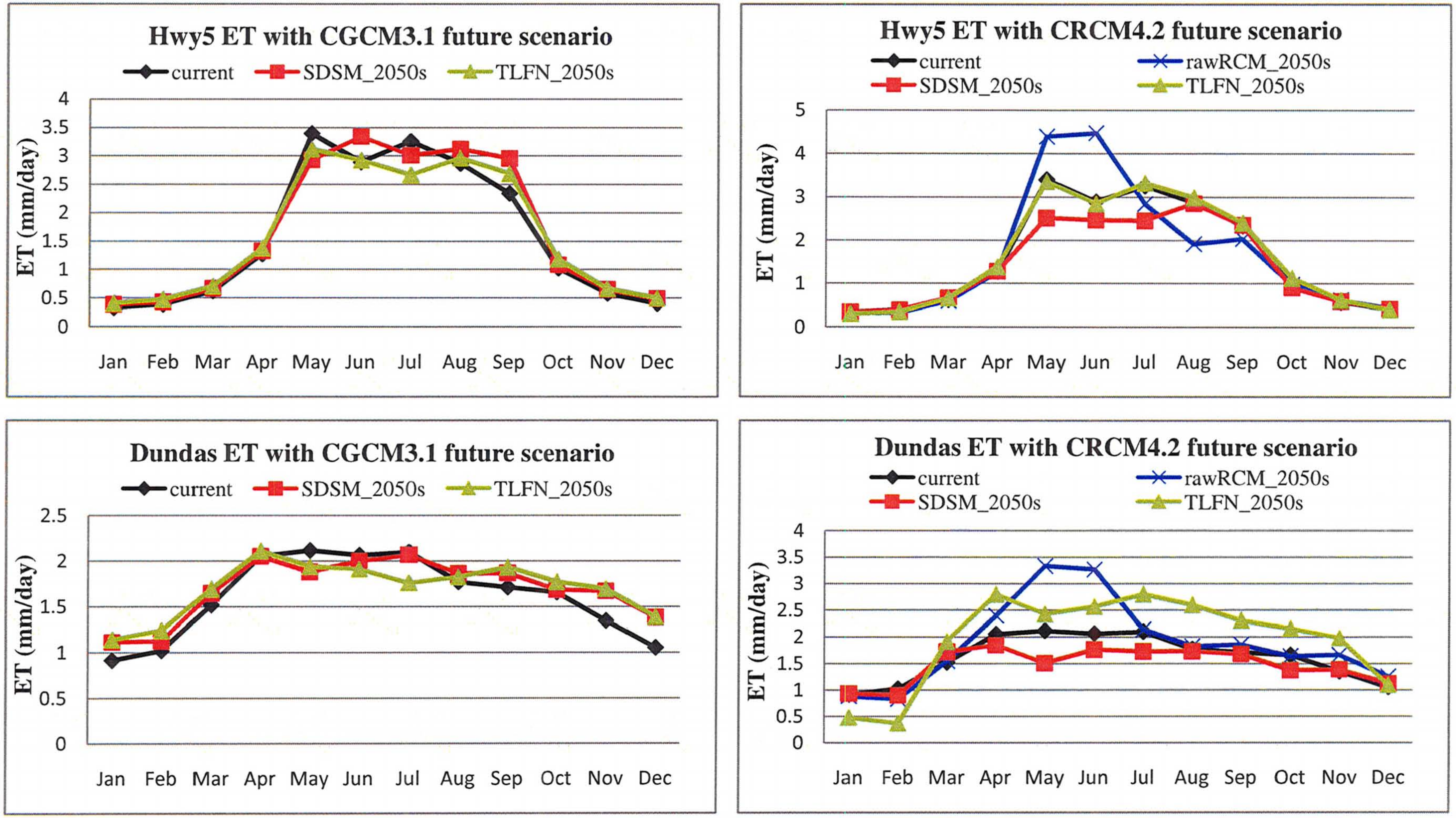

Fig 4C: Evapotranspiration results at Highway 5 and Dundas for 2050s

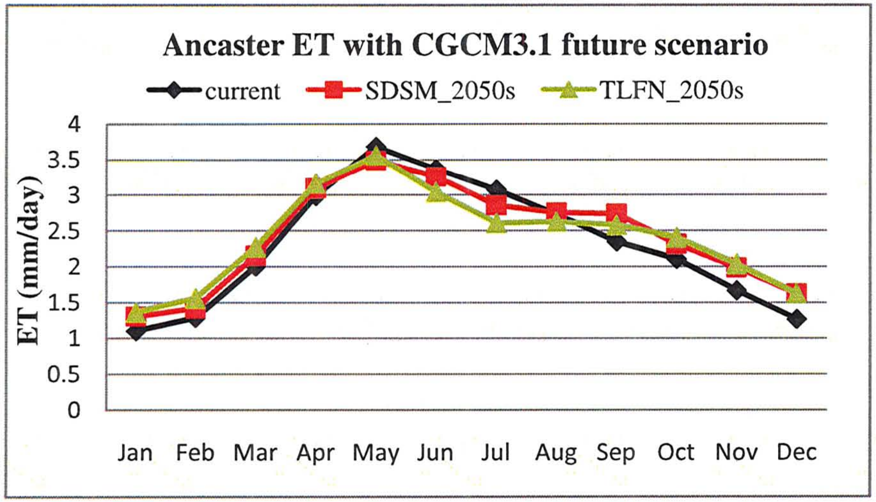

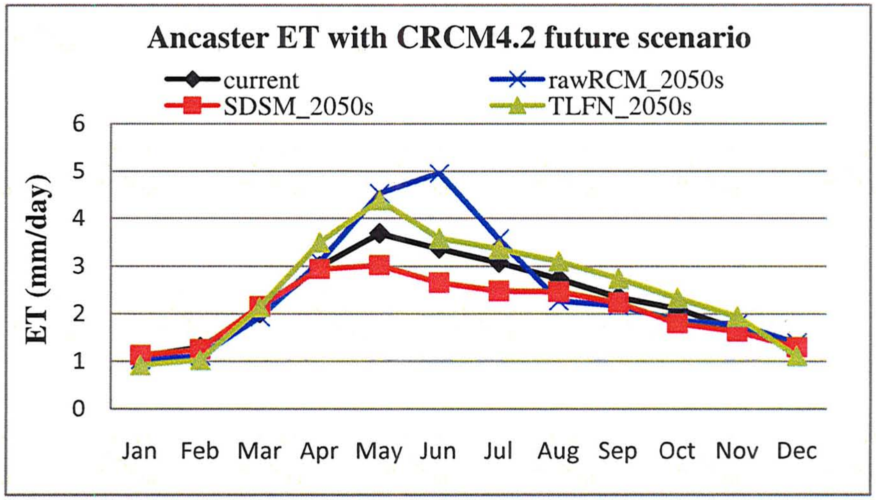

Fig 5C: Evapotranspiration results at Ancaster for 2050s

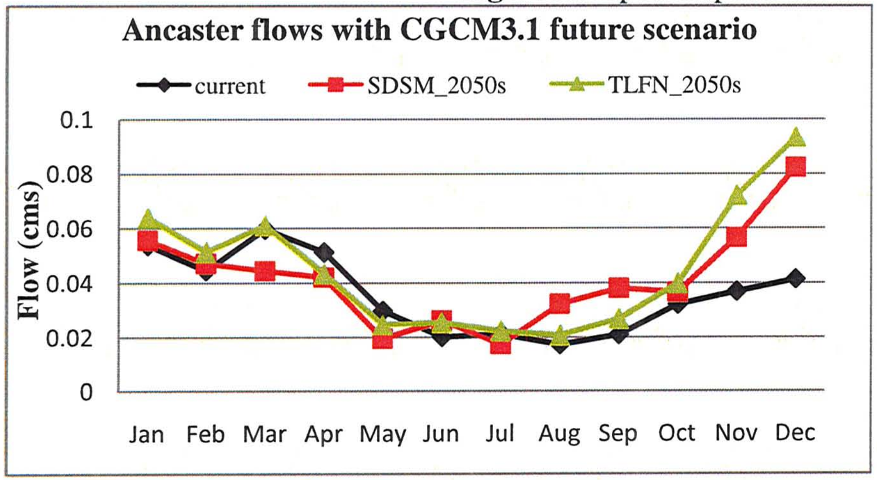

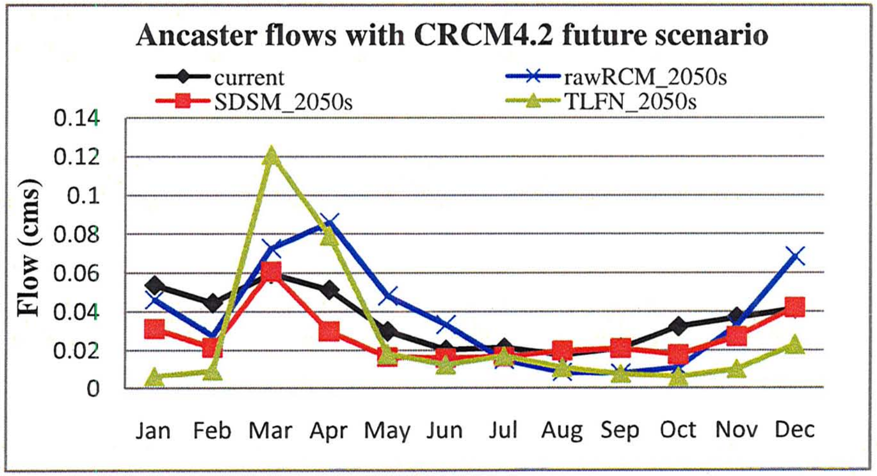

Fig 6C: Ancaster flows for current conditions and 2050s

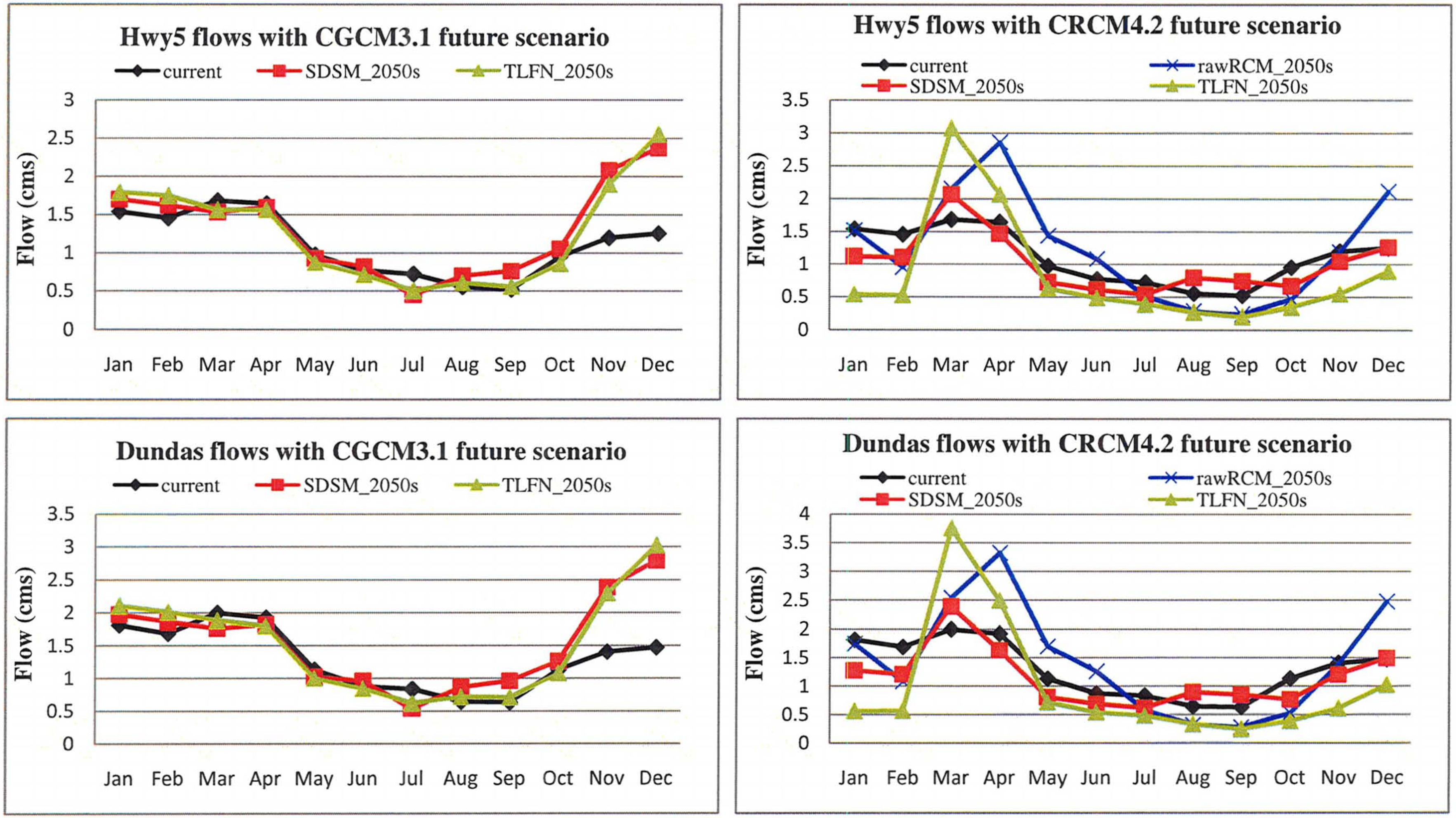

Fig 7C: Highway 5 and Dundas flows for current conditions and 2050s

Table 3C: Changes in average seasonal streamflows for 2050s (2046-2065) from current conditions (1989-2008)

Average increase/decrease in streamflows (%)						
Flow Station			SEASONS			
			Winter	Spring	Summer	Fall
Westover	RAW_RCM		5.34	42.63	-5.32	-11.08
	GCM	SDSM	26.17	0.50	-4.74	35.22
		TLFN	33.16	-3.72	-7.75	14.23
	RCM	SDSM	-12.78	5.14	-0.27	-4.25
		TLFN	-36.42	26.72	-31.90	-30.50
Highway 5	RAW_RCM		7.74	49.77	-8.23	-28.77
	GCM	SDSM	33.95	-5.62	-3.25	45.76
		TLFN	43.25	-7.01	-10.55	23.78
	RCM	SDSM	-17.88	-0.99	-5.02	-8.22
		TLFN	-54.02	33.94	-43.92	-58.84
Dundas	RAW_RCM		6.41	49.13	-8.35	-30.76
	GCM	SDSM	33.05	-8.64	0.35	44.98
		TLFN	43.17	-7.44	-7.69	28.17
	RCM	SDSM	-20.08	-4.53	-6.50	-11.23
		TLFN	-56.81	37.42	-42.65	-60.89
Ancaster	RAW_RCM		1.15	46.13	-4.69	-42.88
	GCM	SDSM	32.41	-24.56	28.08	44.89
		TLFN	48.93	-8.31	15.69	53.21
	RCM	SDSM	-32.44	-24.25	-12.02	-27.47
		TLFN	-72.97	54.40	-32.70	-74.34